Regional groundwater representation by coupling the mesoscale Hydrologic Model (mHM) with OpenGeoSys (OGS): Model development and case studies

Dissertation
(kumulativ)

zur Erlangung des akademischen Grades doctor rerum naturalium
(Dr. rer. nat.)

vorgelegt dem Rat der Chemisch-Geowissenschaftlichen Fakultät der
Friedrich-Schiller-Universität Jena

von M.Sc. Miao Jing
geboren am 24. Oktober 1989 in Dongping, China

Gutachter:

1. Prof. Dr. Sabine Attinger (Universität Potsdam)
2. Prof. Dr. Kai Uwe Totsche (Friedrich-Schiller-Universität Jena)
3. Prof. Dr. Alexander Brenning (Friedrich-Schiller-Universität Jena)

Tag der öffentlichen Verteidigung: 11.09.2019

Declaration on authorship

Declaration on authorship and copyright in a cumulative doctoral thesis

Reprint permissions have been obtained for all manuscripts used as part of the doctoral thesis.

The co-authors of the manuscripts used in the present cumulative doctoral thesis have been informed about the use of the manuscripts and about the declared individual contributions; they have given their consent.

The declared individual contributions of the doctoral candidate and the other doctoral candidates participate as co-authors in the publications are listed in the attachment.

Name of doctoral candidate	Date	Place	Signature
Miao Jing	November 5, 2019	Leipzig	

I give my consent to the submission of a cumulative doctoral thesis and confirm the correctness of the information provided above.

Name of supervisor	Date	Place	Signature
Prof. Dr. Sabine Attinger	November 5, 2019	Leipzig	

Publication #1: Jing, M., Heße, F., Kumar, R., Wang, W., Fischer, T., Walther, M., Zink, M., Zech, A., Samaniego, L., Kolditz, O., and Attinger, S.: Improved regional-scale groundwater representation by the coupling of the mesoscale Hydrologic Model (mHM v5.7) to the groundwater model OpenGeoSys (OGS), Geosci. Model Dev., 11, 1989-2007, https://doi.org/10.5194/gmd-11-1989-2018, 2018.						
Involved in	Miao Jing	Falk Heße	Rohini Kumar	Wenqing Wang	Thomas Fischer	Marc Walther
	Author #1:	Author #2:	Author #3:	Author #4:	Author #5:	Author #6:
Conceptual research design	×	×	×	×		
Plannung of research activities	×					
Data collection	×				×	
Data analyses and interpretation	×	×	×			
Manuscript writing	×	×	×			×
Suggested publication equivalence value	1.0					

Publication #1: Jing, M., Heße, F., Kumar, R., Wang, W., Fischer, T., Walther, M., Zink, M., Zech, A., Samaniego, L., Kolditz, O., and Attinger, S.: Improved regional-scale groundwater representation by the coupling of the mesoscale Hydrologic Model (mHM v5.7) to the groundwater model OpenGeoSys (OGS), Geosci. Model Dev., 11, 1989-2007, https://doi.org/10.5194/gmd-11-1989-2018, 2018.					
Involved in	Matthias Zink	Alraune Zech	Luis Samaniego	Olaf Kolditz	Sabine Attinger
	Author #7:	Author #8:	Author #9:	Author #10:	Author #11:
Conceptual research design				×	×
Plannung of research activities			×		
Data collection	×				
Data analyses and interpretation					
Manuscript writing		×			×
Suggested publication equivalence value					

Publication #2: Jing, M., Heße, F., Kumar, R., Kolditz, O., Kalbacher, T., and Attinger, S.: Influence of input and parameter uncertainty on the prediction of catchment-scale groundwater travel time distributions, Hydrol. Earth Syst. Sci., 23, 171-190, https://doi.org/10.5194/hess-23-171-2019, 2019.						
Involved in	Miao Jing	Falk Heße	Rohini Kumar	Olaf Kolditz	Thomas Kalbacher	Sabine Attinger
	Author #1:	Author #2:	Author #3:	Author #4:	Author #5:	Author #6
Conceptual research design	×	×		×		×
Plannung of research activities	×	×	×			×
Data collection	×		×			
Data analyses and interpretation	×					
Manuscript writing	×	×	×		×	
Suggested publication equivalence value	1.0					

Publication #3: Jing, M., Kumar, R., Heße, F., Thober, S., Rakovec, O., Samaniego, L., and Attinger, S.: Assessing the response of groundwater quantity and travel timedistribution to 1.5, 2 and 3 degrees global warming in a mesoscalecentral German basin, Hydrol. Earth Syst. Sci. Discuss., https://doi.org/10.5194/hess-2019-9, in review, 2019.							
Involved in	Miao Jing	Rohini Kumar	Falk Heße	Stephan Thober	Oldrich Rakovec	Luis Samaniego	Sabine Attinger
	Author #1:	Author #2:	Author #3:	Author #4:	Author #5:	Author #6:	Author #7:
Conceptual research design	×	×	×				×
Plannung of research activities	×	×	×				
Data collection	×					×	
Data analyses and interpretation	×						
Manuscript writing	×	×	×	×	×		×
Suggested publication equivalence value	1.0						

Abstract

Groundwater is the source of approximately twenty percent of the world's freshwater supply. It is also one of the most important sources of water for irrigation. However, groundwater has been over-used and polluted in many places in the world. Climate change and saltwater intrusion are threatening groundwater resources. The groundwater system throughout the world is subject to many potential contamination sources, such as storage tanks, abandoned industrial factories, nitrates from agricultural activities, pesticides, and atmospheric contaminants. Meanwhile, numerical models provide a quantitative framework for integrating field information and for characterizing hydrogeologic processes and have been widely used to forecast the results of a proposed action/inaction.

In reality, the terrestrial hydrologic cycle is a continuous system. The groundwater flow is intricately and tightly linked with the land surface processes and states (e.g., recharge, evapotranspiration, soil moisture, and overland flow). Historically, the surface hydrologic models and groundwater models have been developed separately due to the distinct characteristics of land surface processes and deep groundwater processes. Generally, the surface hydrologic models have a good predictive capability of flood events but constantly fall short in predicting the low flow. The reason behind this is the absence of explicit groundwater representation. Meanwhile, groundwater models focus on representing slow groundwater flow and transport but always use oversimplified upper boundaries (e.g., empirical estimation of recharge). Therefore, the coupling between the surface hydrologic models and the subsurface hydrogeologic models are urgently needed.

This study is devoted to improving the characterization of regional groundwater flow and transport processes through the coupling of the mesoscale Hydrologic Model (mHM) and the hydrogeological model OpenGeoSys (OGS). The proposed mHM-OGS coupled model is applied to assess the regional groundwater resource of a mesoscale catchment in central Germany (Nägelstedt). The mHM-OGS coupled model can reasonably simulate the transient behavior of groundwater levels. It is also a valuable tool in estimating travel time distributions (TTDs) with its capability in explicitly characterizing the subsurface hydraulic heterogeneity and dealing with input and parameter uncertainties. Results of ensemble simulations show that the groundwater TTD in Nägelstedt catchment is strongly dependent on the rate and the spatial pattern of recharge. Meanwhile, the internal hydraulic properties also have a moderate impact on the shape of groundwater TTD. The mHM-OGS coupled model is also a valuable tool in evaluating regional groundwater resources under climate change. An ensemble of climate scenarios are set up to assess the uncertainty in climate projections under 1.5, 2, and 3 °C global warming. Simulation results indicate a small increase in groundwater quantity and a moderate decrease in

groundwater mean travel time in Nägelstedt catchment. Additionally, a large predictive uncertainty is found in the simulation results, which is mainly introduced from the climate projections. The global warming ultimately influences the regional groundwater quality at the long term through the modification of groundwater travel time distributions.

Zusammenfassung

Grundwasser macht etwa zwanzig Prozent der weltweiten Frischwasserversorgung aus. Es ist auch eine der wichtigsten Quellen für landwirtschaftliche Bewässerung. Allerdings wurde das Grundwasser in vielen Teilen der Welt überbeansprucht und verschmutzt. Der Klimawandel und das Eindringen von Salzwasser gefährden die Grundwasserressourcen. Die Grundwassersysteme der gesamten Welt sind permanent zahlreichen potenziellen Kontaminationsquellen ausgesetzt, wie Lagertanks, septischen Abfällen, unkontrollierten gefährlichen Abfällen, Deponien, Chemikalien und Streusalzen sowie atmosphärischen Verunreinigungen. Numerische Modelle bieten eine Möglichkeit die Integration von Feldinformationen und die Charakterisierung hydrogeologischer Prozesse quantitativ durchzuführen. Numerische Modelle wurden häufig zur Vorhersage von Ergebnissen möglicher Szenarien verwendet.

Der terrestrische Wasserkreislauf ist allerdings ein kontinuierliches System. Die Grundwasserströmung ist auf komplizierte Weise eng mit den Bodenoberflächenprozessen und -zuständen gekoppelt (z. B. Grundwasserneubildung, evapotransformation, Bodenfeuchte und Überlandströmung). Historisch wurden die hydrologischen Modelle der Landoberfläche und die Grundwassermodelle aufgrund der unterschiedlichen Eigenschaften von Landoberflächenprozessen und tiefen Grundwasserprozessen getrennt entwickelt. Im Allgemeinen haben die hydrologischen Modelle der Landoberfläche eine gute Vorhersagemöglichkeit für Hochwasserereignisse, sind aber bei der Vorhersage von Niedrigwasser in Flüssen unzureichend. Der Grund dafür ist das Fehlen einer expliziten Grundwasserdarstellung. Grundwassermodelle konzentrieren sich auf die Darstellung langsamer Grundwasserflüsse, verwenden jedoch immer vereinfachte obere Randbedingungen (z. B. empirische Abschätzung der Grundwasserneubildung). Daher ist die Kopplung zwischen Landoberflächenmodellen und Grundwassermodellen dringend erforderlich.

Diese Studie zielt darauf ab, die Anwendbarkeit des mesoskaligen hydrologischen Modells (mHM v5.7) auf die Hydrogeologie zu erweitern, indem es mit dem porösen Mediensimulator OpenGeoSys (OGS) gekoppelt wird. Die Anwendbarkeit des gekoppelten Modells (mHM-OGS v1.0) wird anhand einer Fallstudie im mitteleuropäischen mesoskaligen Einzugsgebiet - Nägelstedt - evaluiert. Die Berechnungen zeigen, dass das einseitig gekoppelte Modell die räumlich expliziten Modellierungsfähigkeiten von hydrologischen Oberflächen- und Grundwassermodellen nutzen kann und eine adäquate Darstellung des raumzeitlichen Verhaltens von Grundwasserspeicher und -köpfen liefert und es somit zu einem wertvollen Werkzeug für Adressierung von Wasserressourcen und Managementproblemen. Das gekoppelte Modell wird verwendet, um die Reisezeitverteilungen (TTD) in einem komplexen realen Aquifersystem zu untersuchen. Die Simulationsergebnisse zeigen

den primären Effekt der Grundwasserneubildung auf die vorhergesagte mittlere Reisezeit (MTT). Die verschiedenen Realisierungen von Kalibrierungsbeschränkten K_s -Feldern vergrößern oder verringern die vorhergesagten MTTs moderat. Zusammenfassend ergibt das Ignorieren der räumlichen Inhomogenitäten und der Unsicherheit der Randbedingungen eine verzerrte Reisezeitvorhersage. In dieser Studie wurde die Reaktion des regionalen Grundwassersystems eines mitteleuropäischen Beckens (Nägelstedt) auf den Klimawandel unter einer Erwärmung von 1.5, 2, and 3 °C untersucht. Die Simulationsergebnisse zeigen eine hohe Wahrscheinlichkeit eines leichten Anstiegs der Neubildung und der Grundwasserstände sowie eine moderate Abnahme der mittleren Verweilzeiten unter 1,5, 2 und 3 °C erwärmung. Die Vorhersageunsicherheit, die durch verschiedene Klimaprojektionen eingeführt wird, steigt mit stärkerer globalen Erwärmung (von 1,5 auf 3 °C) an. Die globale Erwärmung beeinflusst letztendlich die regionale Grundwasserqualität langfristig durch die Änderung der Reisezeitverteilungen.

Contents

List of Figures

List of Tables

Symbols and Abbreviations

c_v	Coefficient of variance
DEM	Digital Elevation Model
DWD	German Meteorological Service
EDK	External Drift Kriging
ET	Evapotranspiration
GCM	General Circulation Model
GIS	Geographic Information System
GW	Groundwater
HBV	Hydrologiska Byråns Vattenbalansavdelning
km	Middle Keuper
K_s	Hydraulic conductivity
ku	Lower Keuper
MAE	Mean Absolute Error
mHM	mesoscale Hydrologic Model
mm	Middle Muschelkalk
mo	Upper Muschelkalk
MPI	Message Passing Interface
MPS	Multiple Point Statistics
mR	mHM Recharge
MTT	Mean Travel Time
mu	Lower Muschelkalk
μ	Arithmetic mean
NSE	Nash–Sutcliffe Model Efficiency
NSMC	Null-space Monte Carlo
ODE	Ordinary Differential Equation

OGS	OpenGeoSys
OpenMP	Open Multi-Processing
PDE	Partial differential equation
QRE	Interquartile Range Error
RCP	Representative Concentration pathway
RMSE	Root-Mean-Square Error
RR	Reference Recharge
RS	Random Sampling
RWPT	Random Walk Particle Tracking
SAS	StorAge Selection
S_{eff}	Effective volume of storage
σ	Standard deviation
SW	Surface Water
TLUG	Thuringian State Office for the Environment and Geology
TTD	Travel Time Distribution
VIC	Variable Infiltration Capacity

Chapter 1

Introduction

This section provides an introduction to the cumulative dissertation. It starts with an overview of current challenges in subsurface hydrology, which is also the motivation of this study. It further introduces the theoretical background of this study. Finally, it ends up with the research questions and thesis structure.

1.1 Current challenges in subsurface hydrology

1.1.1 Surface water-groundwater interaction

Partitioning water budgets are of critical importance in catchment hydrology, while hydrological modeling is one of the most fundamental approaches to cope with this problem. Provided that the land surface fluxes are temporally and spatially highly dynamic, it is impossible to directly measure all water flux components over a real-world catchment with today's technology. For these reasons, hydrological models are designed to interpret hydrological observations and measurements (e.g. runoff, groundwater table, and remote sensing data), unveil water flow and transport dynamics, and project future conditions of the water cycle. Hydrological models partition precipitation into several flow components based on experimental and field observations. Water that goes into a surface water body promptly after individual precipitation events such as rain, is known as *event flow* or *quick flow* [Te Chow, 1988, Beven, 1989, Sophocleous, 2002]. In contrast to quick flow, water can also enter a stream from persistent, slowly varying sources, which is

defined as *baseflow*. Although baseflow can stem from the slow drainage process of water bodies (e.g., lakes or wetlands), it is mainly derived from subsurface groundwater flow [Beven, 1989, Sophocleous, 2002, Fetter, 2018]. Subsurface water can also flow into the stream fast enough such that it can contribute to the event response. This flow is defined as *interflow* [Te Chow, 1988, Beven, 1989, Sophocleous, 2002]. According to Beven [1989] (page 191), "*interflow is the near-surface the flow of water in the soil storage that results in seepage to a stream channel within the time range of a storm hydrograph*". Interflow can be composed of both unsaturated and saturated flows [Beven, 1989, Sophocleous, 2002, Groenendijk and van den Eertwegh, 2004].

Groundwater and surface water are typically well connected in non-arid catchments. Accurate characterization of this coupled surface water-groundwater (SW-GW) interaction can be critical for the partitioning of water budget components. Research on surface-subsurface interactions has expanded into a broad scope that incorporates headwater streams, lakes, wetlands, and estuaries. Coupling of surface and subsurface flows usually happens through shallow saturated/unsaturated soils where subsurface lateral flow infiltrates into or exfiltrates from the saturated groundwater aquifers. Meanwhile, the interaction also happens through a coupled flux in fracture channels for karst or fractured catchments [de Rooij et al., 2013b]. The SW-GW interaction in the large-scale landscape is very complex and varies in time and space. It is mainly controlled by the relative relationship between groundwater and surface water table, the hydraulic conductivity in the river bed or alluvium, and the geometry of surface water channel [Woessner, 2000]. The exchange flux varies in direction with the hydraulic heads, and also in magnitude depending on the hydraulic conductivity of sediments. This exchange flux is typically very dynamic depending on the sudden change in stream stage due to precipitation events and seasonality. Two basic patterns of SW-GW interaction are classified: the influent and effluent condition. The direction of flow is from surface water to groundwater for the influent condition, while it is opposite for the effluent condition [Rozemeijer et al., 2010, Sophocleous, 2002].

Under low precipitation conditions, the baseflow generated by groundwater aquifers is the main source of streamflow. In contrast, with heavy precipitation, the near-surface storages generate quick interflow, producing a higher surface water level, and causing an exchange flux from surface water to groundwater. During the flood, the river loses water

to infiltrate the sediments, reducing flooding amount and recharging the aquifer [Brunke and Gonser, 1997, Sophocleous, 2002].

A big challenge in computational subsurface hydrology is the characterization of highly dynamic surface-subsurface interaction, especially for the large scale models (i.e., 10^3–10^6 km^2). It is difficult to calculate the SW-GW interaction because first, the SW-GW interaction is spatially heterogeneous. Surface-subsurface exchange flow can be diffuse along the river channel, or discontinuous at some certain locations. Depending on the groundwater circulation pattern and the depth of the groundwater table, the surface water body can be either perennial and intermittent [Sophocleous, 2002, Te Chow, 1988]. In the case of multi-year perennial streams, the base stream is somehow continuous, and these streams can be mainly effluent and flowing continuously [Sophocleous, 2002]. Meanwhile, intermittent streams are active only at certain seasons, and can also be influent or effluent streams, depending on its seasonality. Second, SW-GW interaction is temporally dynamic. For those hydraulically well-connected SW-GW systems, the surface-subsurface exchange flux depends on the head difference between the surface water level and the groundwater level. Both the stream stage and groundwater head are highly dynamic, resulting in an essentially highly dynamic exchange flow depending on the climate condition, human activity, and season. Only a limited number of field studies reveal the details of how water migrates from ephemeral river channels or channels to the groundwater [Sophocleous, 2002, Rozemeijer et al., 2010]. Third, it is difficult to accurately obtain the value of hydraulic conductivity of the river bed. Assuming an exchange flux either continuous or discontinuous along the stream, the hydraulic conductivity is also expected to vary nonlinearly along the stream [Maxwell and Miller, 2005]. However, most of the studies rely on simplifications and assumptions to describe the hydraulic conductivity of the river bed [Rozemeijer et al., 2010, Maxwell and Kollet, 2008]. This is partially attributed to the lack of data on hydraulic properties of river beds in real-world catchments.

1.1.2 Subsurface heterogeneity at different scales

The subsurface hydrological system is heterogeneous with diverse hydrogeological patterns. It is also impossible to observe the structure of subsurface hydrological systems. Groundwater flow in the real-world catchment can not be simply conceptualized as a continuous uniform fluid flowing through a homogeneous porous medium. Rather, it is

a non-uniform fluid flowing through porous media where the hydraulic properties are uncertain [Anderson et al., 2015]. The processes and properties in the subsurface system are often difficult to be characterized at a small scale and difficult to upscale to a large scale. Therefore, transformations across scales and heterogeneity aggregation are essential challenges for hydrologists.

On the other hand, the structure of the subsurface porous medium is not accidental. It has predictable properties created by the coupling between the groundwater and the matrix of the porous medium. Patterns for the vegetation or preferential channel flow in soil may have relatively short temporal scales, but drainage patterns on the surface and below the surface, especially groundwater discharge patterns, are evolving at the geological time scales.

In general, given that proper observations are available on proper scales, it is reasonable to ignore, to a certain degree, heterogeneity and make use of the global observations directly for making predictions [de Marsily et al., 2005]. To deal with heterogeneity, it is often tacitly assumed that any problems introduced by spatial heterogeneity will be resolved or masked by inversion and model parameter calibration. Therefore, the effectiveness of hydrologic models is highly dependent on often scale-dependent parameters, which typically need calibration to offer an accurate enough characterization of the catchment area. These calibration activities typically result in significant parameter uncertainty and further lead to biased predictions. The above-mentioned approach is also known as the "top-down" approach. The top-down approach is defined as a hierarchical model refinement scheme that gradually tests and refines the model by adjusting it to data (e.g., calibration) [Hrachowitz and Clark, 2017]. Aiming to understand observed (macroscale) patterns by iteratively adapting the adjustable system properties that can reproduce these observed variables, this approach can be classified as a *deductive* scientific method [Popper, 2005]. Based on system-integrated observations (e.g., streamflow, tracer), the top-down modeling approach aims to depict the system straightforwardly at the same scale of the system, which is often at the catchment scale in the context of hydrology [Hrachowitz and Clark, 2017]. However, the top-down approach is criticized because it does not have a universally valid criterion for rejecting hypotheses, and for its reliance on right testing schemes that are typically not available in reality, because of the lack of adequate high-resolution observations [Savenije and Hrachowitz, 2017, Hrachowitz and Clark, 2017].

In many cases, heterogeneity needs to be characterized explicitly based on the state-of-art geologic characterization. When modeling transport processes in a subsurface porous medium, the dominant heterogeneity pattern such as connectivity metrics is very important to the simulation result. Different realizations of preferential flow channels can differ the simulation results over several orders of magnitude [Renard and Allard, 2013]. The heterogeneity does not only exist in permeability, but also porosity, dispersion coefficient, sorption parameters, among others. Because geological models are typically not conditioned for the data, a geostatistical (facies) model is often used to represent the heterogeneity [Linde et al., 2015, Zech et al., 2015, Danesh-Yazdi et al., 2018]. In the most commonly used geostatistical models, the basic idea is the selection of covariances or the multipoint pattern by the fitting to the images generated by the genetic model [de Marsily et al., 2005]. A current hot spot for the simulation of simple structures, such as to achieve a channel line or the topography of a deposition surface, is to deploy more advanced spatial statistics. Training-image based methods may be used in combination with physically-based techniques for training a Multiple Point Statistics (MPS) model to simulate preferential flow channels [Linde et al., 2015]. With images of real channels, MPS methods can be trained to simulate realistic channels in combination with an object-based simulation approach [Linde et al., 2015].

1.1.3 Integrated modeling of the surface–subsurface hydrological system

The transformation of surface water and groundwater is a critical process of water circulation. Almost all surface water bodies in nature have interactions with groundwater [Huntington and Niswonger, 2012, Barthel and Banzhaf, 2015]. However, due to the complexity of the water cycle itself and the differences in process representation and conceptualization, the process representations and simulation studies of surface water and groundwater have been developed in relatively independent fields for a long time [Jing et al., 2018]. The study of the surface water model also involves the groundwater part, but most of them use the "black-box" representations of groundwater flow and storage. Accordingly, the simulation of the groundwater flow process is rarely carried out substantially and explicitly. On the other hand, the groundwater models include some simple river processing functions and interfaces, but they usually cannot handle complex spatial information of rainfall and temporally dynamic surface runoff.

In the past few years, with the development and maturity of high technologies such as supercomputers, remote sensing techniques, and GIS, the lumped surface water models have been gradually developed into distributed hydrological models [Koirala et al., 2014, Samaniego et al., 2010]. This transformation has created conditions for the new coupled simulation of surface and groundwater based on the dynamics of the water cycle process. The most significant feature of the distributed hydrological model lies in the spatial distribution of the model structures and parameters, which can reflect the influence of the local changes of the underlying surface of the basin on the whole water cycle processes. It can also account for the spatial variation of land use, vegetation cover, soil type, topography, geometry, and other distributed features of watersheds [Beven, 1993].

The coupled model of surface water and groundwater is an emerging tendency for analyzing the interaction between surface water and groundwater [Markstrom et al., 2008, Refsgaard and Storm, 1995, Maxwell and Miller, 2005, Camporese et al., 2010, Bisht et al., 2017]. Integrated hydrological models can be used to analyze complex water-resources issues relevant to the threatens posed by climate change. The reason is that they can effectively compute the dynamic interplay between the surface and the subsurface compartments, and thus enable calculating its second-order impact on evapotranspiration, soil moisture, and runoff generation [Leung et al., 2011]. Most of the existing coupled models are based on some generalizations and conceptualizations of specific exchange fluxes between surface and subsurface domains. Some of them are built based on commercial or well-established surface water and groundwater models, such as the coupling of SWAT and MODFLOW [Kim et al., 2008]. However, because there are distinct features between the two types of models in key issues such as process representation, parameterization, parameter definitions, and division of computational units, the coupled models have been constantly subject to many challenges. The coupled surface-subsurface hydrological models, therefore, should be carefully evaluated to improve their reliability in practical applications.

1.1.4 Catchment-scale travel time distributions

The travel time distribution (TTD) of the catchment is a basic tool to describe the storage, the flow paths through a catchment, and the runoff generation process [McDonnell et al., 2010, Stewart et al., 2012]. This information is also fundamental for comprehending

the streamflow-storage relationship, for understanding the biogeochemical process in the riparian zone, and for revealing the fate of agricultural chemicals in the hydrologic cycle [Pinay et al., 2015, van Meter et al., 2017]. TTDs have distinct shapes and time scales in different components of the hydrological system, with the mean travel time varying from months in the soil profile to hundreds even thousands of years in deep groundwater aquifers [Heße et al., 2017]. The geometry, topography, boundary conditions, and physical properties of subsurface systems strongly affect the flow and transport processes. Therefore, the thorough understanding of the dependence of catchment TTD on geometry, topography, meteorological forcings, and geological structures is challenging for hydrologists. One major challenge lies in the strong topographic and hydrogeologic heterogeneity of catchment.

In the past decades, groundwater TTDs have been widely used worldwide as one state-of-the-art approach to identify sources and rates of groundwater recharge [McCallum et al., 2017]. Groundwater TTDs, which are typically inferred from tracer data, have proved useful to estimate the recharge rate. The groundwater age has the characteristics of increasing along the flow path lines. For this reason, the groundwater recharge rate can be estimated based on the groundwater TTD. For example, in a porous aquifer dominated by vertical recharge and vertical flow paths, the groundwater age increases with depth, and the magnitude of the increase depends on the aquifer structure, porosity, and recharge rate. According to the vertical variation of groundwater age on the transaction, the recharge rate of the aquifer can be broadly constrained [Hartmann et al., 2015, McCallum et al., 2017]. The mean travel time (MTT) of groundwater is a lumped index describing the time required for the groundwater to be fully renewed. This index can reflect the magnitude of the groundwater renewable capacity of the groundwater aquifer as a whole. However, due to many factors such as the complex structure and heterogeneous hydrogeological conditions, the time required for groundwater renewal at different locations is likely to be very different, even in the same groundwater system. Accordingly, the groundwater MTT can only provide a lumped description of groundwater renewable capability [Haitjema, 1995, Engdahl and Maxwell, 2015].

Under the influence of human activities, the actual renewal capacity of groundwater has significantly deviated from that under natural conditions [Treidel et al., 2012]. If the groundwater age becomes larger and larger as the pumping time increases, it means that the groundwater is potentially depleted. Groundwater is increasingly pumped from

relatively old storages, indicating that the groundwater system is less able to receive recharge and that the groundwater system may be in danger [Engdahl and Maxwell, 2015, Kløve et al., 2014]. Conversely, the trend of decreasing MTT means that the extracted water is increasingly pumped from active modern atmospheric precipitation and other recharges. This indicates that the groundwater system is more active in the global water cycle and has a stronger renewable capacity. It also indicates that the current pumping activity is reasonable for the groundwater resources [Engdahl and Maxwell, 2015, Kløve et al., 2014].

Groundwater TTD has great implications for groundwater pollution assessment. If the travel time is very small, the discharged groundwater is expected to be replenished by modern atmospheric precipitation or surface water. This water usually does not undergo sufficient natural cleaning and pollutant decomposition processes. Therefore, the water quality is likely to be poor [Tóth, 1999, Weissmann et al., 2002]. Groundwater TTD can also provide an index for estimating the time water parcels spend to travel through the entire aquifer recharge, runoff, and discharge zones through different runoff paths [Danesh-Yazdi et al., 2018]. This is useful for understanding the migration process of pollutants in groundwater systems.

The main challenge in deriving groundwater TTD is the accuracy of the mathematical model used for either interpreting the tracer data or directly simulating the travel times of water parcels [Stewart et al., 2012, Kirchner, 2016]. These mathematical models can be divided into three categories: the lumped parameter model, the flux tracking model, and the Lagrangian particle tracking model [Sprenger et al., 2019]. The lumped parameter model and flux tracking model are top-down models because they typically characterize heterogeneity and scaling by parameterizing the effects of subgrid heterogeneities on the travel time [Clark et al., 2015].

The historical time series of discharge have been well reproduced by many top-down models [Jencso et al., 2009, Samaniego et al., 2010, Kumar et al., 2013a], but the mechanism of the runoff generation process is still poorly understood in most real-world catchments [McDonnell et al., 2010, Stewart et al., 2012, Hrachowitz et al., 2013, Savenije and Hrachowitz, 2017]. The widely used linear reservoir assumption (equivalent to complete mixing assumption) has been found inadequate to describe real process dynamics in some catchments [Botter et al., 2011, Rinaldo et al., 2011, Hrachowitz et al., 2013]. The

assumption of mixing of different water storages, as well as the conceptualization of evapotranspiration, have a strong impact on the catchment travel time distributions [Hrachowitz et al., 2013, van der Velde et al., 2015]. Typical top-down hydrological models are commonly calibrated using a single target such as runoff [Clark et al., 2008], rather than integrated targets (e.g., tracer data), which hampers the comprehensive understanding of runoff generation process. Moreover, much of these typical hydrological models succeed in linking the dynamics of shallow water storages in thin uppermost soil layer to the streamflow responses, but oversimplify the deep storages below the soil profile and fall short in predicting low flows [Haria and Shand, 2004, Kim et al., 2017]. These inadequacies are particularly problematic in catchment TTD simulations since typical catchment TTDs have long tails, which can hardly be represented by these top-down models [McDonnell et al., 2010].

The explicit representations of flow paths and flow physics are always missing in lumped parameter models. To interpret tracer data, a functional form of TTD has to be predefined based on some assumption of essentially unknown mixing mechanisms. The assumption of the mixing of different water storages, as well as the conceptualization of evapotranspiration, have a strong impact on the catchment TTD [Hrachowitz et al., 2013, van der Velde et al., 2015]. Analytical models aggregate the heterogeneity of stratified groundwater aquifers and cannot accurately characterize low flows [Ameli et al., 2016, Hale and McDonnell, 2016]. This is problematic in catchment TTD simulations since real-world catchment TTDs may have an irregular shape, which can hardly be replicated by the limited number of representative parameters of the analytical model [McDonnell et al., 2010].

Conversely, the Lagrangian particle tracking model is often combined with physically-based hydrological models. The physically-based hydrological model is categorized as a "bottom-up" approach because it explicitly represents the flow and transport processes and satisfies the mass and energy conservation [Clark et al., 2015]. The Lagrangian particle tracking is used in this study to characterize catchment-scale groundwater TTDs.

1.1.5 Error and uncertainty in model inputs and parameters

According to the attributions of uncertainties in the evaluation of groundwater resources, uncertainty sources can be divided into two categories: objective factors and subjective

factors [Wagner and Gorelick, 1987]. The objective factor is caused by the inherent random nature of the groundwater resource system and is mainly related to the temporal and spatial changes of hydrological and hydrogeological variables (such as precipitation, discharge, water quality, groundwater level, and water quality). Subjective uncertainty is caused by the incompleteness of the researchers' understanding of the system, mainly related to the establishment and solution of mathematical models and the uncertainty of parameters in the model [Anderson et al., 2015].

Parameter and predictive uncertainty introduced by constraints on parameter values to reproduce the historical behavior through historical-matching can be effectively described by Bayes equation [Ajami et al., 2007, Xu and Valocchi, 2015]. In practical modeling efforts, the direct use of the Bayes equation is not easy. This stems from the numerical difficulties involved in computing probability distributions, especially where they do not have analytical formulations [Doherty et al., 1994]. Unfortunately, even if the prior probability distribution can be described with an analytical formulation, the nonlinear feature of most models will result in that the posterior parameter probability distribution does not have an analytical formulation [Moore and Doherty, 2006, Doherty and Hunt, 2010].

Another problem that is relevant to hydrological modeling is that models are imperfect simulators of hydrological system behavior. An example of this phenomenon is that a model's calculation of the likelihood function is expected to be biased [Zinn and Harvey, 2003, McInerney et al., 2017]. This is inevitable in most calibration efforts, which means that most model-to-measurement residuals stem from imperfect model structures for most cases [Doherty and Hunt, 2010, Doherty, 2015]. To a degree, the misfit introduced by imperfect model structures can be evaluated utilizing history matching and integrated into the Bayesian representation of posterior parameter pdfs. Unfortunately, this aspect of error in the model's structure, therefore, affects predictive uncertainty [Xu and Valocchi, 2015, Ajami et al., 2007]. The model structural uncertainty leads to an essentially unknown term that exists in any model prediction. Therefore, the posterior probability distribution of that prediction, as indicated by the Bayesian framework, has been essentially changed without being noticed [Doherty and Hunt, 2010, Doherty, 2015].

The potential for error in a prediction of a hydrological model is always larger than the inherent uncertainty [Doherty and Hunt, 2010]. In principle, the latter can be calculated

through the implementation of Bayesian analysis together with a perfect model. However because real-world models are not perfect, their predictions have a higher possibility for error, i.e., a broader posterior probability distribution. This results from the need to make predictions and to analyze their impossibility potential with an imperfect model [Moore and Doherty, 2006, Doherty and Hunt, 2010].

Bayes equation shows that the model's parameters remain uncertain even after they have been restrained through the history-matching process. That is, the model's parameters are still free to adjust, even though a model has been calibrated [Tonkin and Doherty, 2009]. Nevertheless, the post-calibration uncertainty is constrained to some extent. The underlying reasons are: (1) First, one of the conditions under which the uncertainty can be constrained is that the parameters remain realistic and meaningful, which means the physical reality must be respected. This constraint exists in the prior probability distribution of parameters as an inherent component of Bayes theorem [Moore and Doherty, 2006, Doherty and Hunt, 2010]. (2) A second constraint is exerted through the history-matching process. This constraint further restricts the adjustable range of the parameter. It is claimed that the model parameters must be constrained so that the deviation between model and measurement does not increase too much [Moore and Doherty, 2006, Doherty and Hunt, 2010, Doherty, 2015].

The applicability of the Bayesian framework is limited due to the scarcity of data for prior distribution and the expensive computational burden [Anderson et al., 2015]. Alternatively, the software package PEST [Doherty and Hunt, 2010, Doherty, 2015] provides a versatile and efficient platform for parameter estimation and uncertainty evaluation of multiscale hydrological and environmental models. It is a state-of-the-art software in combination with many utility programs that support its use in conjunction with many popular groundwater and surface hydrological models. It is also capable of linear and nonlinear parameter and predictive error and uncertainty analysis [Doherty, 2015]. Specifically, the non-linear uncertainty evaluation is performed using the null-space Monte Carlo (NSMC) method. In this dissertation, most of the inversions and uncertainty analyses in Chapter 2 and Chapter 3 are conducted using PEST.

1.1.6 Climate change and groundwater

Climate change, in which global warming plays a vital part, has become one of the most critical environmental issues in today's world. The research on the impact of climate change on the hydrological cycle and water resources has been attracting more and more attention from researchers worldwide. The key research areas of climate change impacts on hydrology and water resources are: (1) detection and attribution analysis of changes in water cycle elements, (2) reliable estimations of the influences of global warming and human activities on water cycle and water resources, and (3) projection of hydrological fluxes and variables in future climate change scenarios. Other important topics include the estimation of the future trend of water resources, the assessment of influences of changing the climate on extreme hydrological events, and adaptive management strategies for climate impact on water resources [Goderniaux et al., 2009, Wechsung et al., 2008].

With the rapid development of industrialization and economy, the concentration of greenhouse gases (such as carbon dioxide) in the atmosphere has been increasing, and the global temperature has been rising in the past one hundred years [Pachauri et al., 2015]. The fourth assessment report of IPCC indicates that the increasing tendency of global surface temperature from 1906 to 2005 is 0.74 degrees per year [Pachauri et al., 2015]. It is estimated that by 2100, the global average temperature is expected to increase by 1.1–6.4 degrees. Climate change dominated by the increasing temperature has become one of the most urgent challenges for the future of human beings and the global ecosystem.

Water is the main component in atmospheric circulation and one of the most direct and critical factors affected by climate change. Global warming will inevitably lead to changes in the global hydrological cycle, and further significantly influence precipitation, snow melting, overland flow, and soil moisture, among others. It will cause a redistribution of water resources in time and space as well as changes in total water resources, floods, and droughts, among others. The frequency and intensity of extreme disasters seriously affect the development, arrangement, planning, and management of human society, and therefore affect the global ecological conditions and social economy [Samaniego et al., 2018, Thober et al., 2018]. Therefore, studying the mechanism of climate change impact on the water cycle, assessing the impact of water resources security, and proposing an adaptive management strategy for climate change are of great practical significance for

the rational use of water resources and planning management [Taylor et al., 2012, Wada et al., 2010].

The projection of the trends of water resource evolution in future climate change scenarios is one of the most vital topics. This is also highly related to the reliability of projections in climate change impacts on the hydrological cycle and water resources. Many studies have been carried out in this area focusing on the projection of water resources under future climate scenarios [Engdahl and Maxwell, 2015, Goderniaux et al., 2009, Marx et al., 2018, Thober et al., 2018, Samaniego et al., 2018]. Studies on the water-resources response in the context of future climate change often follow the chain of "future climate scenario setting—hydrological simulation—impact evaluation" models [Taylor et al., 2012]. Among them, the choice of climate change scenarios, the construction of hydrological models, and the coupling of climate-hydrological models are of crucial importance.

Groundwater is a critical part of the water cycle and the main source of freshwater. Currently, many pieces of research have been carried out to investigate the effect of climate change on groundwater resources. Meanwhile, some important achievements have been made [Engdahl and Maxwell, 2015, Goderniaux et al., 2009, Tillman et al., 2016, Crosbie et al., 2013]. However, the relationship between groundwater and groundwater recharge pattern introduces a high uncertainty in estimating groundwater responses. As the deepest component of the terrestrial water cycle, groundwater suffers from uncertainties not only in its structure and parameterization but also in inputs introduced from projected precipitations and land surface fluxes. Together with the increasingly prominent crisis in groundwater depletion, these challenges need to be tackled to better assess the influence of climate change on groundwater resources. It is also highly suggested to combine the groundwater research with the results of surface water research to better describe the changing trend of the water cycle and the evolution of water resources [Wada et al., 2010].

1.2 Theoretical background

This section displays equations and basic assumptions for surface and subsurface flows. These equations and assumptions provide the theoretical background for the numerical simulations. Additionally, a benchmark problem is also presented to test the robustness of the RWPT algorithm in OGS source codes.

1.2.1 Surface and groundwater flow

Surface flow (i.e. overland flow) is a thin sheet of water flow that takes place when excess water from rainfall, snowmelt, or other sources flows over the land. In general, surface flow causes a gathering of the runoff into the discrete stream channels. It includes infiltration-excess flow, saturation-excess flow, and subsurface return flow according to the different generation mechanisms.

In two-dimensional problems, the diffusive wave equation (an approximation of the Saint-Venant equations) is given by:

$$\phi_a \frac{\partial H_a}{\partial t} + \nabla \cdot (H\mathbf{q}) = q_s \tag{1.1}$$

where $0 \leq \phi_a \leq 1$ is the surface porosity that is unity for flow over an even flat and variable for flow over an uneven surface [-], H_a is the surface ponding depth [L], H is the mobile water depth [L], and q_s is the source(sink) term [L T^{-1}].

Most large-scale surface hydrologic models do not solve Eq. 1.1 explicitly because of the lack of data and numerical instability. Rather, Muskingum-Cunge routing is widely used by many hydrologic models to represent the river flow [Cunge, 1969, Samaniego et al., 2010, Camporese et al., 2010, Markstrom et al., 2008]. The Muskingum-Cunge method transferred the kinetic wave equation (Eq. 1.1) into a diffusion form by introducing two weighing coefficients [Cunge, 1969, Garbrecht and Brunner, 1991]. This routing algorithm is computationally efficient and numerically robust, while proves reliable in reproducing runoff products.

For physically-based models, the well-known Richards equation is used to describe water flow in unsaturated zone [Maxwell and Miller, 2005]. The van Genuchten model is often used to describe the relationship between the relative saturation and the permeability [van Genuchten, 1981]. In this dissertation, only the saturated form is used to describe the groundwater flow. In saturated groundwater storage, the Richards equation can be simplified to Darcy's law. Darcy's law is a linear equation describing fluid flow in a porous medium. It is a fundamental equation in hydrogeology and geosciences. The description of Darcy's law can be found in Eq. 2.9.

Another important assumption in hydrogeology is the Dupuit–Forchheimer assumption [Dupuit, 1863, Forchheimer, 1986]. This assumption holds that flow path lines are horizontal in unconfined aquifers and that the groundwater drainage rate is proportional to the thickness of the groundwater table. This assumption is a necessary condition for deriving the exponential form of groundwater TTDs [Haitjema, 1995].

1.2.2 Random walk particle tracking

Characterizing the flow paths and travel times in the catchment is significant for understanding the solute and also contaminant transport. The Lagrangian particle tracking algorithm has been widely used to simulate the solute reactive transport process [Eberts et al., 2012, de Rooij et al., 2013a, Benson et al., 2017, Yang et al., 2018]. It also provides the possibility to gain information on flow paths and travel times at the catchment scale. The Lagrangian approach can be considered as the discretization of the mass, and the Eulerian method can be considered as the discretization of space. One of the most-widely used Lagrangian particle tracking method is the random walk particle tracking (RWPT) method. The RWPT assumes that the advection process is deterministic and that the diffusion/dispersion process is probabilistic [Park et al., 2008a, Kolditz et al., 2016]. RWPT methods have been widely used in applications in the context of catchment travel times [Engdahl and Maxwell, 2015, Kollet and Maxwell, 2008, Tompson et al., 1999].

RWPT method has been extensively applied for geochemical simulations and groundwater age dating [Park et al., 2008a, Kolditz et al., 2012, Jing et al., 2019a]. The PDEs and a benchmark example for the RWPT method can be found in Appendix A.

1.2.3 RWPT in porous medium: 2-D benchmark example

To test the functionality of the RWPT algorithm in simulating the groundwater transport process, a solute transport problem in 2-D homogeneous porous media is used as the benchmark example. Note that the term OGS stands for OGS5 because OGS5 is used exclusively in this dissertation. In this benchmark example, a steady-state uniform flow field is assumed, in which a point-source contaminant is injected into the system at time $t = 0$. The numerical model is used to replicate the temporal and spatial patterns of concentration distribution. The modeling domain is a horizontal rectangle with a length

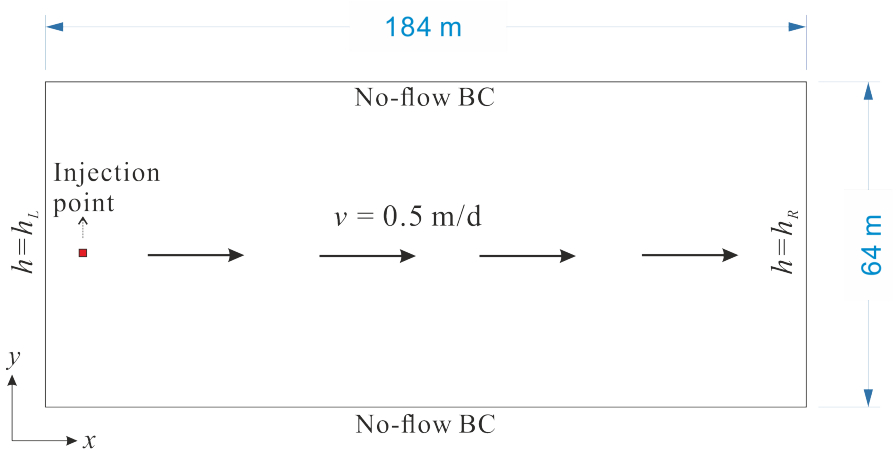

FIGURE 1.1: Schematic of the 2-D homogeneous aquifer benchmark example.

of 184 m and a width of 64 m. A uniform flow field is established with fixed-pressure boundary conditions being assigned at the left and right boundaries (Figure 1.1).

For the 2-D transport problem with a uniform velocity field in homogeneous porous media, a simple analytical solution is provided by Otaga et al. [Ogata, 1961]. Assuming that a point-source contaminant with a concentration of C_0 is injected into the domain at the location (x_0, y_0) and the contaminant is subjected to dispersion and advection, then the concentration of a contaminant at location(x, y) at time t can be described as [Ogata, 1961]:

$$C(x,y,t) = \frac{C_0 A}{4\pi t\sqrt{D_{xx}+Dyy}}\exp\Big[-\frac{(x-x_0)^2}{4D_{xx}t} - \frac{(y-y_0)^2}{4D_{yy}t}\Big] \tag{1.2}$$

where C_0 is the initial concentration of the contaminant at location (x_0, y_0).

In OGS model, the 2-D rectangular domain is discretized into a structure mesh with 0.5 m $\times$ 0.5 m quadrilateral elements. The identical grid density has also been applied to transfer the spatial pattern of particles to concentrations. This grid density is also used to transfer the particle density to element concentrations. Boundary conditions of isolation in flow are assigned at the upper and lower boundaries. Fixed-pressure boundary conditions are exerted at the left and right boundaries to achieve the uniform flow field. The flow velocity is 0.5 m $\cdot$ d^{-1} uniformly.

The point-source contaminant is injected into the system with a concentration of 1 kg $\cdot$ m^{-3}. For doing so, 1000 particles are released in a square area (0.1m $\times$ 0.1m) near the left side of the domain. The parameters used in the flow and transport modeling are

TABLE 1.1: Parameters used in the 2-D homogeneous porous medium benchmark problem.

Symbol	Parameter	Value	Unit
k	Permeability	1.114×10^{-11}	m^2
A	Weighting factor	0.9	–
α_L	Longitudinal dispersivity	0.1	m
α_T	Transverse dispersivity	0.1	m

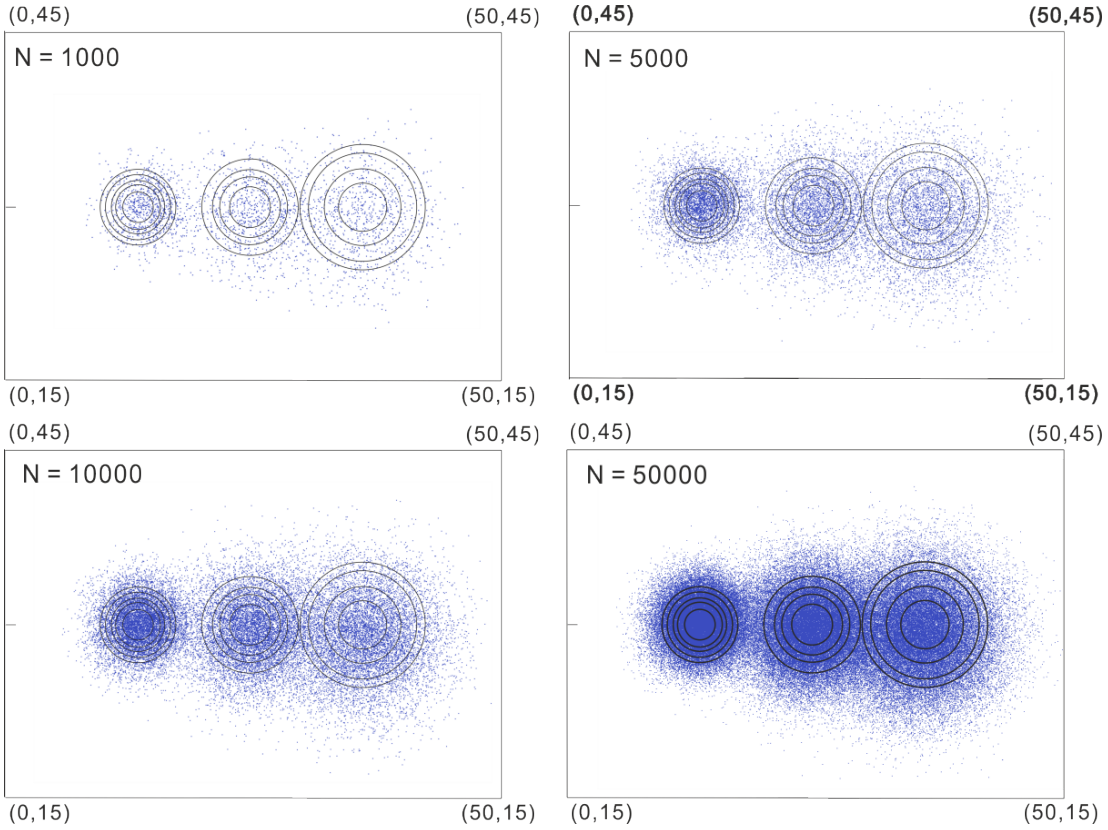

FIGURE 1.2: Simulations (dots) and analytical solutions (circles) of the 2-D benchmark example using 1000, 5000, 10000, and 50000 particles, respectively. The analytical solutions show the concentration contours for $C = 2.6 \times 10^{-4}, 1.6 \times 10^{-4}, 1.0 \times 10^{-4}$, and 4×10^{-5}, respectively.

shown in Table 1.1. Specifically, the molecular diffusion coefficients D_{xx} and D_{yy} can be calculated using Equation A.3:

$$D_{xx} = \alpha_T \cdot v \tag{1.3}$$

$$D_{yy} = \alpha_T \cdot v \tag{1.4}$$

The simulation results of the spatial distribution of released particles at 20, 40, and

60 days using 1000, 5000, 10000, and 50000 particles are shown in Figure 1.2. The analytical solutions using Equation 1.2 are also shown in Figure 1.2. In general, the simulation results have a good agreement with the analytical solutions. Although not shown in this figure, the converted concentrations from the particle density also show good correspondence with the analytical solutions [Park et al., 2008a]. Following the increase of released particle numbers, the stability of simulation results increases as well. Many past studies suggest that at least 50000 particles should be used to reach the convergence state [Park et al., 2008a, Danesh-Yazdi et al., 2018]. This test case demonstrates the predictive capability of the RWPT method of OGS.

1.3 Research questions and thesis structure

To deal with challenges in computational hydrogeology, it is urgently needed to combine the surface hydrological model and groundwater model for a better characterization of highly-correlated components in the terrestrial water cycle. Applicability and accuracy of such coupled systems must be carefully tested through a case study in real-world catchments. Besides, a warming world also poses challenges for hydrologists concerning properly project future changes in groundwater resources. In this regard, some research questions are raised and itemized below.

1. Is it able to couple a bucket-type hydrological model with a physically-based hydrogeological model? If yes, how is the capability of the coupled model in predicting discharge and groundwater heads?

   One of the main challenges for answering this question is the bucket-type hydrological model has its representation of groundwater storage. It is a big challenge to replace the original highly-conceptualized groundwater storage with physically-based groundwater storage and keep the water budget closed at the same time.

2. Is the coupled model capable to investigate regional groundwater TTDs, meanwhile explicitly accounting for subsurface heterogeneity?

3. Is the coupled model capable to explore the climate impact on regional groundwater resources concerning different potential warming levels?

4. How is the contribution of input and parameter uncertainties to the final TTD predictions?

5. How do the uncertainties of climate and groundwater model contribute to the projection in groundwater resources under different warming levels?

This cumulative dissertation is designed to answer these major research questions. The following chapters are logically structured to ensure the ideas are accurately delivered.

Chapter 2 describes the development of the coupled model (mHM-OGS v1.0), including the description of two models, the coupling mechanism, and an example application in a mesoscale catchment. Some highly-relevant topics such as the sensitivity of groundwater head dynamics to the spatial distribution of groundwater recharge and the head difference between historically dry and wet years in the studied region are also comprehensively discussed.

Chapter 3 describes the application of mHM-OGS in quantifying the TTDs for a real-world catchment. It also incorporates a comprehensive uncertainty study of model inputs and parameters. Some related topics including the sensitivity of discharging young or old water to the spatial pattern of recharge and its implications for applied hydrological modeling are also discussed.

Chapter 4 describes another application of the coupled model – quantification of climate impact on regional groundwater flow and transport processes. The uncertainty propagation from different sources to the simulation results is also systematically evaluated.

In Chapter 5, the main findings and limitations of this dissertation are discussed in detail. A comparison of this study to the past studies as well as the advantages and disadvantages of the current approach have been included in this chapter.

Finally, in Chapter 6, conclusions are drawn based on the analyses in the above chapters. Summary and outlook are also presented in this chapter.

Three chapters in this dissertation has been published or submitted to international peer-reviewed journals. Chapter 2 was published in *Geoscientific Model Development* [Jing et al., 2018]. Chapter 3 was published in *Hydrology and Earth System Sciences* [Jing et al., 2019a]. Chapter 4 was submitted to *Hydrology and Earth System Sciences* and published online as a discussion paper [Jing et al., 2019b].

(Author's note: The formats of figures, tables, and literature have been slightly changed for the consistency of this dissertation. Chapter 4 is slightly different from the original submitted version as it incorporates some revisions based on the review comments. Materials in Chapter 2, Chapter 3, and Chapter 4 are available via license: CC BY 4.0. Please check the original journal version.)

Chapter 2

Improved regional-scale groundwater representation by the coupling of the mesoscale Hydrologic Model (mHM v5.7) to the groundwater model OpenGeoSys (OGS)

Acknowledgements

This research received funding from the Deutsche Forschungsgemeinschaft via Sonderforschungsbereich CRC 1076 AquaDiva. We kindly thank Sabine Sattler from Thuringian State office for the Environment and Geology (TLUG) for providing the geological data. We kindly thank our data providers: the German Weather Service (DWD), the Joint Research Center of the European Commission, the Federal Institute for Geosciences and Natural Resources (BGR), the European Environmental Agency (EEA), the European Water Archive (EWA), and the Global Runoff Data Centre (GRDC). We thank the two reviewers Prof. Olaf Cirpka and Dr. Edwin Sutanudjaja very much for their comprehensive reviews.

published as:

Jing, M., Heße, F., Kumar, R., Wang, W., Fischer, T., Walther, M., Zink, M., Zech, A., Samaniego, L., Kolditz, O., and Attinger, S.: Improved regional-scale groundwater representation by the coupling of the mesoscale Hydrologic Model (mHM v5.7) to the groundwater model OpenGeoSys (OGS), Geosci. Model Dev., 11, 1989-2007, https://doi.org/10.5194/gmd-11-1989-2018, 2018.

2.1 Abstract

Most large-scale hydrologic models fall short in reproducing groundwater head dynamics and simulating transport process due to their oversimplified representation of groundwater flow. In this study, we aim to extend the applicability of the mesoscale Hydrologic Model (mHM v5.7) to subsurface hydrology by coupling it with the porous media simulator OpenGeoSys (OGS). The two models are one-way coupled through model interfaces GIS2FEM and RIV2FEM, by which the grid-based fluxes of groundwater recharge and the river-groundwater exchange generated by mHM, are converted to fixed-flux boundary conditions of the groundwater model OGS. Specifically, the grid-based vertical reservoirs in mHM are completely preserved for the estimation of land-surface fluxes, while OGS acts as a plug-in to the original mHM modeling framework for groundwater flow and transport modeling. The applicability of the coupled model (mHM-OGS v1.0) is evaluated by a case study in the central European mesoscale river basin - Nägelstedt. Different time steps, i.e. daily in mHM and monthly in OGS, are used to account for fast surface flow and slow groundwater flow. Model calibration is conducted following a two-step procedure using discharge for mHM and long-term mean of groundwater head measurements for OGS. Based on the model summary statistics, namely the Nash–Sutcliffe model efficiency (NSE), the mean absolute error (MAE), and the interquartile range error (QRE), the coupled model is able to satisfactorily represent the dynamics of discharge and groundwater heads at several locations across the study basin. Our exemplary calculations show that the one-way coupled model can take advantage of the spatially explicit modeling capabilities of surface and groundwater hydrologic models and provide an adequate representation of the spatiotemporal behaviors of groundwater storage and heads, thus making it a valuable tool for addressing water resources and management problems.

2.2 Introduction

Large-scale hydrologic models had been primarily developed to predict river discharge. To that end, these models typically use simplified representation of underlying hydrological processes, usually bucket-type expressions to describe water storage and flow inside the catchment [Refsgaard and Storm, 1995, Wood et al., 1997, Koren et al., 2004, Samaniego et al., 2010, Niu et al., 2011]. Water is transmitted among different vertical and horizontal

buckets by means of an infiltration-runoff partitioning algorithm, which can be normally expressed as a function of the water storage [Hrachowitz and Clark, 2017]. Model parameters in these types of models are usually obtained via calibration to match the observed dynamics of streamflow time series. As a result, these types of conceptual models are generally good at predicting streamflow dynamics. However, all (bucket-type) hydrologic models simplify water flow processes by ignoring lateral flow, especially at a large scale. Thus, such models inevitably fall short of characterizing subsurface groundwater dynamics, where such lateral flows are dominant. In addition, estimates of groundwater storage and heads are particularly error prone due to the low sensitivity of groundwater (storage) to river flows.

The groundwater representation in these conceptual (bucket-type) hydrologic models is consequently not adequate in several aspects. First,these models aggregate the heterogeneity of typically stratified groundwater aquifers, and fall short in adequately representing groundwater heads and low-flow conditions [Ameli et al., 2016, Hale and McDonnell, 2016]. Second, these models often do not properly capture the dynamics of solute transport and retention at the catchment scale. For example, Van Meter (2017) [van Meter et al., 2017] found that current nitrogen fluxes in rivers can be dominated by groundwater legacies. An oversimplified groundwater representation is inadequate for understanding travel time distributions (TTDs) at a catchment scale and is therefore not capable of describing such legacy behavior [Botter et al., 2010, Benettin et al., 2015, 2017]. Finally, a more accurate groundwater representation including lateral subsurface flow is needed to predict the response of groundwater to climate change [Scibek and Allen, 2006, Green et al., 2011, Ferguson et al., 2016].

Parallel to such conceptual surface hydrologic models, three-dimensional (partial differential equation, PDE) subsurface models, which allow for both steady-state and transient groundwater flow, have been developed, accounting for the representation of subsurface heterogeneity and a varying degree of sources and sinks. Such models are good at tackling the aforementioned problems encountered in application of conceptual models. PDE-based models usually contain a complete representation of subsurface physics, but fall short in contain good representation of surface and shallow soil processes. For example, models for evaluating the effects of pumping and surface-water interactions on ground-water flow typically take recharge using long-term mean of precipitation and evaporation, without considering flow through the soil and unsaturated zones [Danskin, 1999, Selle et al., 2013].

The groundwater numerical models may contain some packages or interfaces to simulate surface water or unsaturated zone processes [Harbaugh et al., 2000, Kalbacher et al., 2012, Delfs et al., 2012]. Those packages always need extra data and right characterization of many topographical and geological properties. Parameterization of topographical and geological parameters is a big challenge due to the strong spatial and temporal heterogeneity and lack of data [Moore and Doherty, 2006, Arnold et al., 2009]. At this end, a variety of numerical codes/models are available such as InHM [VanderKwaak and Loague, 2001, Smerdon et al., 2007], ParFlow [Maxwell and Miller, 2005, Maxwell et al., 2015], OpenGeoSys [Delfs et al., 2012, Kolditz et al., 2012], tRIBS [Ivano et al., 2004], CATHY [Camporese et al., 2010], HydroGeoSphere [Therrien et al., 2010, Hwang et al., 2014], MODHMS [Panday and Huyakorn, 2004, Phi et al., 2013], GEOtop [Rigon et al., 2006], IRENE [Spanoudaki et al., 2009], CAST3M [Weill et al., 2009], PIHM [Kumar et al., 2009, Qu and Duffy, 2007], and PAWS [Shen and Phanikumar, 2010]. PDE-based hydrologic models usually represent subsurface flow by accounting for both saturated and unsaturated groundwater flows. The flow fields can be directly computed on the basis of spatial gradients of the modeled primary variable, e.g., the hydraulic head. The PDE-based models are flexible in coping with subsurface heterogeneity by means of proper characterization of the aquifer system (e.g. stratification or geostatistical approach), and thus are able to reduce aggregation errors caused by geological heterogeneity [de Marsily et al., 2005, Cirpka and Attinger, 2003, Zech et al., 2015]. Furthermore, these models can explicitly compute flow path lines and provide direct estimates of travel times of water and solute particles. These properties of PDE-based models provide a significant advantage over (bucket-type) conceptual models especially in complex real-world applications [Park et al., 2008a, Engdahl and Maxwell, 2015, Danesh-Yazdi et al., 2018].

However, despite these advantages in modeling the deeper subsurface flows, PDE-based models are not without problems, in particular in capturing the near-surface flow dynamics i.e., in shallow portions of the subsurface. For example, the PDE-based models often encounter problems in the unsaturated zone for simulating the quick flow components, which are mainly dependent on subgrid heterogeneities of topographic variation as well as soil and land-cover characteristics [Paniconi and Putti, 2015]. Using a complex PDE-based surface hydrologic model to simulate near-surface processes is possible in general, but it does require a model implementation at a fine spatial resolution to resolve the sub-grid features (e.g., root-water uptake) and include a tremendous number of uncertain model

parameters. Furthermore these models have dramatically increased numerical complexity and computation time, and thus calibrating these models is a cumbersome task, and doing this in a stochastic framework is computationally not feasible.

To summarize these points, bucket-type hydrologic models, such as mHM [Samaniego et al., 2010, Kumar et al., 2013b], VIC [Liang et al., 1994], and HBV [Lindström et al., 1997], are good at predicting water fluxes, such as discharge, but are highly conceptual and their model results are difficult to interpret with respect to certain processes (e.g., groundwater flows). The outputs of PDE-based hydrologic models, such as ParFlow, CATHY, and HydroGeoSphere, are highly interpretable but show consistently worse performance than bucket-type models when predicting discharge dynamics [Gulden et al., 2007, Paniconi and Putti, 2015]. The differing capabilities of bucket-type and PDE-based models are the result of the different challenges that are posed by the various compartments of the terrestrial water cycle. One of the main challenges in modeling surface and near-surface storage is process uncertainty. The process uncertainty is caused by the strong non-liearities of hydrological processes and the fine-scale variability in land-surface features. Thus it can be hardly solved by PDE-based models, but can be well handled by bucket-type models through the parameterization process.

In the deeper subsurface storage, the temporal and spatial scale of groundwater process is significantly larger than the shallow storage, and the flow is governed by linear PDE (Darcy's law), thus makes the PDE-based model standard at a large scale [Dagan, 2012]. Meanwhile, the data uncertainty becomes more significant in the deep subsurface storage in comparison to shallow storage due to the spatially sparse hydrogeological data. Moreover, a recent study reveals the strong spatial and temporal heterogeneity of processes and properties at the surface/groundwater (SW/GW) interface, and underlines the importance of quantifying variability across several scales at the SW/GW interface and its significance to water resources management [McLachlan et al., 2017]. It therefore stands to reason, that the use of a hybrid of both these model frameworks is a good choice for a joint representation of surface and subsurface water storages and fluxes. Several well-tested coupled models have been developed in recent years, including ParFlow-CLM [Maxwell and Miller, 2005, Maxwell et al., 2015, Kurtz et al., 2016], GSFLOW [Markstrom et al., 2008, Hunt et al., 2013], PCR-GLOBWB-MOD [Sutanudjaja et al., 2011, 2014], and CP(v1.0) [Bisht et al., 2017].

In this study, we present a coupling between the conceptual mesoscale Hydrologic Model (mHM v5.7) and the PDE-based model OpenGeoSys (OGS) is presented [Kolditz et al., 2012, 2016]. The overall aim is to provide a proper representation of groundwater flows and storages and enabling the coupled model to provide reliable estimates of groundwater heads. mHM has demonstrated its preeminence in coping with near-surface process uncertainty while providing reliable representation of observed discharge behavior across a range of scales and locations [Samaniego et al., 2010, Kumar et al., 2013b, Huang et al., 2017]. Conversely, OGS has demonstrated its capability of dealing with data uncertainty in aquifers [Sun et al., 2011, Walther et al., 2012, Selle et al., 2013]. The general idea behind the coupling is to use the hydrological simulation of with mHM, including the simplified linear groundwater storage, extract fluxes into and out of groundwater from mHM, and use this as the Neumann boundary condition for the PDE-based groundwater model OGS. By doing so, the predictive power of mHM is augmented to also predict hydraulic heads in groundwater. The one-way coupling approach considered here has a number of advantages. First, the one-way coupling can be regarded as a conservative approach, such that the parametrization process, which is one of the most significant features of mHM, remains fully intact. In particular, this means that the whole body of confidence in the predictive power of mHM, which has been build up over the years, can be fully relied on. Second, using such a one-way coupling will allow users of mHM to simply extend currently established catchment models and enhance their abilities in the aforementioned way. Using a more sophisticated two-way coupling, would entail users having to rebuild their models almost entirely. Third, a one-way coupling allows for ready future expansion of the functionality of the coupled model, e.g., legacy of solutes in groundwater, should the need arise. Finally, one-way coupling takes less computational effort and achieves better numerical stability than two-way coupling.

By coupling two well-tested model codes, we want to answer the following scientific questions: (1) can spatially distributed groundwater heads and their dynamics be reasonably captured by expanding the capabilities of a surface hydrologic model, such as mHM at the regional scale, while conserving its excellence in predicting discharge? (2) Can spatially resolved groundwater recharge estimates, provided by mHM, improve the prediction of head measurements of groundwater models such as OGS? To answer these questions, we applied the coupled model mHM-OGS v1.0 in a central German meso-scale catchment (850 km^2), and evaluated the model skills using measurements of streamflow

and groundwater heads from several wells located in the study area. The coupled (surface) hydrologic and groundwater model (mHM-OGS v1.0) presented in this paper is our first attempt toward the development of a large-scale coupled modeling system with the aim to analyze the spatiotemporal variability in groundwater flow dynamics at a regional scale.

To answer these questions, the paper is structured as follows. In the next section, we describe the model concept, model structure, and the coupling scheme. In Sect. 2.4.1, the study area and model setup used for illustration in this study are comprehensively described. In Sect. 2.5, we present the simulation results of mHM-OGS v1.0 in a catchment in the application. In the Sect. 2.6, we discuss the model results as well as advantages and limitations of current modeling approach.

2.3 Model description

2.3.1 Mesoscale Hydrologic Model (mHM)

The mesoscale Hydrologic Model (mHM, www.ufz.de/mhm) is a spatially explicit distributed hydrologic model that uses grid cells as a primary modeling unit, and accounts for the following processes: canopy interception, snow accumulation and melting, soil moisture dynamics, infiltration and surface runoff, evapotranspiration, subsurface storage and discharge generation, deep percolation, baseflow, discharge attenuation, and flood routing (Figure 2.1). The runoff generation applies a robust scheme, which routes runoff in upstream cells along river networks using the Muskingum-Cunge algorithm. The model is driven by daily meteorological forcings (e.g., precipitation, temperature), and utilizes observable physical properties or signals of the basin (e.g., soil textural, vegetation, and geological properties) to infer the spatial variability in the required parameters. mHM is an open-source project written in Fortran 2008. Parallel versions of mHM using OpenMP concepts are available.

A unique feature of mHM is the application of multiscale parameter regionalization (MPR). The MPR method accounts for subgrid variability in physical characteristics of the catchment such as topography, soil and vegetation. The MPR methodology facilitates the flexibility of the model for hydrological simulations at various spatial scales [Samaniego et al., 2010, Kumar et al., 2013a,b, Rakovec et al., 2016a,b, Samaniego et al., 2017]. mHM

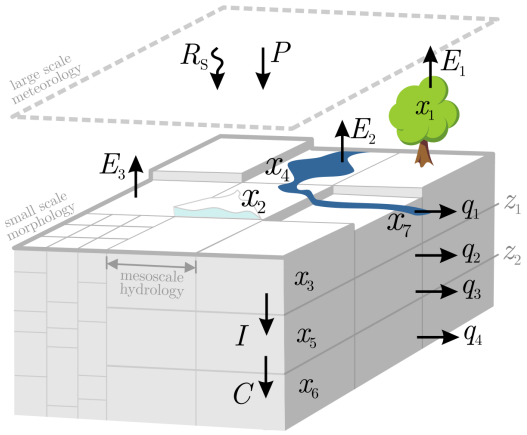

FIGURE 2.1: The concept of the mesoscale hydrologic model, mHM [Samaniego et al., 2010]. This figure is a property of Helmholtz-Zentrum für Umweltforschung GmbH - UFZ.

differentiates three levels to better represent the spatial variability in state and input variables. The effective parameters at different spatial scales are dynamically linked by a physically based upscaling scheme. A detailed description of MPR, as well as the formulations governing hydrological processes, is given by Samaniego et al. [2010] and Kumar et al. [2013b].

Below, we list the equations that describe near-surface processes in the deep soil and groundwater layers. The comprehensive system of equations of mHM can be found in Samaniego et al. [2010]. Here, weonly listed the equations needed for the coupling. In the subsurface reservoir, which is the second vertical layer (x_5 in Figure 2.1), interflow is partitioned into fast interflow (q_2) and slow interflow (q_3):

$$q_2(t) = max\{I(t) + x_5(t-1) - \beta_1(z_2 - z_1),\ 0\}\beta_2 \tag{2.1}$$

$$q_3(t) = \beta_3(x_5(t-1))^{\beta_4} \tag{2.2}$$

where $q_2(t)$ is fast interflow at time t [LT^{-1}], I is the infiltration capacity [L], x_5 is the water depth of water storage in the deep soil reservoir [L], β_1 is the maximum holding capacity of the deep soil reservoir [-], z_i is depth of the subsurface layer i [L], β_2 is the fast-recession constant [T^{-1}], $q_3(t)$ is slow interflow at time t [LT^{-1}], β_3 is the slow-recession constant, and β_4 is the exponent that quantifies the degree of nonlinearity of the cell response.

The groundwater recharge is equivalent to the percolation to the groundwater reservoir (the third vertical layer, see x_6 in Figure 2.1). The groundwater recharge $C(t)$ can be expressed by

$$C(t) = \beta_5 x_5(t-1) \tag{2.3}$$

where $C(t)$ is the groundwater recharge in cell i [LT^{-1}], and β_5 is the effective percolation rate coefficient [T^{-1}].

In the groundwater reservoir, baseflow is generated following a linear relationship between storage and runoff:

$$q_4(t) = \beta_6 x_6(t-1) \tag{2.4}$$

where $q_4(t)$ is the baseflow [LT^{-1}], β_6 is the baseflow recession rate coefficient [T^{-1}], and x_6 is the depth of the groundwater reservoir [L].

The runoff from upstream grid cells and the internal runoff in cell i are routed into streams using the Muskingum algorithm:

$$Q_i^1(t) = Q_i^1(t-1) + c_1(Q_i^0(t-1) - Q_i^1(t-1)) + c_2(Q_i^0(t) - Q_i^0(t-1)) \tag{2.5}$$

with

$$Q_i^0(t) = Q_{i'}(t) + Q_{i'}^1(t) \tag{2.6}$$

$$c_1 = \frac{\Delta t}{\kappa(1-\xi) + \frac{\Delta t}{2}} \tag{2.7}$$

$$c_2 = \frac{\frac{\Delta t}{2} - \kappa\xi}{\kappa(1-\xi) + \frac{\Delta t}{2}} \tag{2.8}$$

where Q_i^0 and Q_i^1 denote the runoff entering and leaving the river reach located in cell i [LT^{-1}], respectively, $Q_{i'}$ is the contribution from the upstream cell i' [LT^{-1}], κ is the Muskingum travel time parameter [T], ξ is the Muskingum attenuation parameter [-], Δt is the time step size [T], and t is the time index for each Δt interval.

2.3.2 OpenGeoSys (OGS)

OpenGeoSys (OGS) is an open-source project with the aim of developing robust numerical methods for the simulation of thermo-hydro-mechanical-chemical (THMC) processes in porous and fractured media. OGS is written in C++ with a focus on the finite element

analysis of coupled multi-field problems. Parallel versions of OGS based on both MPI and OpenMP concepts are available [Wang et al., 2009, Kolditz et al., 2012, Wang et al., 2017]. To date, two OGS versions are available: OGS5 (https://github.com/ufz/ogs5) and OGS6 (https://github.com/ufz/ogs). In this study, the term "OpenGeoSys (OGS)" represents OGS5 if not stated otherwise.

OGS has been successfully applied in different fields, such as water resources management, hydrology, geothermal energy, energy storage, CO_2 storage, and waste disposal [Kolditz et al., 2012, Shao et al., 2013, Gräbe et al., 2013, Wang et al., 2017]. In the field of hydrology-hydrogeology, OGS has been applied to regional groundwater flow and transport [Sun et al., 2011, Selle et al., 2013], contaminant hydrology [Beyer et al., 2006, Walther et al., 2014], reactive transport [Shao et al., 2009, He et al., 2015], and seawater intrusion [Walther et al., 2012], among others.

Saturated groundwater flow follows the continuity equation and Darcy's law:

$$S\frac{\partial \psi_p}{\partial t} = -\nabla \cdot \vec{q} + q_s \tag{2.9}$$

$$\vec{q} = -K_s \nabla(\psi_p + z) \tag{2.10}$$

where S is the specific storage coefficient in confined aquifers, and the specific yield in unconfined aquifers [1/L], ψ_p is the pressure head in the porous medium [L], t is time[T], $\vec{q}$ is the specific discharge or Darcy velocity [LT^{-1}], q_s is the general source or sink term [T^{-1}], K_s is the saturated hydraulic conductivity tensor [LT^{-1}], and z is the vertical coordinate (positive upward) [L].

The stream network is normally represented by a set of polylines in the geometry file of OGS. In the case of a 3-D model, a common way to set up the polyline system is to utilize the mapping tool embedded in OGS source codes, by which the shape file obtained from GIS software representing streams can be easily mapped onto the upper surface of OGS mesh and converted into a set of polylines. Each reach of the stream network can be represented by one polyline or several continuous polylines, depending on the demand of the user. Each polyline consists of a set of continuous mesh nodes, to which Dirichlet, Neumann or Robin boundary conditions can be applied.

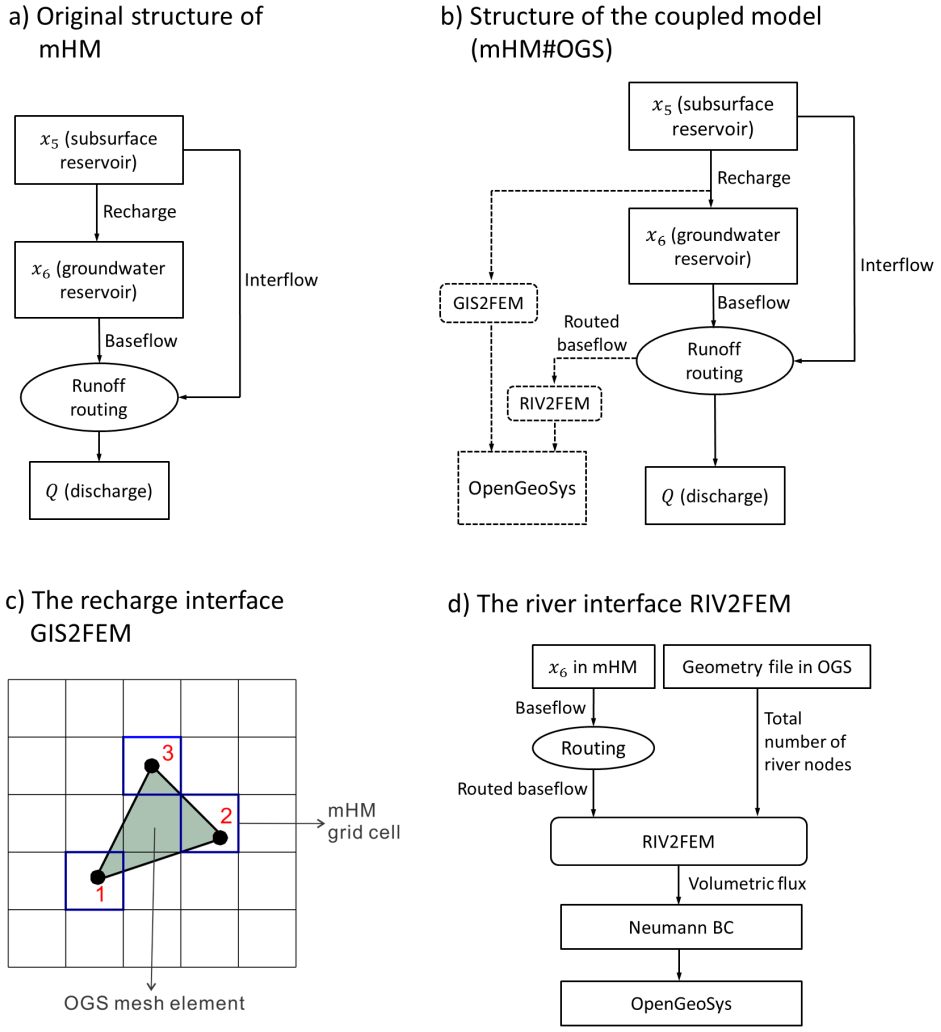

FIGURE 2.2: Schematic of the coupled model mHM-OGS v1.0. a) Original structure of the vertically layered reservoir of mHM. b) Structure of the coupled model (mHM-OGS v1.0). c) Illustration of data interpolation and transformation through the coupling interface GIS2FEM. d) Scheme of the river interface RIV2FEM. For the sake of simplicity, the figure only displays mHM layers relevant to this study and neglects the other mHM layers (i.e. x_1 - x_4). In Figure 2.2c, the grid-based mHM fluxes (e.g., recharge) are linearly interpolated to the top surface of the OGS mesh, and further transferred into volumetric values and directly assigned to the surface mesh nodes of the OGS grid.

2.3.3 Coupling mechanism

The coupled model mHM-OGS v1.0 is developed to simulate SW-GW flow in one or more catchments by simultaneously calculating flow across the land surface and within the groundwater. mHM-OGS v1.0 simulates flow within three hydrological regions. The first region is limited by the upper boundary of the plant canopy and the lower boundary of the soil zone bottom. The second region includes open-channel water, such as streams. The third region is the water-saturated aquifer. mHM is used to simulate the processes

in the first and second regions, while OGS is used to simulate the groundwater flow for prescribed fluxes at all boundaries in the third region.

The coupling initiative aims to add additional predictive capability of groundwater heads, which is achieved by OGS, to the existing capability of predicting discharges that is achieved by mHM. mHM is used to estimate a water budget stepwise and component-wise through model calibration against discharge. In contrast, OGS serves as a post-processor to obtain groundwater heads by using mHM-simulated recharge and baseflow as driving forces. Two model interfaces, namely GIS2FEM and RIV2FEM, have been developed to link the two models by transferring recharge and baseflow from mHM to Neumann boundary conditions in OGS.

The two models are executed separately and sequentially, typically with different temporal (e.g., daily in mHM and weekly or monthly in OGS) and spatial resolutions (e.g., rectangular, structured grids with coarse resolution in mHM and smaller, potentially unstructured grids with fine resolution in OGS). The original vertically layered reservoirs in mHM, namely the soil-zone reservoir and the subsurface reservoir are preserved, implying that all well-tested features of mHM (e.g., MPR, infiltration-runoff partitioning) are retained in the coupled model.

To illustrate the coupling mechanism in detail, the coupling workflow is itemized below.

1. mHM is run independently of OGS to calculate land surface fluxes including exchange fluxes of the groundwater storage.

   Using gridded meteorological forcings (precipitation, temperature, and potential evapotranspiration), the grid-based infiltration rates (e.g., groundwater recharge) and runoff components (e.g., interflow, baseflow) are estimated and saved as mHM output files. The original linear groundwater reservoir (depth x_6 in Figure 2.1) is used to estimate baseflow. Moreover, MPR is used in the calibration process such that subgrid variabilities can be validly calculated. The spatially distributed groundwater recharge and total routed baseflow are written into raster files for later use.

2. After the mHM run has finished, the stepwise routed baseflow estimated by mHM is transformed to distributed river discharges along streams and spatially distributed exchange rates between streams and groundwater needed in OGS.

Most PDE-based models characterize river-groundwater interaction based on either first-order flow exchange or boundary condition switching [Paniconi and Putti, 2015]. However, these approaches inevitably introduce extra parameters describing geometric, topographic, and hydraulic properties of the stream channel (e.g., river bed conductance, river bed and drain elevations, channel width). Unfortunately, these parameters are essentially unknown at a large scale due to the lack of data and the subgrid-scale variability in these parameters. Due to these limitations, an alternative approach which is based on the routed baseflow estimated by mHM is used.

mHM and OGS conceptualize streams differently: streams in mHM are implicitly defined based on preprocessing of digital elevation model (DEM) data and a routing scheme, while OGS uses an explicit predefined river geometry. In OGS, each reach of the stream network is defined by a polyline in the OGS geometry file. To coordinate the two different approaches, a model interface, RIV2FEM, is developed to convert the routed baseflow estimated by mHM to Neumann boundary conditions assigned at stream nodes of the OGS mesh (Figure 2.2d). Via RIV2FEM, the routed baseflow estimated by mHM is transferred to the uniformly disaggregated groundwater discharges by distributing it uniformly along the predefined stream network in OGS (Figure 2.2d):

$$\overline{q}_4(t) = \frac{Q_4(t)}{\sum_{i=1}^{N} A_i} \tag{2.11}$$

where $\overline{q}_4(t)$ denotes the normalized flux of disaggregated groundwater discharge at time t [LT^{-1}], $Q_4(t)$ denotes the routed baseflow at the outlet of catchment at time t [L^3T^{-1}], A_i is the nodal area of the ith stream node [L^2], and N is the total number of stream nodes. The uniformly disaggregated groundwater discharges are then assigned to every stream node in OGS to serve as the Neumann boundary condition (Figure 2.2d). This approach significantly reduces the number of parameters, avoids the uncertainty caused by the unknown river properties, and is suitable for many real-world applications that suffer from scarce data. Moreover, as recharge and baseflow are directly taken from mHM, the mass conservation criterion is naturally satisfied in this approach.

3. The distributed groundwater recharge generated by mHM is fed to the coupling

interface GIS2FEM, and then transferred to the upper surface boundary conditions of the OGS model.

The coupling interface GIS2FEM is used to interpolate and transfer mHM grid-based recharge to OGS nodal recharge values. GIS2FEM interpolates the flux value to the top surface elements of the OGS mesh. The detailed workflow is:

- GIS2FEM reads the raster file generated by mHM and the mesh file of OGS.
- In the case of a 3-D mesh, GIS2FEM extracts the upper surface of the OGS mesh. For each of the nodes on this surface, GIS2FEM searches for the mHM grid cell that the node is located in, and assigns the recharge value of this grid cell to the corresponding node (marked as C^m).
- After all top surface elements have been processed, GIS2FEM undertakes the face integration calculation, by which the specific recharge C^m [LT^{-1}] calculated by mHM is converted into volumetric recharge C^{in} [L^3T^{-1}] and assigned to the corresponding OGS mesh nodes (Figure 2.2c). Specifically, the specific recharge C in a certain element is calculated as:

$$C(\mathbf{x}) = \sum_{i=1}^{N} W_i(\mathbf{x}) C_i^m, \tag{2.12}$$

where $\mathbf{x}$ is the spatial coordinate on the surface, N is the total number of nodes in a surface element, W_i is the weighting function of ith node of the OGS surface element, and C_i^m is the specific recharge at the ith node of OGS surface element (calculated by mHM) [LT^{-1}]. Then the volumetric recharge C_i^{in} at the ith node (here i is the global node index) is calculated by the face integration calculation:

$$C_i^{in} = -\int_{\partial\Omega} W_i(\mathbf{x}) C(\mathbf{x}) d(\mathbf{x}), \tag{2.13}$$

where C_i^{in} is the volumetric recharge of node i [L^3T^{-1}], $\partial\Omega$ is the surface boundary of the FEM domain, and W_i is the weighting function of the ith node.

4. After the mHM-generated recharge and baseflow have been transferred into boundary conditions at the upper surface of the OGS mesh, the groundwater model is run to simulate the groundwater flow and transport.

In this step, additional boundary conditions can be set up in OGS mesh on the basis of expert knowledge. The exclusive use of Neumann boundary condition is not recommended and may lead to nonuniqueness of solutions. At least one specified head boundary should be set at the perimeter or internal nodes to constrain the model solution. The groundwater model simulates groundwater flow to obtain hydraulic heads in the example application. The groundwater model may also be used to compute travel times and solute transport within the groundwater domain, requiring additional boundary conditions; but this is not described in the present chapter.

2.4 Example application

2.4.1 Study area and model setup

We use a mesoscale catchment (about 850 km^2) upstream of the Nägelstedt gauge located in central Germany to test our coupled model (Figure 2.3). The Nägelstedt catchment comprises the headwaters of the Unstrut River, a tributary of the river Saale. This study area is selected because many of the groundwater monitoring wells in the area are operated by the Thuringian State Office for the Environment and Geology (TLUG) and the Collaborative Research Center AquaDiva [Küsel et al., 2016]. The elevation within the catchment ranges between 164 m and 516 m, whereby the higher regions are in the west and south and belong to the forested hill chain of the Hainich (Figure 2.3). The Nägelstedt catchment is one of the most intensively used agricultural regions in Germany. In terms of drinking water supply, about 70% of the water requirement is satisfied by groundwater [Wechsung, 2005]. About 17% of the land in this region is forested area, 78% is covered by crop and grassland, and 4% is urban and transport area. The mean annual precipitation in this area is about 660 mm.

In this study, mHM runs were executed for a time period of 35 years (from January 1, 1970 to December 30, 2004), with the period 1970 - 1974 being used for spin-up. OGS was run for the period from January 1, 1975 to December 30, 2005. mHM was run with a daily time step, while OGS was run with a monthly time step. The resolution of mHM grid cells is 500 m $\times$ 500 m. OGS uses a structured, hexahedral 3-D mesh, with a spatial resolution of 250 m $\times$ 250 m in the horizontal direction and 10 m in the vertical direction

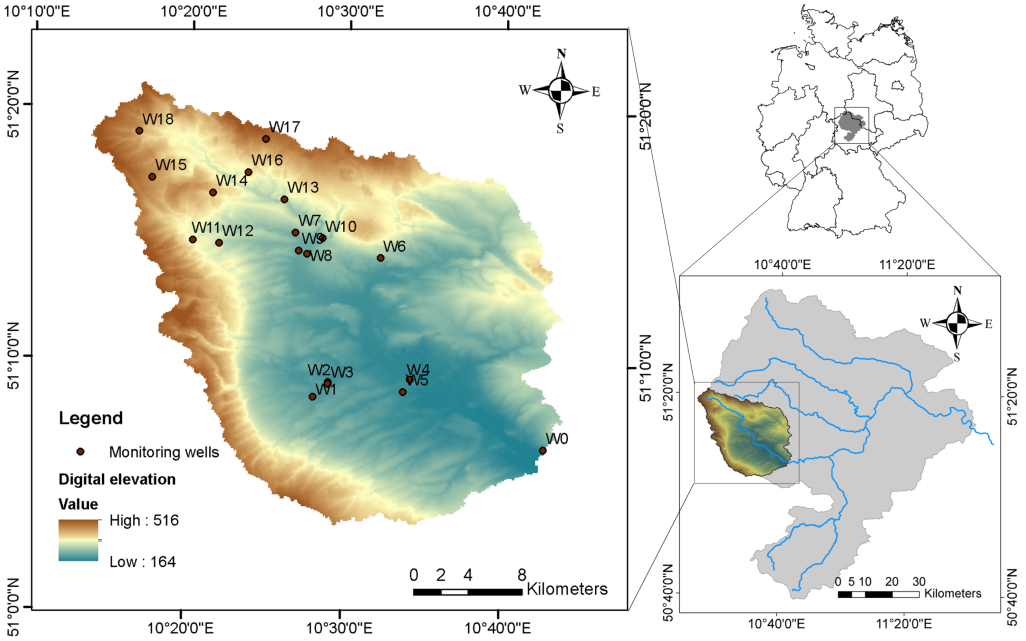

FIGURE 2.3: The Nägelstedt catchment used as the test catchment for this study. The left-hand map shows elevation and locations of monitoring wells used in this study. The lower right-hand map shows the relative location of Nägelstedt catchment in the Unstrut Basin. The upper right-hand map shows the location of the Unstrut Basin in Germany.

over the whole domain. The detailed input data and parameter set to run both models are detailed in the following sections.

2.4.2 Meteorological and surface properties

We started the modeling by performing the daily simulation of mHM to calculate near-surface hydrological processes. The mHM model is forced by daily meteorological conditions, including distributed precipitation and atmospheric temperature. The spatial patterns of precipitation and atmospheric temperature were based on point measurements of precipitation and atmospheric temperature at weather stations from the German Meteorological Service (DWD). The point data at weather stations were subsequently kriged onto a 4 km precipitation field, and then downscaled to mHM grid cells. Moreover, the potential ET was estimated based on the method from Hargreaves and Samani [1985]. Other datasets used in mHM are the DEM data, which is the basis for deriving properties such as slope, river beds, and flow direction; soil and geological maps, and derived properties such as sand and clay contents, bulk density; CORINE land-cover information (in the years 1990, 2000 and 2005); and discharge data at the outlet of the catchment.

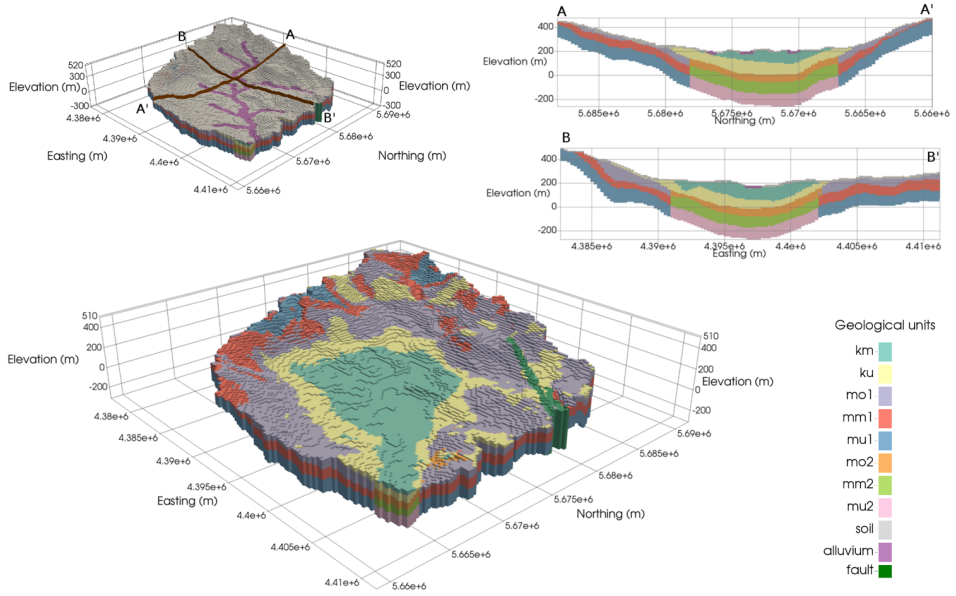

FIGURE 2.4: Three-dimensional and cross-sectional views of the hydrogeologic zonation in the Nägelstedt catchment. The upper left-hand figure highlights the distribution of alluvium and soil zones. The upper right-hand figure shows two vertical geological cross-sections. The lower map shows the detailed zonation of geological sub-units beneath the soil zone and alluvium.

2.4.3 Aquifer properties

A stratigraphic model is used to explicitly represent the heterogeneous distribution of hydraulic properties (hydraulic conductivity, specific yield, and specific storage). The stratigraphic model is based on well log data and geophysical data obtained from the Thuringian State Office for the Environment and Geology (TLUG). The workflow developed by Fischer et al. [2015] is used to convert the data format, by which the complex 3-D geological model was converted into the open-source VTK format file that can be directly read by OGS.

The major stratigraphic units in the study site are the Muschelkalk (Middle Triassic) and the Keuper (Upper Triassic). Younger Tertiary and Quaternary deposits are less important for the large-scale hydrogeology of the basin. The Keuper deposits mainly lie in the center of the Unstrut basin and act as permeable shallow aquifers. In the Nägelstedt catchment, the Keuper deposits are further subdivided into two geological sub-units: Middle Keuper (km) and Lower Keuper (ku) (see Figure 2.4). The Muschelkalk is marked by a prevailing marine environment and is subdivided into three sub-units the Upper Muschelkalk (mo), Middle Muschelkalk (mm, dolomites and residues of eroded salt layers) and Lower Muschelkalk (mu, limestones). According to previous geological

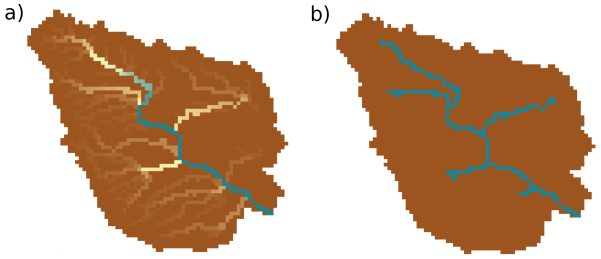

FIGURE 2.5: Illustration of the stream network used in this study. (a) Original stream network based on the streamflow routing algorithm of mHM; (b) Processed stream network that was used in this study. The small tributaries where the runoff rates are below the threshold (0.145 m^3/s) as shown in panel (a), have been removed to form the panel (b).

surveys [Seidel, 2004], the sub-units of the Muschelkalk have varying hydraulic properties depending on their positions and depths. They are further divided into sub-units with higher permeabilities (mo1, mm1 and mu1) and sub-units with lower permeabilities (mo2, mm2 and mu2) (Figure 2.4). The mo has been widely considered as a karstified formation. Recent research by Kohlhepp et al. [2017] has revealed that in the Hainich Critical Zone, the intense karstification and the conduit are limited at the base of the mo formation. Accordingly, we use the equivalent porous medium approach to characterize the mo. The uppermost layer with a depth of 10 m is set as a soil layer (Figure 2.4). A high-permeability alluvium layer is set along the mainstream and major tributaries to represent granite and stream deposits (Figure 2.4).

2.4.4 Boundary conditions

Based on the steep topography along the watershed divides, groundwater is assumed to be naturally separated and unable to pass across the boundaries of the watershed. In general, no-flow boundaries are set at the outer perimeters surrounding the basin as well as at the lower aquitard, except for the northwestern and northeastern edges. On the basis of the measurements, a Dirichlet boundary condition is assumed at the northwestern and northeastern edges.

The stream network was delineated by processing a grid-based runoff raster file generated by mHM. The grid-based runoff was converted to a valid stream network compatible with OGS. The necessity of transferring the mHM runoff raster file to the OGS stream network has been elaborated in Section 2.3.3. Particularly in this case study, weremoved the small intermittent tributaries by setting a threshold value of long-term averaged routed runoff.

Only streams with a runoff rate higher than the threshold (in this case study, 0.145 m^3/s) are delineated as valid streams. In other words, the intermittent streams to the upper stream reaches are neglected (Figure 2.5). The preprocessed stream network consists of a main stream and four tributaries (Figure 2.5b). The reach of each stream is defined as a polyline in a geometry file. As illustrated in Section 2.3.3, uniformly disaggregated groundwater discharges processed by the interface RIV2FEM were assigned to every OGS mesh node within the stream network.

2.4.5 Calibration procedure

The calibration of the coupled model follows a two-step procedure. In the first step, mHM was calibrated independently of OGS for the period from 1970 to 2005 by matching the observed runoff at the outlet of the catchment. The first 5 years were used as spin-up period to set up initial conditions in the near-surface soil zone. The calibration quality is quantified by the Nash-Sutcliffe coefficient of efficiency (NSE):

$$NSE = 1 - \frac{\sum_{i=1}^{n} |(q_m - q_s)|_i^2}{\sum_{i=1}^{n} |(q_m - \overline{q}_m)|_i^2} \tag{2.14}$$

where q_s is the simulated discharge [L^3T^{-1}], q_m is the measured discharge [L^3T^{-1}], and $\overline{q}_m$ is the mean of measured discharge [L^3T^{-1}].

In the second step, the steady-state groundwater model in OGS was calibrated to match the long-term mean of observed groundwater levels. The long-term mean of recharge and baseflow estimated by mHM were fed to the steady-state groundwater model as Neumann boundary conditions. The calibration was performed using the software package PEST [Doherty et al., 1994]. The model parameters were adjusted within a fixed interval until the value of objective function, which is the sum of weighted squared residuals of modeled and observed groundwater heads, was minimized. Specifically, the intervals of adjustable parameters were taken from the literature [Wechsung, 2005, Seidel, 2004], and the weights assigned to each observation were set uniformly to 1. The calibration result is assessed using the root-mean-square error (RMSE).

2.4.6 Model evaluation and sensitivity analysis

We used the time series of groundwater levels in 19 monitoring wells to evaluate the predictive capability of the transient model. In the transient model, hydraulic conductivities are obtained from the calibrated steady-state model. Meanwhile, the initial condition of the groundwater head is directly taken from the result of the steady-state model. The Pearson correlation coefficient R_{cor} and the interquartile range error (QRE) are used as two summary statistics to evaluate the predictive capability. The (relative) QRE is defined by:

$$QRE = \frac{IQ_{7525}^{md} - IQ_{7525}^{dt}}{IQ_{7525}^{dt}} \tag{2.15}$$

where IQ_{7525}^{md} and IQ_{7525}^{dt} are the interquartile ranges of simulations and observations, respectively.

We sought to quantify the sensitivity of groundwater flows to the different spatial pattern of recharge. For this purpose, a uniform recharge scenario was established as the reference scenario. The sensitivity analysis follows a two-step workflow. First, the steady-state groundwater models are calibrated for the two recharge scenarios independently. Second, transient simulations are conducted by assigning the same values of storage parameters, and then observed their corresponding performances in two recharge scenarios. With the exception of recharge scenario and hydraulic-conductivity values, all model parameters (e.g., specific yield and specific storage) and inputs are set to be identical in both scenarios. The mean absolute error (MAE), and the QRE are used as two summary skill scores to assess model performances in the two recharge scenarios.

2.5 Results

2.5.1 Calibration

As the first part of calibration, mHM is calibrated against discharge. The calibration results demonstrate the predictive capability of mHM in reproducing the time series of catchment discharge (Figure 2.6). The NSE is 0.88. Other fluxes, such as evapotranspiration measured at eddy-covariance stations inside this area, also show quite reasonable correspondence to the modeled estimate [Heße et al., 2017].

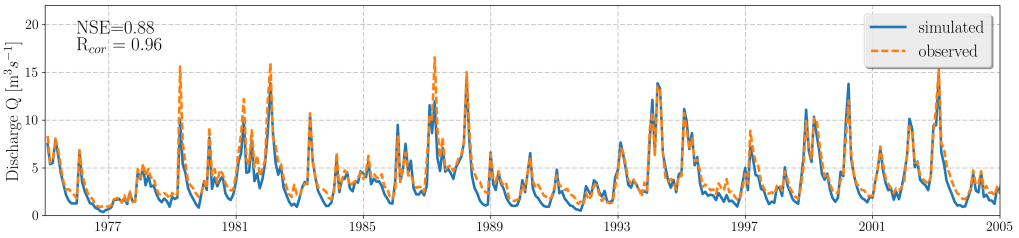

FIGURE 2.6: Observed and simulated monthly discharge at the outlet of the Nägelstedt catchment.

In the second step, the steady-state groundwater model is calibrated against the long-term mean of groundwater heads. Table 2.1 shows the calibrated hydraulic conductivities in each of the geological units. The objective function of calibration, which is the sum of squared weighted residuals, converged from an initial value of 8625 m^2 to 464.74 m^2 after a total of 114 model runs. Broadly speaking, the steady-state model can plausibly reproduce the finite numbers of observed groundwater heads in the catchment. Figure 2.7 shows the one-to-one plot of simulated and observed groundwater heads (locations of those wells are shown in Figure 2.3). In general, the model is capable of reproducing spatially distributed groundwater heads over a wide range, with an overall RMSE of 6.45 m. Most of the discrepancies between individual observations and simulations are within a reasonable range (i.e., less than 6 m). Nevertheless, some monitoring wells show larger discrepancies between observations and simulations (i.e., greater than 6 m), which is due to the unknown local or even subgrid-scale properties. For the sake of simplicity, no further attempt was made to add more model complexity to improve the model fit.

The simulated depth to groundwater over the whole catchment using the calibrated hydraulic-conductivity values is shown in Figure 2.7c. Broadly speaking, the calibrated model reasonably reproduces the spatial groundwater table distribution. Groundwater depth varies between greater than 40 m in the higher southwestern and northern mountainous areas, to less than 5 m in the central lowlands. The plausibility of steady-state simulation results can be assessed through regionalized observations of groundwater heads [Wechsung, 2005].

2.5.2 Spatiotemporal patterns of recharge and baseflow

Groundwater recharge has a spatially variable and dynamic behavior depending on the sporadic, irregular, and complex features of precipitation, geological structure, and

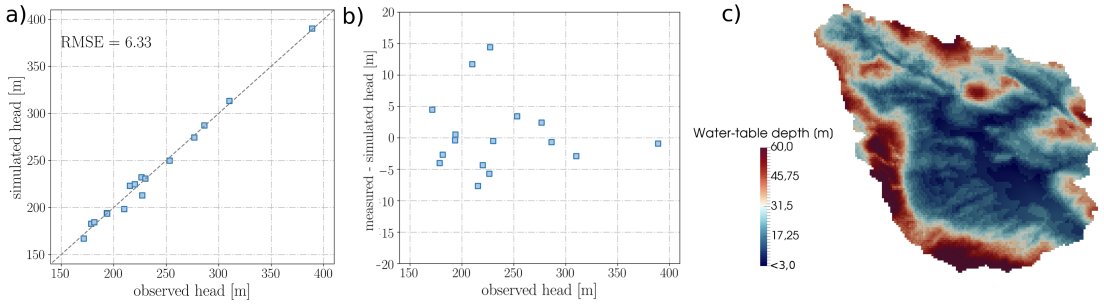

FIGURE 2.7: Illustration of steady-state groundwater model calibration and simulated heads. (a) Observed and simulated groundwater head (including RMSE); (b) Difference between simulated and observed head related to the observed head values; c) Simulated long term mean water table depth across the Nägelstedt catchment.

morphological features. The temporal and spatial variability in groundwater recharge and baseflow is estimated by mHM over a period of 30 years from 1975 to 2005.

Figure 2.8 shows the spatial variability in groundwater recharge in three months: March (Figure 2.8a), May (Figure 2.8b), and January (Figure 2.8c). The results indicate that the location of highest recharge rate is in the upstream mountainous areas where the Muschelkalk aquifer crops out, but varies in different seasons. The maximum value of monthly groundwater recharge varies from 26 mm in March, to 51 mm in May and 14 mm January. I also evaluated the plausibility of groundwater recharge simulated by mHM through comparison to other reference datasets. At the large scale, the groundwater recharge simulated by mHM agrees quite well with estimates from the Hydrological Atlas of Germany [Zink et al., 2017].

Figure 2.9a shows the distribution of monthly groundwater recharge and monthly baseflow. Over the entire year, groundwater inflow (recharge) and outflow (baseflow) are balanced, exhibiting a mean value of 8 mm/month. The difference between the two values is merely 2%. The Figure 2.9a, however, indicates that the distribution of monthly groundwater recharge is skewed to the right, whereas the distribution of monthly baseflow is more peaked. Figure 2.9b depicts the time series of groundwater recharge and baseflow, which further demonstrates that the deviation of monthly groundwater recharge is larger than the baseflow. This phenomenon further reveals the significant buffering effect of the linear groundwater storage in mHM.

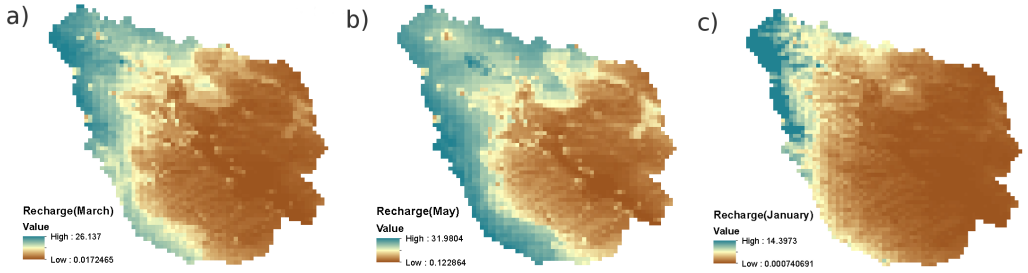

FIGURE 2.8: Spatial distributions of groundwater recharge in the Nägelstedt catchment (unit: mm/month) (a) in March (b) in May, and (c) in January 2005.

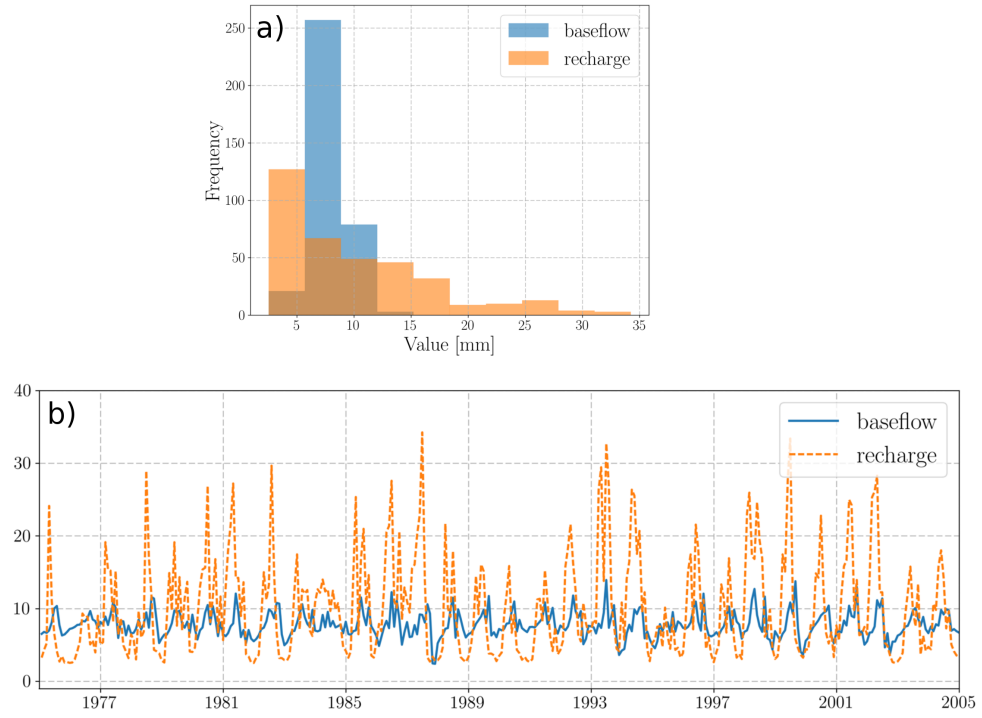

FIGURE 2.9: Analysis of groundwater inflow (recharge) and outflow (baseflow) over the Nägelstedt catchment. a) Distribution of groundwater balance components. b) Monthly time series of groundwater recharge and baseflow.

2.5.3 Model evaluation against dynamic groundwater heads

In this subsection, the head observations of several monitoring wells in the catchment were used to evaluate the model performance. Discrepancies between the modeled and observed groundwater heads are analyzed by subtracting long-term mean values, $\overline{h}_{mod}$ and $\overline{h}_{obs}$. Four model-skill scores including the mean value, the median value, the Pearson correlation coefficient R_{cor}, and the QRE are used to evaluate the model performance.

Six wells with different geological and morphological properties were chosen as samples to exhibit the model performance (Figure 2.10). Specifically, well W10 is located in

TABLE 2.1: Main hydraulic properties used in the case study under the default mHM-generated recharge scenario.

Geological units	Hydraulic conductivity [m/s]			Specific yield [-]
	Lower limit	Upper limit	Calibrated value [m/s]	
km	1.0×10^{-6}	5.5×10^{-3}	1.844×10^{-5}	-
ku	1.0×10^{-7}	3.4×10^{-4}	2.848×10^{-5}	-
mo1	8.0×10^{-8}	2.0×10^{-3}	3.570×10^{-5}	0.10
mm1	1.0×10^{-7}	9.0×10^{-4}	3.594×10^{-5}	-
mu1	5.0×10^{-9}	2.0×10^{-4}	6.202×10^{-6}	-
mo2	1.0×10^{-8}	5.0×10^{-4}	3.570×10^{-6}	-
mm2	3.0×10^{-8}	9.0×10^{-5}	3.594×10^{-6}	-
mu2	5.0×10^{-10}	2.0×10^{-5}	6.202×10^{-7}	-
soil	5.0×10^{-5}	1.0×10^{-2}	6.617×10^{-5}	0.10
alluvium	4.0×10^{-5}	1.0×10^{-2}	3.219×10^{-4}	0.18

the northern uplands and is near the main stream, whereas well W1 is located in the southwestern lowlands. As can be observed from Figure 2.10, they provide good fits between simulated and observed heads, with a R_{cor} of 0.87 and 0.76, and QRE of -23.34% and -1.65%. Well W17 is located in the Lower Keuper unit, while well W16 is located in the Upper Muschelkalk formation. In these two monitoring wells, the simulations are highly correlated with observations with high values of R_{cor} (0.71 and 0.82), in spite of their different geological properties (Figure 2.10). The simulation results at monitoring wells W13 (located in the northern mountainous area) and W7 (located at the northern upland) also exhibit good correspondence with the observations (Figure 2.10). In general, the model is capable of capturing the historical trends of groundwater dynamics, even though the mean values of simulations and observations may deviate to some extent. Due to the limited spatial resolution and complex hydrogeological structure, this degree of discrepancy is acceptable.

2.5.4 Model sensitivity to different recharge scenarios

As described in Section 2.4.6, a reference recharge scenario (RR), i.e., a spatially uniform recharge scenario, is set up to assess the effect of spatial patterns of recharge on groundwater heads. In RR the steady-state groundwater model was re-calibrated using the long-term mean of spatially uniform recharge (Table 2.2). For the purpose of showing discrepancies between two recharge scenarios, I compared the values of MAE and |QRE| at each monitoring well among the spatially distributed recharge, mR, and RR (Figure 2.11). The mean value and the median value of |QRE| were also calculated and are

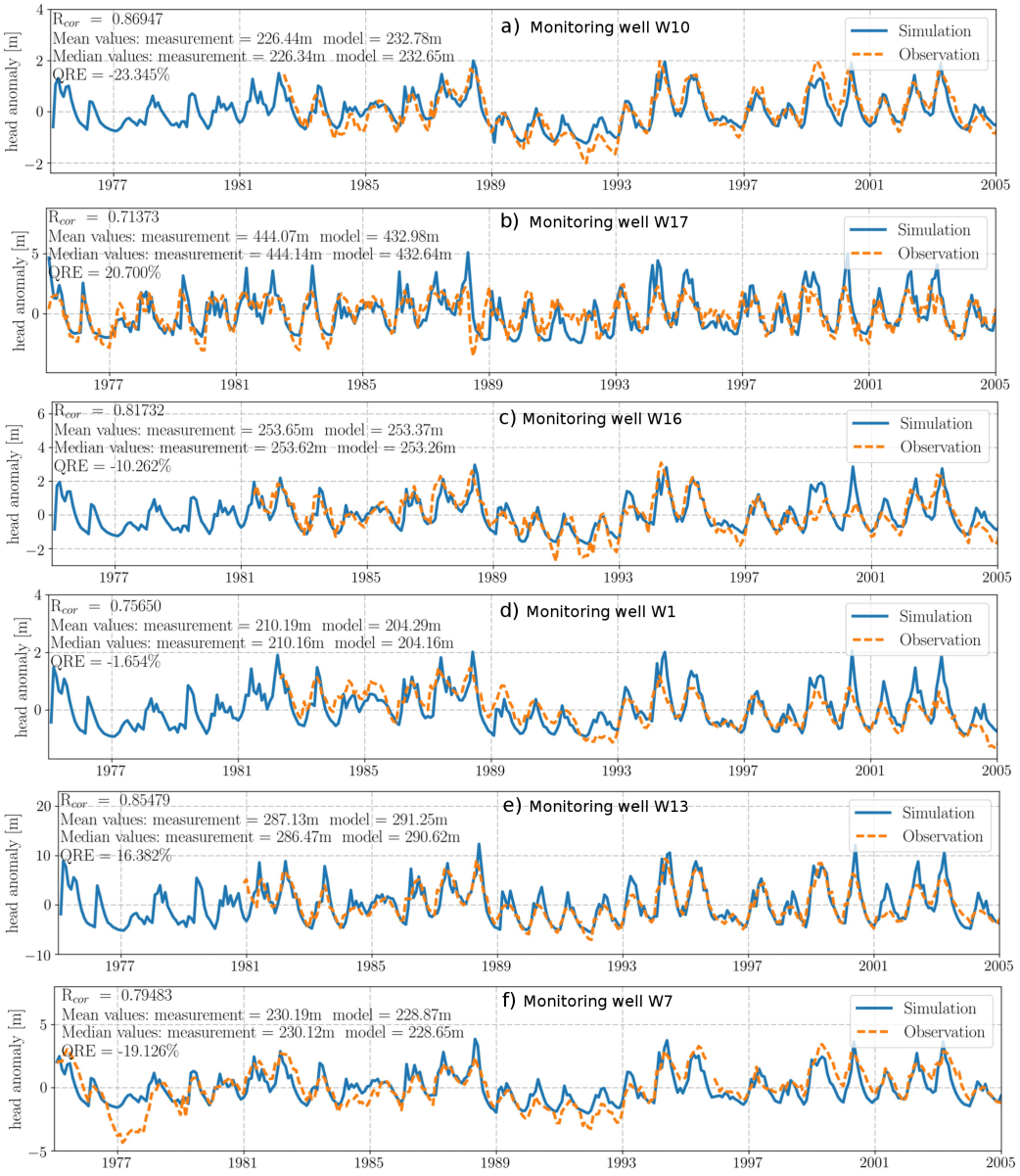

FIGURE 2.10: Comparison between measured (green dashed line) and simulated groundwater head anomalies (blue solid line). (a) W10 is located in uplands, near a stream. (b) W17 is located in a mountainous area. (c) W16 is located at a hillslope in the northern uplands. (d) W1 is located in the lowlands. (e) W13 is located in the northern mountains. (f) W7 is located in the northern uplands.

shown in Figure 2.11. Figure 2.11a indicates that the MAE using the spatially distributed recharge mR (4.04 m) is lower than that using the RR (4.61 m). Considering that the only difference between the two recharge scenarios is their spatial patterns, it is concluded that accounting for spatially- distributed recharge provides a moderate improvement in the model.

Figure 2.11b shows the absolute values of the QRE (|QRE|) in simulations using the two recharge scenarios (mR and RR). It is found that the deviation of |QRE| is significantly

TABLE 2.2: Hydraulic properties used in the uniform recharge scenario (RR).

Geological units	Hydraulic conductivity [m/s]
km	5.023×10^{-5}
ku	6.216×10^{-5}
mo1	8.608×10^{-5}
mm1	2.990×10^{-5}
mu1	5.316×10^{-6}
mo2	8.604×10^{-6}
mm2	2.997×10^{-6}
mu2	5.317×10^{-7}
soil	5.239×10^{-5}
alluvium	7.302×10^{-4}

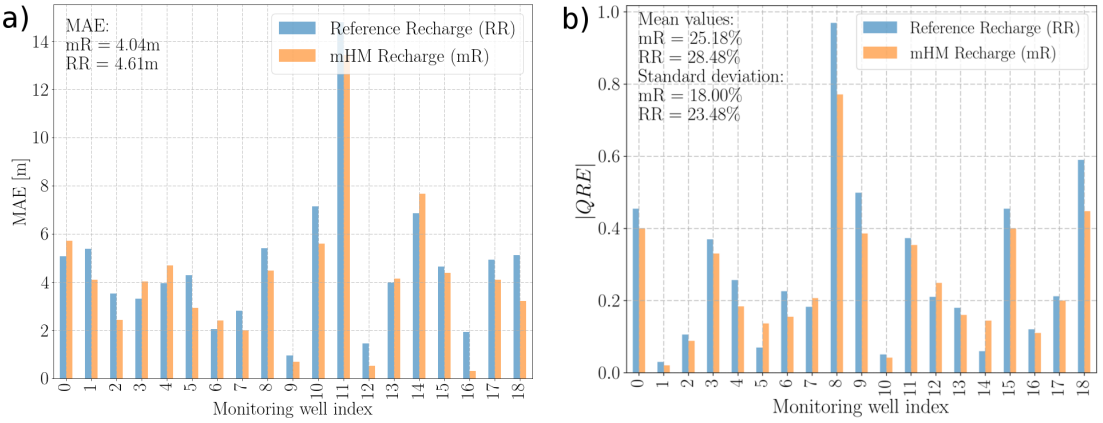

FIGURE 2.11: Barplots of a) the mean absolute error MAE and b) the absolute inter-quartile range error |QRE| in all monitoring wells in two recharge scenarios.

larger than R_{cor}, i.e., the |QRE| in two wells is abnormally higher than the other wells. The higher values of |QRE| at W8 and W18 may be caused by their proximity to model boundaries, as the two wells are located either near a river or near the catchment perimeter. This deviation indicates that accurate quantification of the amplitude of head fluctuations at certain locations is difficult, which may be due to the proximity of boundaries or complex local topography and geology. Nevertheless, 16 out of 19 wells exhibit low QREs, with the values of |QRE| in a range of ±40% in the spatially distributed mR scenario. A smaller mean and standard deviation of |QRE| in the spatially distributed mR than in the RR, has been observed. The 19 chosen monitoring wells cover the geological units of the alluvium, Keuper, and Muschelkalk, and range from high mountains to lowlands across the catchment. These results demonstrate the promising modeling capability of the model and highlight the moderately better historical matching when using a spatially distributed pattern of groundwater recharge.

Figure 2.12 illustrates the seasonality of groundwater heads by showing the spatial

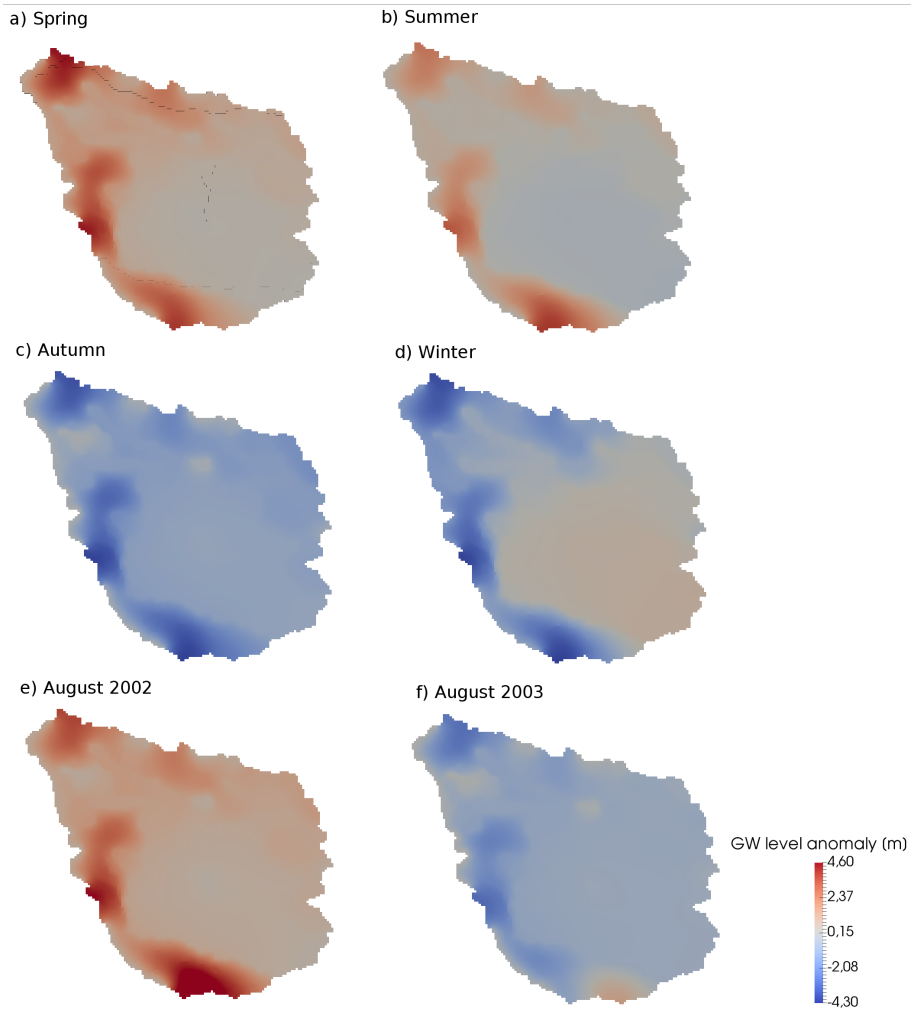

FIGURE 2.12: Seasonal variation of spatially distributed groundwater heads by their anomalies after removing the long-term mean groundwater heads (unit: m). (a) Long-term mean groundwater head distribution in spring; (b) long-term mean groundwater head distribution in summer; (c) long-term mean groundwater head distribution in autumn; (d) long-term mean groundwater head distribution in winter; (e) monthly mean groundwater head distribution in the wet season (August 2002); (f) monthly mean groundwater head distribution in the dry season (August 2003).

distribution of groundwater heads averaged over the spring, summer, autumn, and winter seasons. A strong spatial variability can be observed. For example, the fluctuation amplitudes of groundwater heads in the northern, eastern, and southeastern mountainous areas are larger than in the central plains area. In order to illustrate predicted groundwater levels and droughts caused by extreme climate events, I selected a meteorologically wet month (August 2002) and a meteorologically dry month (August 2003), and show the corresponding variations in groundwater heads in Figures 2.12e and 2.12f. In general, the groundwater heads in the wet season are higher than the long-term mean values (Figure 2.12e). The variation of groundwater heads in the dry season, however, shows a strong

spatial variability. Such a strong spatial variability in groundwater head variation has also been reported by Kumar et al. [2016].

2.6 Discussion and conclusions

Our simulation results demonstrate that the coupled model mHM-OGS v1.0 can generally reproduce groundwater head dynamics very well. It is also able to reasonably reproduce fluctuation amplitudes of groundwater heads, although with less accuracy. The simulation results also reveal that the stochastically and physically based representations of groundwater dynamics can be intrinsically linked on the condition that the geometry and geological structure of groundwater aquifer are reasonably characterized. Compared to the good predictive capability of capturing the general trend behavior, the amplitude of head time series is hard to reproduce. This might be because local geological formations in the vicinity of monitoring wells may significantly alter local groundwater flow behavior, and thus further affect groundwater head fluctuations.

The results of this study demonstrate the successful application of the well-established hydrologic model, mHM, in estimating spatially heterogeneous groundwater recharge and baseflow at a regional scale. At a spatial scale of 10^3 km^2 (the scale in this study), the distributed recharge estimated by mHM is superior to using homogeneous recharge. mHM has been successfully applied at the continental scale covering all of Europe [Thober et al., 2015, Kumar et al., 2013b, Rakovec et al., 2016b, Zink et al., 2017]. The successful application of the coupled model in this study suggests a huge potential for extending the applicability of mHM-OGS v1.0 to a larger scale (e.g., 10^4 - 10^6 km^2) or even a global scale.

The results of this study demonstrate a viable strategy for improving classic meso- to large-scale distributed hydrologic models, such as the current version of mHM [Samaniego et al., 2010, Kumar et al., 2013b], VIC [Liang et al., 1994], PCR-GLOBWB [van Beek and Bierkens, 2009], and WASMOD-M [Widén-Nilsson et al., 2007]. These distributed hydrologic models do not calculate spatiotemporal groundwater heads and are therefore unable to represent groundwater head dynamics in their groundwater compartment. The physical representation of groundwater flow is, however, relevant in future regional-scale and possibly global hydrologic models to accurately determine travel times, solute export

from catchments, and water quality in rivers [Botter et al., 2010, Benettin et al., 2015, van Meter et al., 2017]. The coupled model mHM-OGS v1.0 also offers the potential for predicting groundwater drought in analyzing the dynamic behavior of groundwater heads. Thus, it could be a useful tool for understanding groundwater anomalies under extreme climate conditions [Kumar et al., 2016, Marx et al., 2018].

For example, building on previous work of Heße et al. [2017], who calculated travel time distributions (TTDs) using mHM, it is possible to expand the range of their work to the complete critical zone, which is important for comprehensively understanding particle (e.g., pollutant) transport behavior and the historical legacy in soil zone and groundwater storage [Basu et al., 2010, Beniston et al., 2014]. mHM-OGS v1.0 fits well with the long-term simulation of nitrogen transport in the terrestrial water cycle. The coupled model is also able to evaluate surface water and groundwater storage changes under different meteorological forcing conditions, which allows the comprehensive evaluation of hydrologic response to climate changes (e.g., global warming). Additionally, OGS demonstrates its capability in addressing thermo-hydro-mechanical-chemical (THMC) coupling processes in large-scale hydrologic cycles (not reflected in this study), which is significant for a wide range of real-world applications, including nutrient circulation, saltwater intrusion, drought, and heavy metal transport [Kalbacher et al., 2012, Selle et al., 2013, Walther et al., 2014, 2017].

In addition to improving the predictive capabilities of mHM, some improvements can also be demonstrated for the groundwater model OGS. Our results showed a modest improvement using mHM-generated recharge compared to a simpler, uniform recharge rate. A strong advantage has been gained for the description of the top boundary condition, i.e. the recharge, which is temporal and spatially variable through the input of mHM. Even more, the recharge fluxes provided are based on mHM's phenomenological process description, which significantly better describes the surface level recharge fluxes than common approaches through recharge rates derived by empirical relations.

In this study, we have focused our efforts on extending the applicability of mHM from surface hydrology to subsurface hydrology by a simple one-way coupling. Consequently, we do not account for any feedback between river and groundwater head fluctuations. This approach is parsimonious and numerically efficient, and meanwhile fully preserves the well-tested parameterization algorithm in mHM. Unlike two-way coupling, the one-way

coupling described here allows the user to expand the abilities of mHM without sacrificing any of its well-known and well-established properties. Nevertheless, in a next step, we will devote to incorporate a full, two-way coupling using the next version of the mHM-OGS model. The main limitation of one-way coupling is that the effects of a shallow depth to groundwater on actual ET, maintained by lateral groundwater flow, cannot be explicitly addressed. However, the dynamic interactions between overland flow and groundwater flow, as well as between soil moisture dynamics and groundwater dynamics can explicitly be modeled and investigated using a full coupling scheme. This approach is open to a broader spectrum of calibration options, such as calibration by remotely sensed soil moisture data.

In conclusion, we can state that the coupled model mHM-OGS v1.0 retains the predictive capability of mHM for discharge volumes. In addition, it is capable of reproducing groundwater head dynamics. The simulation results indicate a promising predictive ability, confirmed by calibration and comparison to observed discharge and groundwater heads. Based on the historical match of discharge and groundwater heads in the case study, we conclude that the coupled model mHM-OGS v1.0 is a valuable tool for addressing many challenging problems in the field of water management, including pollutant transport and legacy, climate change, and groundwater drought.

Chapter 3

Influence of input and parameter uncertainty on the prediction of catchment groundwater travel time distributions

Acknowledgements

This study receives support from the Deutsche Forschungsgemeinschaft via Sonderforschungsbereich CRC 1076 AquaDiva. We kindly thank Sabine Sattler from Thuringian State office for the Environment and Geology (TLUG) for providing basic geological data. We acknowledge the EVE Linux Cluster team at UFZ for their support for this study. We also acknowledge the Chinese Scholarship Council (CSC) for supporting Miao Jing's stay in Germany.

published as:

Jing, M., Heße, F., Kumar, R., Kolditz, O., Kalbacher, T., and Attinger, S.: Influence of input and parameter uncertainty on the prediction of catchment-scale groundwater travel time distributions, Hydrol. Earth Syst. Sci., 23, 171-190, https://doi.org/10.5194/hess-23-171-2019, 2019.

3.1 Abstract

Groundwater travel time distributions (TTDs) provide a robust description of the subsurface mixing behavior and hydrological response of a subsurface system. Lagrangian particle tracking is often used to derive the groundwater TTDs. The reliability of this approach is subjected to the uncertainty of external forcings, internal hydraulic properties, and the interplay between them. Here, we evaluate the uncertainty of catchment groundwater TTDs in an agricultural catchment using a 3-D groundwater model with an overall focus on revealing the relationship between external forcing, internal hydraulic properties, and TTD predictions. Eight recharge realizations are sampled from a high-resolution dataset of land surface fluxes and states. Calibration-constrained hydraulic conductivity fields (K_s fields) are stochastically generated using the null-space Monte Carlo (NSMC) method for each recharge realization. The random walk particle tracking (RWPT) method is used to track the pathways of particles and compute travel times. Moreover, an analytical model under the random sampling (RS) assumption is fitted against the numerical solutions, serving as a reference for the mixing behavior of the model domain. The StorAge Selection (SAS) function is used to interpret the results in terms of quantifying the systematic preference for discharging young/old water. The simulation results reveal the primary effect of recharge on the predicted mean travel time (MTT). The different realizations of calibration-constrained K_s fields moderately magnify or attenuate the predicted MTTs. The analytical model does not properly replicate the numerical solution, and it underestimates the mean travel time. Simulated SAS functions indicate an overall preference for young water for all realizations. The spatial pattern of recharge controls the shape and breadth of simulated TTDs and SAS functions by changing the spatial distribution of particles' pathways. In conclusion, overlooking the spatial nonuniformity and uncertainty of input (forcing) will result in biased travel time predictions. We also highlight the worth of reliable observations in reducing predictive uncertainty and the good interpretability of SAS functions in terms of understanding catchment transport processes.

3.2 Introduction

Travel/transit time distributions (TTDs) of groundwater provide a description of how aquifers store and release water and pollutants under external forcing conditions, which has significant implications for interdisciplinary environmental studies. For example, remarkable time lags of the reaction of streamflow with outer forcings and considerable amounts of "old water" (i.e., water with an age of decades or longer) in streamflow have been observed in many studies [Howden et al., 2010, Stewart et al., 2012]. Moreover, the legacy nitrogen in groundwater storage may dominate the annual nitrogen loads in agricultural basins [Wang et al., 2016, van Meter et al., 2016, van Meter et al., 2017]. Groundwater TTDs offer important insights into the vulnerability of aquifers to pollution spreading, and they are critically important for the environmental assessment of non-point-source agricultural contamination [Böhlke and Denver, 1995, Böhlke, 2002, Molnat and Gascuel-Odoux, 2002, Eberts et al., 2012]. TTDs shed light on the quantification of the long-term influence of agricultural contamination, which is crucial for water quality sustainability.

The accurate quantification of groundwater travel time at a regional scale is extremely challenging. A primary difficulty is that the complex geometric, topographic, meteorologic, and hydraulic properties of hydrologic systems control the flow and mixing processes and therefore define the unique shape of the TTD [Leray et al., 2016, Hale and McDonnell, 2016, Engdahl et al., 2016]. The other difficulty is that the groundwater system is intricately and tightly coupled to land surface hydrologic processes. The fundamental characteristics and the coupled nature determine the response of a catchment to outer forcings such as anthropogenic climate change, artificial abstraction, and agricultural and chemical contamination [Tetzlaff et al., 2014, van der Velde et al., 2015, Heße et al., 2017].

The techniques for determining groundwater TTDs can be categorized into two groups: geochemical approaches and numerical modeling approaches [McCallum et al., 2014]. In geochemical approaches, the lumped parameter models are often used to interpret the catchment-scale observation of an environmental tracer concentration. Environmental tracer datasets can be divided into those representing the concentration distribution of young water (e.g., ^{3}H, SF_6, ^{85}K, and CFCs) and those representing the concentration distribution of old water (e.g., ^{36}Cl, ^{4}He, ^{39}Ar, and ^{14}C). Additionally, the analytical StorAge Selection (SAS) function is a cutting-edge tool for characterizing transport

processes in lumped, time-varying hydrologic systems at the hillslope/catchment scale [Botter et al., 2011, Rinaldo et al., 2011, van Der Velde et al., 2012, Harman, 2015, Danesh-Yazdi et al., 2018]. This framework provides a clear distinction between the travel time (the time spent by a water parcel or a solute from its entrance to the control volume until its exit) and the residence time (the age of the water parcel or the solute existing in the control volume at a particular time). The SAS function has been successfully applied to interpret environmental tracer data through some assumptions of the mixing mechanism [Benettin et al., 2015, 2017]. However, analytical approaches fall short in representing the dispersion of transport processes caused by catchment heterogeneity. Strong heterogeneity leads to significant aggregation error of mean travel times (MTTs) when using analytical models to interpret the tracer data [Kirchner, 2016, Stewart et al., 2016].

In contrast to such an analytical approach, physically based numerical models can explicitly describe the geometry, topography, and geological structures, and they can represent the flow paths of individual water particles. Physically based numerical models are structurally complex and computationally expensive and often have more parameters than lumped parameter models do. These models can be classified as Eulerian approaches or Lagrangian approaches [Leray et al., 2016]. The Eulerian approach directly solves the partial differential equations (PDEs) derived from mass conservation with "age mass" as the primary variable [Goode, 1996, Ginn, 2000, Engdahl et al., 2016]. The Lagrangian approach, including the smoothed particle hydrodynamics (SPH) approach and the random walk particle tracking (RWPT) approach, is numerically robust and less restrictive on time-step size in solving advection-dominated problems [Tompson and Gelhar, 1990]. Consequently, Lagrangian methods are more promising in simulating complex real-world transport processes, as they avoid spurious mixing error in grid-fixed Eulerian methods [Benson et al., 2017]. Therefore, the Lagrangian approach has been widely used to simulate large-scale reactive transport and biogeochemical problems [Park et al., 2008a, de Rooij et al., 2013a, Selle et al., 2013].

A reliable application of groundwater transport modeling is subject to many sources of uncertainty, including measurement, model structural, and parameter uncertainty [Beven, 1993]. Specifically, the reliability of model prediction suffers from the uncertainty of external forcings, the uncertainty of internal hydraulic characteristics, and the interplay between them [Ajami et al., 2007]. The spatially sparse measurements of recharge lead

to a biased characterization of spatiotemporal patterns of recharge [Healy, 2010, Cheng et al., 2017]. On the other hand, the spatial scarcity of hydrogeological data always hampers the right characterization of aquifer properties such as porosity and permeability, thus allowing a range of various realistic parameter values. The best-fit parameter may suffer from a fitting error caused by overparameterization and equifinality [Schoups et al., 2008]. Such biased parameters cause uncertain predictions because parameter error may compensate for model structural defects [Doherty, 2015]. Accordingly, predictive uncertainty can be hardly assessed in a precise way.

Biased characterization of the hydrodynamic system and oversimplified assumptions will lead to a problematic prediction of TTDs. Many past studies offer insights into the influence of recharge and hydrogeological configuration on the prediction of TTDs. For example, some research studies have been devoted to the development of analytical solutions for the idealized catchment (or aquifer) under some essential assumptions and simplifications [Neuman, 1972, Haitjema, 1995, Engdahl et al., 2016, Leray et al., 2016]. Among them, Haitjema [1995] derived an analytical solution in an idealized groundwatershed under steady-state conditions and the Dupuit–Forchheimer assumption and found that the groundwater mean travel time appears to be only dependent on recharge, saturated aquifer thickness, and porosity, provided that the hydraulic conductivity is locally homogeneous. Basu et al. [2012] evaluated analytical, GIS, and numerical approaches for the prediction of groundwater TTDs and found that the simulated TTDs show a moderate difference. Many recent studies have reported the dependency of transient TTDs on the temporal variability of input forcings [Benettin et al., 2015, Yang et al., 2018, Remondi et al., 2018, Kaandorp et al., 2018], but the dependency of TTDs (as well as SAS functions) on the spatial variability of input forcings has rarely been studied.

Although studies on catchment-scale groundwater TTDs are numerous, comprehensive uncertainty analysis that aims to unveil the different roles of external forcing and internal hydrostratigraphic structure using both a numerical model and SAS functions is scarce. In this regard, two important questions are the following: (1) How does the uncertainty of recharge (including its spatial nonuniformity) and hydraulic conductivities affect the TTD predictions in a mesoscale agricultural catchment, provided that the model is constrained to reality and groundwater head observations? (2) How does the uncertainty of inputs (forcings) and parameters influence the prediction of systematic preference for young/old water?

In this paper, we aim to answer these questions through a detailed (uncertainty) analysis of an example application in a mesoscale real-world catchment. In doing so, we establish a detailed groundwater model coupled to a random walk particle tracking system for predicting groundwater TTDs. The OpenGeoSys (OGS) groundwater model is used to simulate the groundwater flow, while the input forcing is fed by the mesoscale hydrologic model (mHM) via the mHM-OGS coupling interface [Jing et al., 2018]. The numerical model follows the steady-state assumption of groundwater flow systems. This assumption is made because at the regional scale, the groundwater flow process has a much larger timescale than that of the high-frequency oscillation of recharge, which essentially dampens the effect of recharge oscillation [Leray et al., 2016]. An ensemble of simulations using multiple recharge realizations and multiple equifinal hydraulic conductivity (K_s) fields is established. An analytical model is used as a reference for unveiling the mixing mechanism of the system. The StorAge Selection function is also used to interpret the simulation results of the numerical model, with an overall aim to quantify the predictive uncertainty of systematic preference for young/old water.

3.3 Site description

The candidate site in this paper is the Nägelstedt catchment, located in central Germany (see Figure 2.3). With an area of approximately 850 km^2, the Nägelstedt catchment is a headwater catchment of the Unstrut river. The terrain elevation of this area varies from 164 m to 516 m a.m.s.l. (above mean sea level). It is a subcatchment of the Unstrut basin, one of the most intensively used agricultural regions in Germany. About 88% of the land in this site is marked as arable land, which is significantly higher than the average level of Thuringian [Wechsung et al., 2008]. The agricultural nitrogen input has varied over the years and locations, from 5 - 24 kg ha^{-1} in the soils of the lowlands to 2 - 30 kg ha^{-1} in the feeding area [Wechsung et al., 2008]. The mean annual precipitation is approximately 660 mm.

The dominating sediment in the study area is the Muschelkalk (Middle Triassic). The Muschelkalk has an overall thickness of about 220 m, and it has been divided into three subgroups according to mineral composition: Upper Muschelkalk (mo), Middle Muschelkalk (mm), and Lower Muschelkalk (mu). The Upper Muschelkalk (mo) is mainly composed of limestone, marlstone and claystone, and it forms fractured aquifers [Jochen

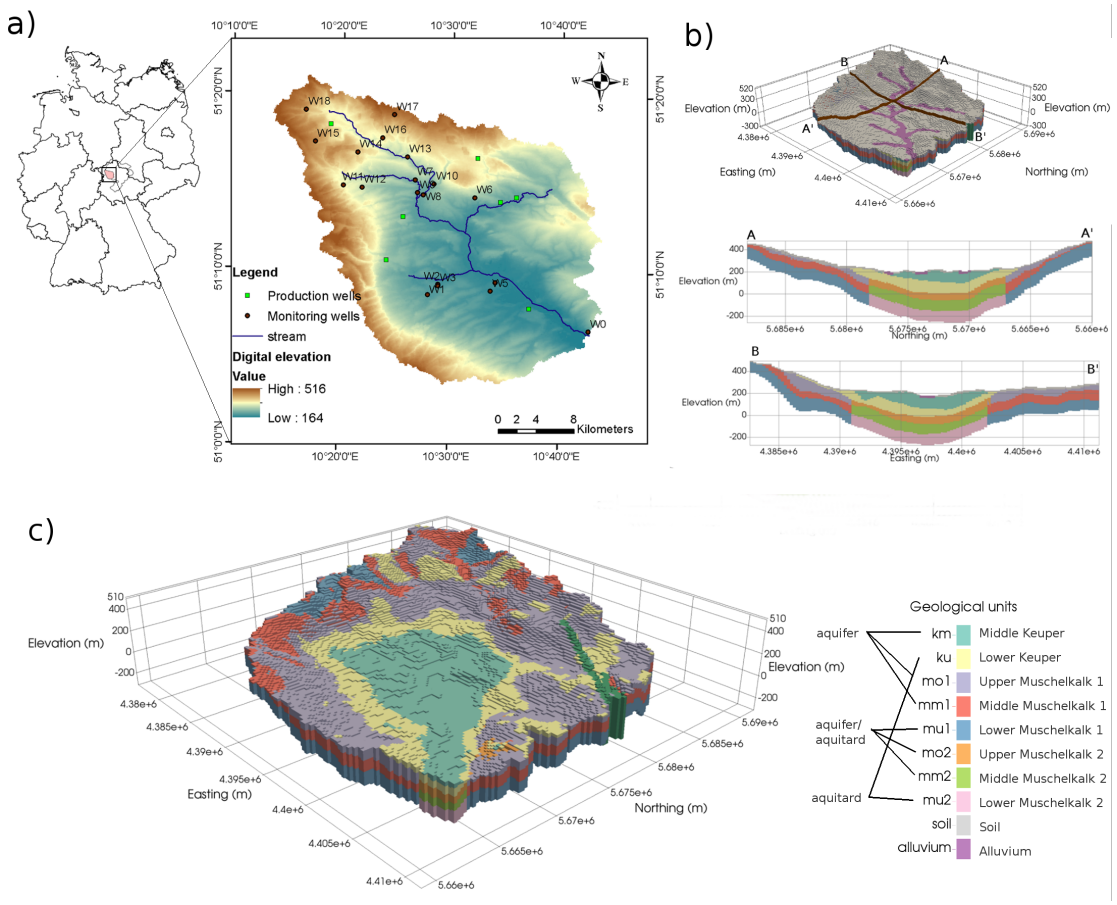

FIGURE 3.1: The Nägelstedt catchment used as the test catchment for this study. a) An overview of the Nägelstedt catchment and the locations of the monitoring wells used in this study. b) 3-D view highlighting the arrangement of alluvium and soil and cross-sectional view of the study area. c) 3-D view highlighting the zonation of the sedimentary aquifer-aquitard system. Note that the Muschelkalk layers (mo, mm and mu) are divided into more permeable subunits (mo1, mm1 and mu1) and less permeable subunits (mo2, mm2, and mu2).

et al., 2014, Kohlhepp et al., 2017]. The Middle Muschelkalk (mm) deposits are composed of evaporites, including dolomit marlstone, gypsum, dolomit limestone and eroded salt layers. The Lower Muschelkalk (mu) is composed of massive limestone [McCann, 2008, Jochen et al., 2014]. The Muschelkalk formation consists of limestone sediments, which may form fractured and karst aquifers. A recent study demonstrated that karstification and the development of conduits are limited at the base of the Upper Muschelkalk at the Hainich critical zone in the Nägelstedt catchment [Kohlhepp et al., 2017]. In the middle of the study area, Keuper deposits, including Middle Keuper (km) and Lower Keuper (ku), overlay the Muschelkalk formation. The Lower Keuper formation forms the low permeable aquitard on top of the Upper Muschelkalk aquifer [Kohlhepp et al., 2017]. Lithologically, the Muschelkalk aquifer system is a "layer-cake" aquifer system that

contains interbedded marlstone aquitards [Aigner, 1982, Merz, 1987, Kohlhepp et al., 2017].

Eighteen monitoring wells distributed in this area are used to calibrate the model (Figure 2.3a, in which well W0 is abandoned in this study due to the proximity to the outer edge). The geological layers to which the wells belong are listed as follows: five wells in Middle Keuper (km), four in Lower Keuper (ku), six in Upper Muschelkalk (mo), two in Middle Muschelkalk (mm), and one in alluvium.

3.4 Methodology and materials

3.4.1 Numerical model

We use mHM-OGS coupled model, proposed by Jing et al. [2018], is used to simulate terrestrial hydrological processes. This coupled model was developed for extending the predictive capability of mHM from land surface processes to the subsurface flow and transport processes. Specifically, the mesoscale hydrologic model (mHM) [Samaniego et al., 2010, Kumar et al., 2013b] is used to partition water budget components, while the OGS porous media simulator [Kolditz et al., 2012] is used to compute groundwater flow and transport processes by using mHM-generated recharge as driving forces. For details on the mHM-OGS coupled model, please refer to Jing et al. [2018].

The catchment water storage is conceptually partitioned into soil-zone storage and deep groundwater storage; the two corresponding components are computed by mHM and OGS, respectively. The soil zone dynamics of TTD has been well studied using mHM in a previous work [Heße et al., 2017]. Hence, in this chapter, explicit forward modeling of the saturated-zone TTD through a 3-D OGS groundwater model is performed by using the mHM-generated recharge as the external forcing.

In this study, we focus on the travel times in the saturated zone. Saturated groundwater flow is characterized by the continuity equation and Darcy's law:

$$S\frac{\partial \psi_p}{\partial t} = -\nabla \cdot \vec{q} + q_s \tag{3.1}$$

$$\vec{q} = -K_s \nabla(\psi_p - z) \tag{3.2}$$

where S is the specific storage coefficient in confined aquifers, or the specific yield in unconfined aquifers (1/L); ψ_p is the pressure head in the porous medium (L); t is the time (T); $\vec{q}$ is the specific discharge or the Darcy velocity (LT^{-1}); q_s is the general source/sink term (T^{-1}); K_s is the saturated hydraulic conductivity tensor (LT^{-1}); and z is the vertical coordinate (L).

We use the RWPT method to track the particle movement. The RWPT method is embedded in the source codes of OGS [Kolditz et al., 2012, Park et al., 2008a]. Derived from stochastic physics, RWPT is under the assumption that the advection process is deterministic and the diffusion-dispersion process is stochastic. The theoretical background of the RWPT method is described in detail in Appendix.

3.4.2 Numerical model setup

3.4.2.1 Boundary conditions

The steady-state model configuration is achieved using a temporally averaged recharge over a long period (1955–2005). The gridded recharges estimated by mHM are interpolated and then assigned to each grid node on the upper surface of the OGS mesh using a bilinear interpolation approach. No-flow boundaries are assumed at the outer edges that are defined by catchment divides, except for the northwestern and northeastern edges, where fixed-head boundaries are applied [Wechsung et al., 2008]. The streams are assigned with fixed-head boundaries, wherein the heads are equal to the long-term-averaged water levels. For the steady-state system and the one-way coupled model, the baseflow component generated by OGS proves to be consistent with the baseflow estimated by mHM, implying that the water budget in the subsurface system is essentially closed [Jing et al., 2018]. Neumann boundaries are prescribed for seven drinking water production wells. However, the amount of pumping makes up only around 3% of the total amount of outflow, and it therefore has a marginal influence on the water budget [Wechsung et al., 2008].

3.4.2.2 Modeling procedures

The numerical experiment to explore the uncertainty of TTDs is performed through the following workflow:

TABLE 3.1: Adjustable ranges of parameters.

Parameters	Hydraulic conductivity [m/s]	
	Upper limit	Lower limit
soil	9.0×10^{-4}	5.0×10^{-5}
alluvium	2.0×10^{-3}	4.5×10^{-6}
km	9.0×10^{-4}	1.0×10^{-6}
ku	8.5×10^{-5}	9.6×10^{-7}
mo1	8.0×10^{-4}	9.0×10^{-7}
mm1	9.1×10^{-4}	3.1×10^{-7}
mu1	2.0×10^{-5}	2.0×10^{-8}

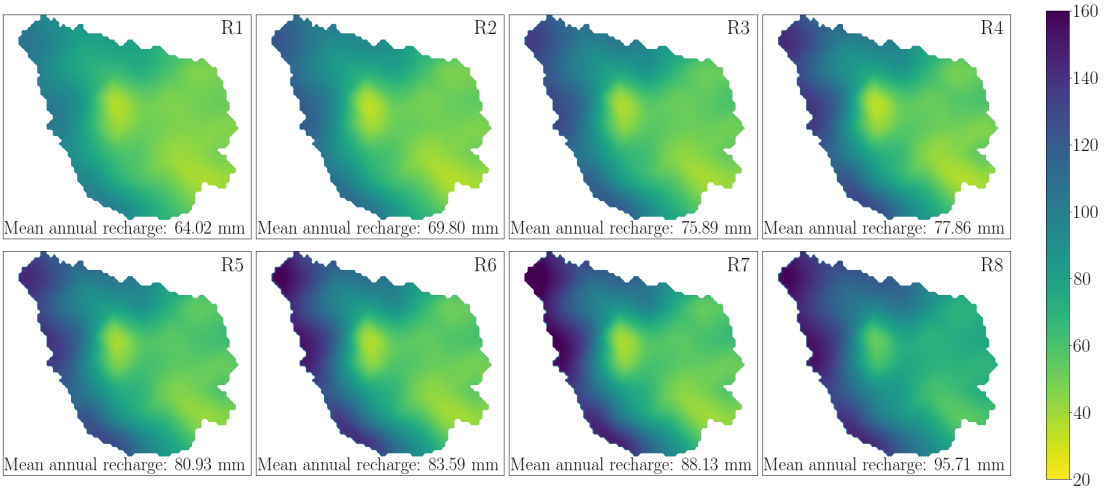

FIGURE 3.2: Recharge realizations used in this study (unit: mm). They were sampled from a high-resolution dataset of land surface fluxes for Germany [Zink et al., 2017].

1. Eight spatially distributed recharge realizations are sampled from a high-resolution dataset of land surface fluxes for Germany, in which mHM is used to simulate land surface hydrological processes. The details of the dataset and the sampling method are described in the following section.

2. For each recharge realization, a series of equally probable realizations of K_s fields are generated using the null-space Monte Carlo (NSMC) method.

   The NSMC method takes advantage of the hybrid Tikhonov-TSVD method in the PEST parameter estimation code to produce Monte Carlo realizations of parameters [Tonkin and Doherty, 2009, Doherty and Hunt, 2010]. This approach is able to efficiently generate an ensemble of parameter fields that are conditioned to expert knowledge and measurements. Here, the observations of groundwater levels from 18 spatially distributed monitoring wells are used to calibrate the OGS model (the locations of monitoring wells are illustrated in Figure 2.3a). Before generating

parameter sets, the model is calibrated to obtain the best-fit hydraulic conductivities, as well as a covariance matrix of the parameter probability distributions. On the basis of this information, many fully distributed K_s fields are randomly generated from a uniform distribution of hydraulic conductivity values [Doherty, 2015]. As shown in Table 3.1, the range of hydraulic conductivities is predefined based on values obtained from a geological survey [Wechsung et al., 2008]. As a result, a total of 400 parameter sets conditioned on both observations and reality are generated for the uncertainty analysis.

3. In each parameter realization, a large number of particles are injected through the top surface of the groundwater model. The spatial density of particles is proportional to the spatially distributed recharge rates.

   To accurately interpret the travel time distribution, a large number of particles (e.g., approximately 80 000 particles in the case study) is released into the top surface of the groundwater model. The released particles serve as samples of water parcels for deriving their travel time distributions. In doing so, the density of particles is set proportional to the recharge at the corresponding grid cell (Figure 3.3). Each particle tracer represents a volumetric recharge rate of around 700 m^3/year.

4. An ensemble of forward simulations using the RWPT method is performed over all realizations of K_s fields.

   In each realization of the ensemble parameter sets, forward simulations of particle tracking are performed. In this study, the focus is on the predictive uncertainty within the convection process. Therefore, the molecular diffusion coefficients are universally set to 0 for all ensemble simulations. The porosity of the study domain is set to 0.2 universally. Through the above procedures, the flow paths and the corresponding residence times can be fully traced in the model at random times and locations, facilitating the detailed characterization of TTDs.

In parallel to this analysis, a sensitivity analysis for the spatial variability of recharge is also performed. Two different recharge scenarios are compared for this purpose: (1) the spatially distributed recharge generated by mHM and (2) the uniform recharge that is equal to the spatial average of the distributed recharge. Other parameters, including the porosity and the hydraulic conductivity, remain identical in these two recharge scenarios.

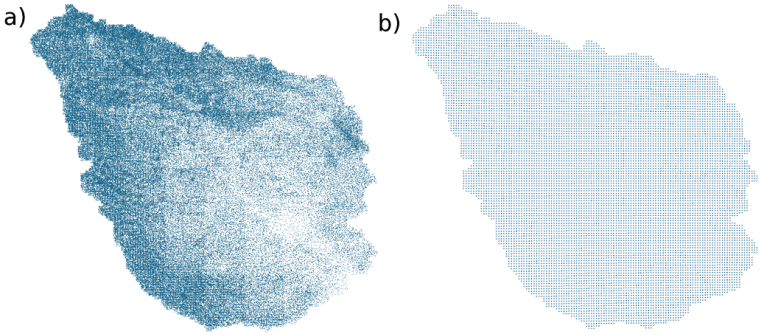

FIGURE 3.3: Two different spatial distributions of particle tracers for the random walk particle tracking (RWPT) method. a) The mass-weighted distribution of particles based on the recharge estimated by mHM. This is the default spatial pattern of particle tracers in this study. b) The uniformly distributed particle tracers used in the uniform recharge scenario.

3.4.2.3 Recharge realizations

A high-resolution dataset of land surface fluxes and states across Germany is used for sampling recharge scenarios. This dataset was established on the basis of a daily simulation with 4 km spatial resolution using the mesoscale hydrologic model (mHM) for a time span of 60 years (1951–2010) [Zink et al., 2017]. This dataset consists of an ensemble (100 realizations) of land surface variables, including evapotranspiration, groundwater recharge, soil moisture and discharge, with a spatial resolution of 4 km. A total of 100 realizations of land surface states are all conditioned on the observed daily discharge, and each of them has been derived by incorporating the uncertainty of parameterization caused by the heterogeneity of geometry, topography and geology. The modeled datasets are further validated against observation-based evapotranspiration and soil moisture data from eddy covariance stations [Heße et al., 2017]. The derived recharges show a good correspondence to the estimation from the Hydrologic Atlas of Germany [Zink et al., 2017].

Eight representative recharge realizations (R1-R8) are sampled from 100 realizations for this study to save computational time. To enhance the representativeness of the samples, the 100 recharge realizations are sorted in an ascending order by their spatial averages. The selected recharge realizations are uniformly sampled from the sorted recharge realizations. In doing so, the maximum and minimum recharges are included in the samples such that the whole range of recharge realizations is fully covered.

3.4.2.4 3-D stratigraphic model

A 3-D stratigraphic mesh is established on the basis of hydrogeological characterizations elaborated in Section 3.3 (Figure 2.3). The structured mesh is composed of 310 599 nodes (132 rows, 140 columns, and 82 vertical layers). The 3-D cell size of 250 m, 250 m, and 10 m in the x, y and z directions is used in this study. Based on the German stratigraphy [Menning, 2002], the Middle Muschelkalk, the Upper Muschelkalk, the Lower Keuper, and the Middle Keuper outcrop in the Nägelstedt catchment. Accordingly, a stratigraphic aquifer system with 10 geological units is set up. The uppermost 10 m of the mesh has been separated as a soil layer, while an alluvium layer consisting of high-permeability sandy gravel is set at the nodes beneath and near streams (Figure 2.3). Each of the Muschelkalk layers is further divided into two categories: the more permeable parts (mo1, mm1, and mu1) and the less permeable parts (mo2, mm2, and mu2) (see Figure 2.3). For each of the Muschelkalk units, the permeability of the less permeable part is tied to the corresponding more permeable part with a factor of 0.1. The equivalent porous medium approach is applied to characterize the karst aquifer of the Upper Muschelkalk (mo). This approach translates the parameters describing highly heterogeneous hydraulic properties at the point scale into the equivalent homogeneous medium at the regional scale to avoid adding redundant parameters and therefore avoid overfitting.

3.4.2.5 Parameter uncertainty

Multiple calibration-constrained K_s fields were stochastically generated for each recharge realization. Figure 3.4 shows the box-plot of generated hydraulic conductivities in all realizations categorized by geological unit. The hydraulic conductivity of the Lower Muschelkalk (mu) has the highest uncertainty (10^{-8} - 10^{-5} m/s) because the conductivity of mu is insensitive to groundwater head observations, given that it is the deepest geological layer and that no monitoring well is located in this layer (Table B.1). The other parameters fluctuate moderately and are constrained within 1 order of magnitude in most of the recharge realizations. Hydraulic conductivities of several permeable layers (mo, mm, alluvium, and soil) increase from R1 to R8, which is not surprising because the hydraulic conductivity increases with increasing recharge and constant groundwater head. Moreover, the hydraulic conductivities of the above layers are roughly linearly correlated with the corresponding recharge in each recharge realization. Figure 3.5 shows

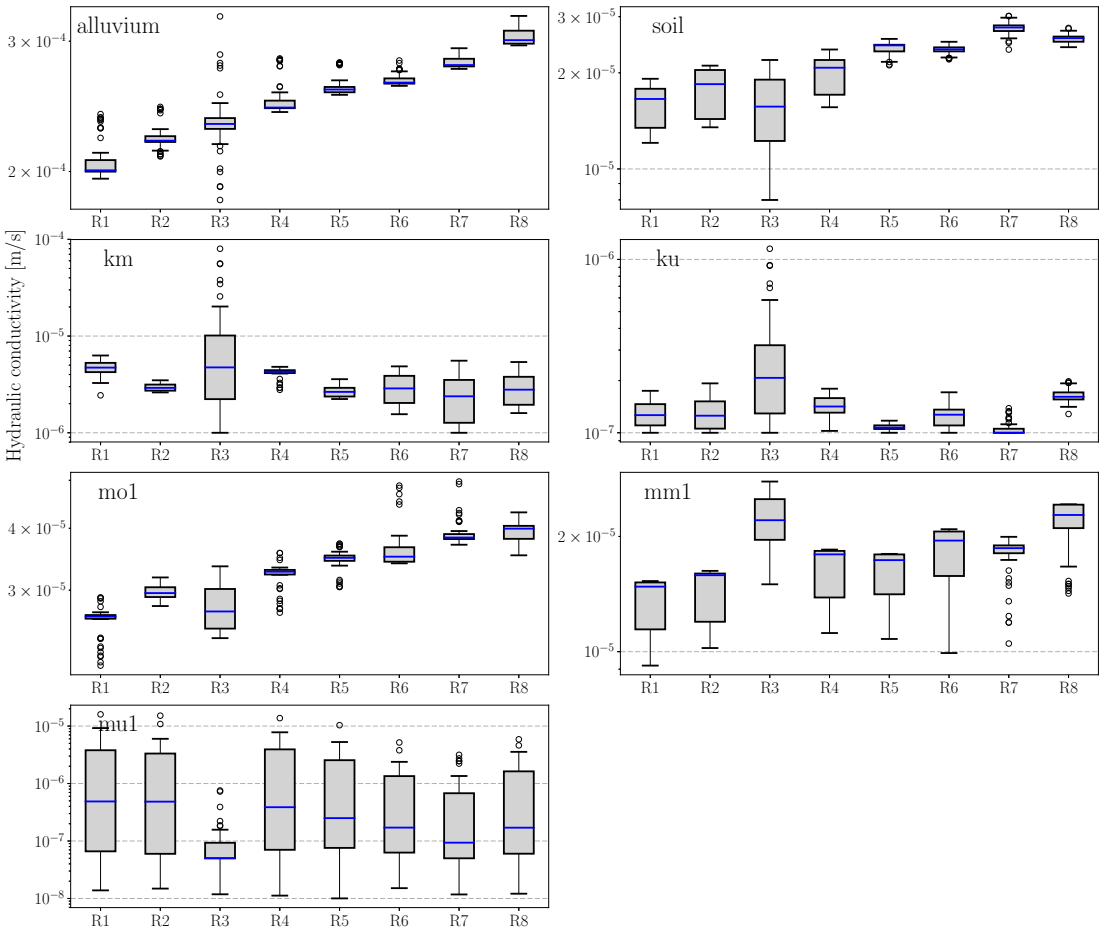

FIGURE 3.4: Box-plot of stochastically generated hydraulic conductivity (K_s) for each geological layer in 8 recharge realizations. Note that the parameters mo2, mm2, and mu2 are not shown in this figure because the less permeable subunits of the Muschelkalk (mo2, mm2, and mu2) are tied with the respective more permeable subunits (mo1, mm1, and mu1) with a factor of 0.1.

the simulated and observed groundwater heads for all 400 realizations. All of the 400 realizations are well constrained to observations, with the root mean square error (RMSE) of groundwater level residuals being lower than 4.6 m in all of the considered recharge realizations.

3.4.3 Theory of analytical StorAge Selection function

The travel time is defined as the time spent by a moving element (either a water particle or a solute) in a control volume of a hydrologic system. In principle, the control volume can be defined at arbitrary spatial scales (i.e., from the molecular scale to the regional scale). Considering a hydrologic system in which the input flux (J) and the output fluxes ($Q_1, Q_2, ..., Q_n$) are known, each parcel of water within the system is tagged using its

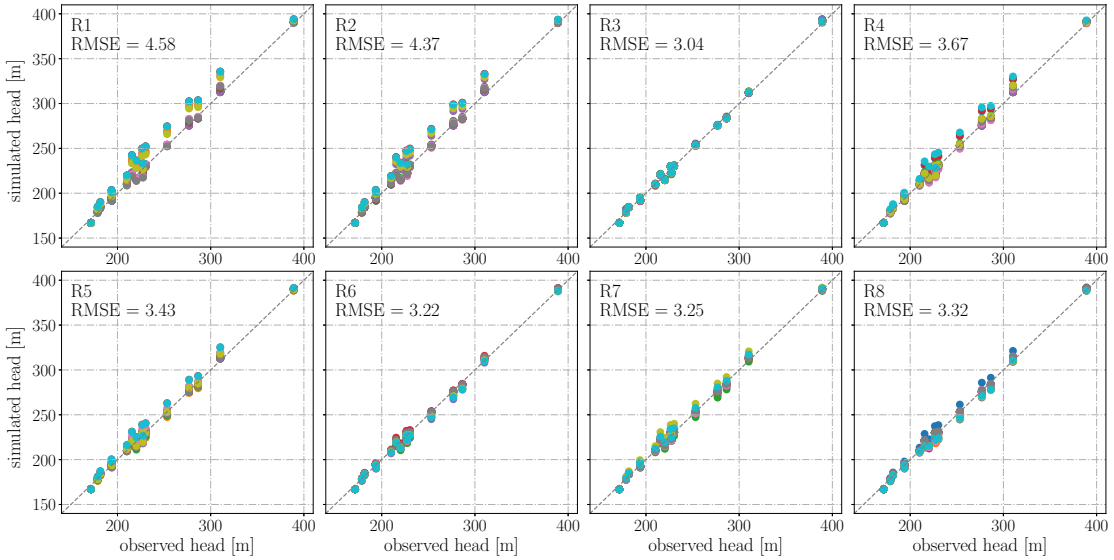

FIGURE 3.5: Observed and simulated groundwater heads for each parameter and recharge realization. The results of 400 realizations (R1K1 - R8K50) are categorized by recharge realization and shown in different panels.

current age τ. The age-ranked storage $S_T = S_T(T,t)$ is defined as the mass of water in the system with age $\tau < T$. The backward form of the master equation (ME) for TTD in a control volume can be expressed as follows [Botter et al., 2011, van Der Velde et al., 2012, Harman, 2015]:

$$\frac{\partial S_T}{\partial t} = J(t) - \sum_{j=1}^{n} Q_j(t) \overleftarrow{P}_{Q_j}(T,t) - \frac{\partial S_T}{\partial T} \tag{3.3}$$

with boundary condition $S_T(0,t) = 0$, where T is the residence time of the oldest water parcel in storage S_T; t is the chronological time; $\overleftarrow{P}_{Q_j}(T,t)$ is the cdf of the backward travel time distribution of output flux Q_j; $J(t)$ is the input flux at time t; and $Q_j(t)$ is the output flux at time t. Specifically in this study, J is the groundwater recharge, and Q is composed of two components: the stream baseflow and the abstraction at production wells.

The SAS function describes the fraction of water parcels leaving the control volume at time t, which is selected from the age-ranked storage S_T. Following the above definition, the SAS function can be linked with the backward travel time distribution $\overleftarrow{P}_Q(T,t)$ [Harman, 2015]:

$$\Omega_Q(S_T,t) = \overleftarrow{P}_Q(T,t) \tag{3.4}$$

for $S_T = S_T(T,t)$. Ω_Q is the cumulative form of the SAS function.

Three instances of SAS functions using gamma distribution are shown in Figure 3.9a. In case the age distribution of each outflow is uniformly selected from all water storages with various ages, the outflux TTDs turn into a random sample (RS) of the storage residence time distribution (RTD). The random sampling is equivalent to the uniform SAS function (Figure 3.9a). Many past studies have also considered the random sampling as a proper description of the sampling behavior for heterogeneous catchments [Cartwright and Morgenstern, 2015, Benettin et al., 2015, Heße et al., 2017]. Eq. (3.4) in this case has the analytical solution [Harman, 2015, Danesh-Yazdi et al., 2018]:

$$p_S(T,t) = \overleftarrow{p}_Q(T,t) = \frac{J(t-T)}{S(t)} \exp\Big[- \int_{t-T}^{t} \frac{Q(\tau)}{S(\tau)} d\tau \Big] \tag{3.5}$$

where $p_S(T,t)$ is the pdf of the residence time distribution and $S(t)$ is the storage at time t. Specifically, in the case of a steady-state hydrodynamic system, Eq. (3.5) is further simplified into an exponential form:

$$\overleftarrow{p}_Q(T) = \frac{J}{S} \exp\Big(- \frac{J}{S} T \Big) \tag{3.6}$$

Eq. (3.6) is the analytical solution of backward TTD under the RS assumption.

In the idealized saturated groundwater aquifer, Eq. 3.6 is equivalent to the analytical solution derived by Haitjema [1995]. Based on the Dupuit–Forcheimer's assumption, Haitjema [1995] derived a formula about the frequency distribution of residence time:

$$p_s(T) = \frac{1}{\overline{T}} \exp\Big(- \frac{T}{\overline{T}} \Big) \tag{3.7}$$

$$\overline{T} = \frac{nH}{J} \tag{3.8}$$

provided that nH/J is constant over the entire domain, the recharge is spatially uniform, and the aquifer is locally homogeneous, where n is the porosity, H is the saturated aquifer thickness, and $\overline{T}$ is the weighted mean travel time in the aquifer.

3.4.4 Linking the SAS functions to the physically based numerical model

Danesh-Yazdi et al. [2018] developed an approach to link the analytical SAS functions to the fully distributed numerical model. Although differing in numerical model and

particle tracking scheme, we apply the same approach to link the SAS functions and the numerical model in this study. Eq. (3.3) under the steady-state condition can be further simplified as

$$\frac{\partial S_T}{\partial T} = Q(1 - \Omega_Q(S_T)). \tag{3.9}$$

By combining Eq. (3.4) and Eq. (3.9), the age-ranked storage S_T can be calculated directly under the steady-state assumption:

$$S_T(T) = Q\Big(T - \int_0^T \overleftarrow{P}_Q(\tau)d\tau\Big). \tag{3.10}$$

Combining Eq. 3.10 with Eq. 3.4, the SAS function can be directly computed from the simulated backward TTD using the numerical model.

3.4.5 Predictive Uncertainty of TTDs

The theoretical framework of predictive uncertainty in this chapter is based on Doherty [2015]. As indicated in Bayes' theorem, the parameters of a model retain uncertainty, given that they have been adjusted to best-fit values achieved during calibration. Nevertheless, the uncertainty of parameters is subject to constraints. One of the constraints resides in the fixed adjustable range of parameters, in which expert knowledge must be respected. Another constraint is exerted by the parameterization process.

While the computationally expensive Bayesian approach offers a complete theoretical framework for predictive uncertainty evaluation, practical modeling efforts are often based on model calibration and a subsequent analysis of error or uncertainty in post-calibration predictions [Doherty, 2015]. Ideally, the best-fit parameters achieved through calibration can reduce the predictive error to a minimum, with the minimum predictive error being the inherent uncertainty. However, the best-fit parameter is always biased from the true parameter because the essential imperfection of the model may facilitate or hamper the achievement of the minimum. Therefore, the motivation of uncertainty analysis in this study is to quantify and minimize the predictive uncertainty of travel time distributions, given that the parameters are plausible and that the model can reproduce well the groundwater heads.

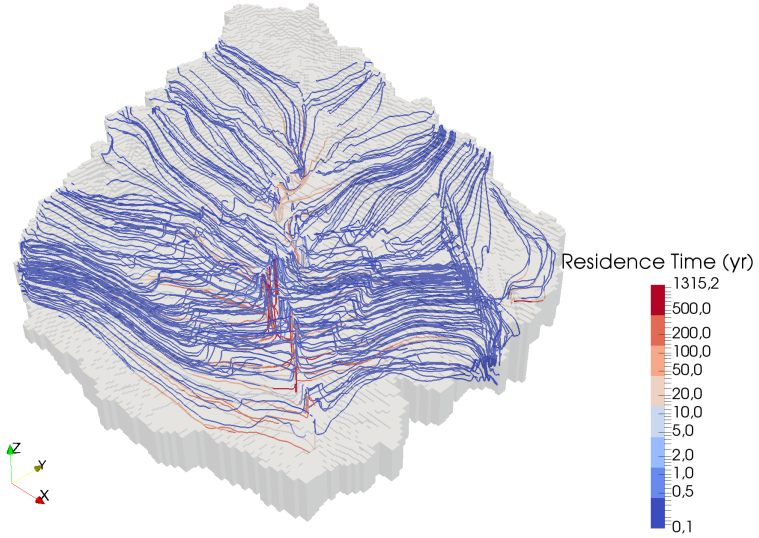

FIGURE 3.6: 3-D view of flow pathlines of some particles in realization R5K1. Note that only a limited number of particle pathlines are displayed here.

3.5 Results

For the sake of clarity, we number the recharge realizations from R1 (with the lowest recharge rate) to R8 (with the highest recharge rate). For each recharge realization, 50 K_s fields are numbered from K1 to K50. Accordingly, R1K1 represents K_s field K1 in recharge realization R1.

3.5.1 Uncertainty of TTD predictions

Flow paths of particle tracers in a random parameter realization (R5K1) are displayed in Figure 3.6, serving as a visual reference for the regional groundwater flow pattern and the residence time distributions. In this realization, the deep low-permeability geological layers (e.g., mm2 and mu2) act as low-permeability aquitards. Therefore, the majority of streamlines do not enter these geological layers (Figure 3.6).

Figure 3.7 displays both the simulated TTDs using 50 K_s fields for eight recharge realizations (orange solid lines) and the reference TTDs, represented by fit blue dash-dot curves using the exponential model (Eq. 3.6). The ensemble average (μ) and the coefficient of variation (c_v) of MTTs for each recharge realization are also calculated and shown in Figure 3.7. Note that if the number of parameter realizations is sufficiently large, the ensemble average of MTTs (μ) will converge to the simulation result using the best-fit parameters achieved through model calibration [Doherty, 2015]. Noticeable variability of

TTDs can be observed with respect to different recharge realizations. Generally, the μ values show a decreasing trend from 166.5 yrs in recharge realization R1 to 110.9 yrs in recharge realization R8, with only two exceptions (R3 and R6), which is not surprising based on the inversely linear dependency between recharge J and μ, indicated by Eq. 3.8. In each recharge realization, the different realizations of K_s fields manipulate the mean travel time. c_v varies from 7.81% (for R5) to 15.56% (for R3), indicating a modest degree of uncertainty propagated from K_s estimation to TTD prediction.

The exponential model under the RS assumption is fit to the ensemble-averaged TTD of numerical solutions (see the black lines in Figure 3.7) using Eq. 3.6. As shown in Figure 3.7, the shapes of numerically simulated TTDs significantly deviate from the exponential distribution under the RS assumption, indicating a nonuniform sampling behavior of different water ages. The TTDs of numerical simulations are more right-skewed than the analytical TTDs under the RS assumption. This phenomenon reveals that the catchment TTD cannot be replicated by the single random sampling store.

Based on Eq. 3.8, the "effective volume" of water involved in the transport process in the aquifer can be approximated. The effective volume of groundwater storage related to the transport process is calculated and shown in Table 3.2. The effective volumes of storage (S_{eff}) estimated by the numerical solutions range from 9.8 m to 12.0 m, whereas the S_{eff} estimated by the analytical solution range from 6.8 m to 7.5 m. The groundwater storage that contributes to the streamflow is significantly smaller than the total groundwater storage (48.3 m). This difference is because most of the released particles only exist in the upper permeable layers rather than being spread evenly over the whole aquifer-aquitard system. Note that this is only a first-order approximation because the analytical solution is only rigorously valid for the idealized homogeneous aquifer system [Haitjema, 1995].

Moreover, we assess the propagation to the MTT predictions from input and parameter uncertainty yielded by the eight recharge realizations and the Monte Carlo realizations of hydraulic conductivities. Figure 3.8a depicts the distribution of MTTs of the ensemble simulations. The MTTs of the 400 realizations range from 87 to 212 yrs. At the same time, the ensemble average of MTTs over all realizations of recharges and K_s fields ($\overline{\mathrm{MTT}}$) is 135.1 yrs, and the coefficient of variation is 18.93%. Figure 3.8b depicts the relationship between the ensemble average of MTTs and the spatially averaged recharge rates. A roughly inversely proportional relationship between the ensemble average of

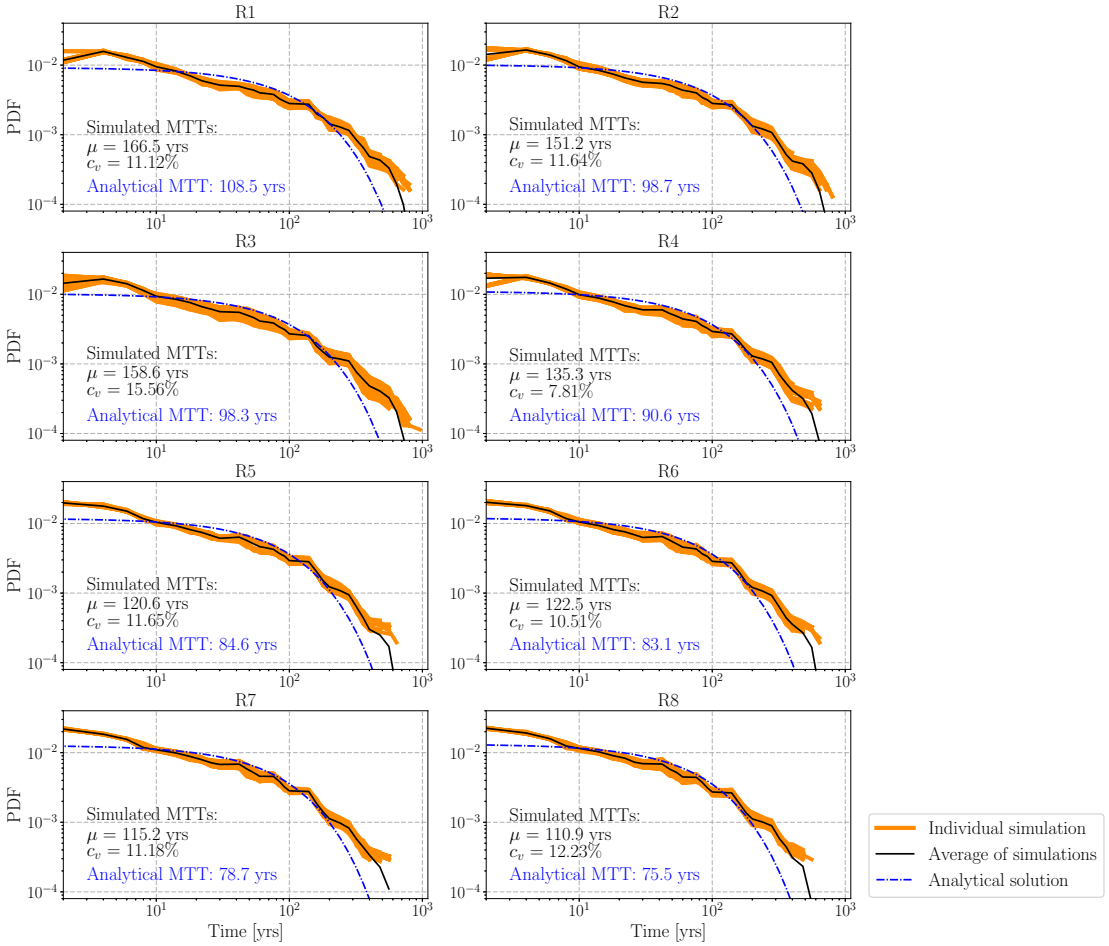

FIGURE 3.7: Travel time distributions of ensemble simulations and analytical solutions categorized by recharge realization. The orange lines show the simulated TTDs of all realizations of K_s fields for each recharge realization. The black lines denote the ensemble averaged TTDs of each recharge realization. The blue dash-dot line is the fit analytical TTD under the random sampling (RS) assumption. The analytical MTT, the mean (μ), and the coefficient of variance (c_v) of the simulated MTTs are also shown in this figure.

TABLE 3.2: Effective groundwater storages related to the transport process for each recharge realization.

	Effective volume of storage [m]								
	R1	R2	R3	R4	R5	R6	R7	R8	mean
S_{eff} (numerical)	10.7	10.6	12.0	10.5	9.8	10.2	10.2	10.6	10.6
S_{eff} (analytical)	6.9	6.9	7.5	7.1	6.8	6.9	6.9	7.2	7.0

MTTs and the spatially averaged recharge rates (Figure 3.8b) can be observed. The standard deviations (σ) of simulated MTTs range from 12.9 yrs (for R6) to 24.7 yrs (for R3).

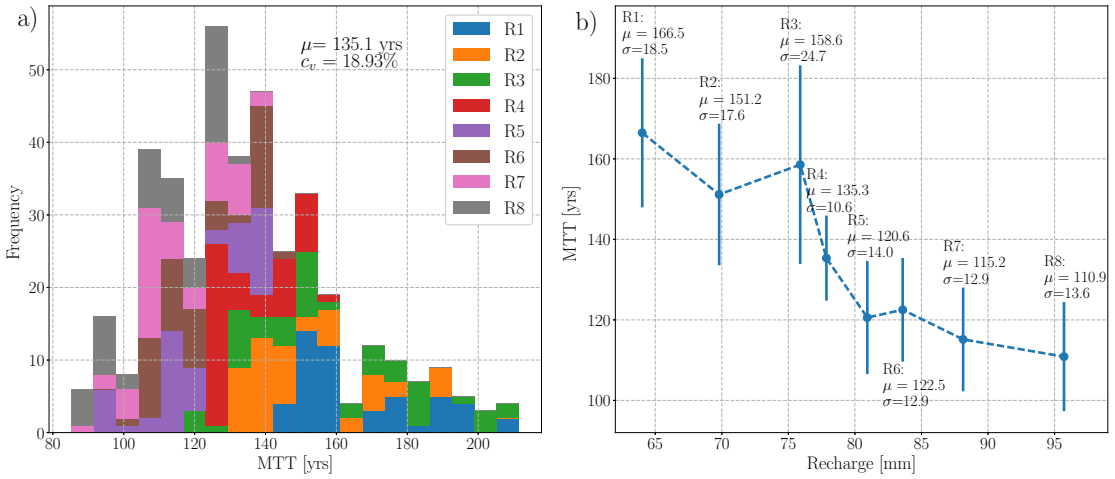

FIGURE 3.8: Uncertainty quantification: Monte Carlo simulations of MTT predictions categorized by recharge realization. Panel a) shows a histogram of MTT predictions. Panel b) shows the relationship between the ensemble averaged MTT (μ) and the spatially averaged recharge. The error bars represent the standard deviation of MTTs (σ) for each recharge realization.

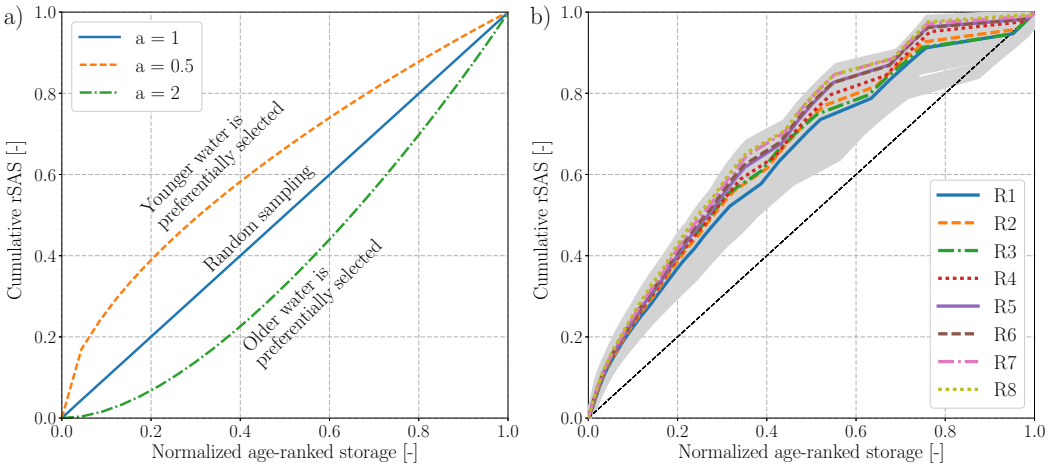

FIGURE 3.9: Cumulative rank SAS functions as a function of normalized age-ranked storage. (a) Schematic of cumulative rank SAS functions parameterized by gamma distribution with the shape parameter a = 0.5, 1, and 2. (b) Cumulative rank SAS functions of the ensemble simulations (light grey lines) and the ensemble average for each recharge realization.

3.5.2 Uncertainty of young/old water preference

Figure 3.9a provides an intuitive illustration of the relationship between the cumulative rank SAS functions and the systematic preference for discharging water with different ages. Figure 3.9b shows the cumulative rank SAS functions of all ensemble simulations (obtained from 400 realizations of K_s fields in 8 recharge scenarios). The figure is categorized into 8 groups by different colors and line styles, each representing a recharge realization. Generally, the system has a weak preference to select younger water as discharge, despite

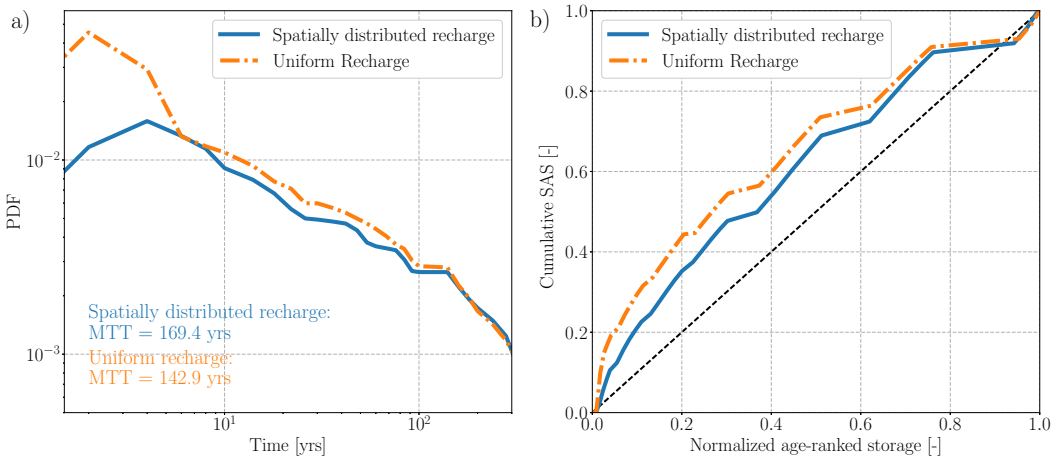

FIGURE 3.10: Sensitivity of a) TTDs and MTTs, and b) SAS functions to the spatial pattern of recharge.

different recharge realizations and K_s realizations. Nevertheless, a moderate variation in SAS functions for the ensemble simulations can be observed. The variation of interest is introduced by the spatial distribution and velocity of flow pathlines that are controlled by different K_s fields. For example, a more permeable shallow aquifer layer will activate more flow pathways in this layer and thus will introduce a stronger preference for young water. In particular, the significant variation in hydraulic conductivities in the deepest geological layer (e.g., Lower Muschelkalk) has a pronounced impact on the discharge of old water. With a thickness of up to 100 m, the hydraulic conductivity of this layer controls how many water parcels can enter into this layer and how deep the flow paths can develop. This effect can be evidenced by a large difference in the SAS functions related to old ages and a relatively smaller difference in those related to young ages in Figure 3.9b.

3.5.3 Sensitivity to the spatial pattern of recharge

Figure 3.10a depicts the sensitivity of simulated TTDs and mean travel times (MTTs) to the spatial distribution of recharge, while Figure 3.10b shows the sensitivity of the cumulative SAS function to the spatial pattern of recharge. The reference simulation is set up using the spatially uniform recharge that is equal to the spatial average of the spatially distributed recharge, while all of the other parameters in these two simulations are held identical. The different spatial distributions of recharge have a clear effect on the shape of TTDs. It appears that the most evident difference between the TTDs

of the two recharge scenarios occurs at the early period. Additionally, the simulated MTT using the uniform recharge appears to be smaller than that using the spatially distributed recharge. Figure 3.10b indicates that the simulation using uniform recharge has a consistently stronger preference for sampling young water than the simulation using spatially distributed recharge. Nevertheless, both scenarios show a general preference for young water. This phenomenon further underlines the dependency of SAS functions on the spatial pattern of recharge and the importance of reliable characterization of the spatial distribution of recharge for the TTD estimation.

The difference in TTDs and SAS functions is not induced by the variability in internal hydraulic properties, since the two simulations share the same K_s field. Rather, it is mainly induced by the different flow paths of particle tracers in the two recharge scenarios. The spatially distributed recharge simulated by mHM reveals that the upstream mountainous area has higher recharge rates than those in the lowland plain. By contrast, the uniform recharge scenario neglects this spatial nonuniformity. This difference results in the following: (a) under a uniform recharge scenario, more particle tracers enter the system from locations near the streams at lowland plains (Figure 3.3b), indicating that more particle tracers are transported in the local flow system rather than in the regional flow system [Toth, 1963]; and (b) higher recharge rates at lowland plains accelerate the particles' movement in this area and shorten their travel times. As such, local particle flow paths within the shallow aquifer layer at lowland plains are activated, leading to a stronger preference for sampling local flow paths in shallow aquifer layers and therefore a stronger preference for young ages. Our findings are in line with the observations by Kaandorp et al. [2018], wherein the authors found a relatively higher preference for the selection of older water in the upstream area than that in the downstream area of the Springendalse Beek catchment.

3.6 Discussion

3.6.1 Uncertainty of external forcing, internal property, and TTD predictions

In the idealized aquifers where groundwater flow is of the Dupuit–Forchheimer type, the recharge is uniform, and the aquifer is locally homogeneous. TTD is controlled by recharge,

saturated aquifer thickness, and porosity, and it is independent of hydraulic conductivity [Haitjema, 1995]. In a real-world catchment with complex geometry and topography, stratigraphic aquifers, and nonuniform recharge, our numerical exploration demonstrates that the groundwater TTD is dependent on both recharge and the hydrostratigraphic K_s field.

The mechanisms behind the effects of the recharge rate and the K_s field are different. Given that the spatial pattern of recharge remains the same, a higher recharge rate intensifies the fluxes for the complete range of flow pathways. This process forces water downward in the recharge zones and upward to the discharge area. As such, flow rates through all flow pathways are increased equally, and the spatial distribution of flow pathways is not changed. The corresponding SAS function is also not changed [Botter et al., 2010, Cartwright and Morgenstern, 2015, Kaandorp et al., 2018]. In contrast, a different K_s field activates flow pathways in more permeable layers, deactivates flow pathways in less permeable layers, changes the spatial distribution of flow pathways, and therefore changes the shape of the SAS function [Harman et al., 2016, Kim et al., 2016].

The value of observational data in reducing predictive uncertainty in simulated TTDs is also underlined. In this study, the majority of model parameters can be adequately conditioned by spatially distributed groundwater head observations (Figure 3.4). Provided that most of the hydraulic conductivities are constrained to the model-to-measurement misfit and reality, the TTD predictions can also be effectively bounded. This is evidenced by Figure 3.7, from which moderate values of c_v ranging from 7.81% to 15.56% in different recharge realizations can be observed. The ensemble-averaged MTTs for different recharge realizations also have a high c_v (15.70%), implying that the TTD prediction appears highly sensitive to recharge. Our findings are in line with Danesh-Yazdi et al. [2018], in which the interplay between recharge and subsurface heterogeneity was investigated and a strong dependency of TTDs on the recharge was observed.

3.6.2 Analytical model and SAS functions

The analytical solution of TTD, assuming a random sampling of water, cannot properly replicate the TTD of numerical simulation in the study domain. In the stratigraphic aquifer with complex topography and diffuse recharge, the analytical solution using Eq. 3.6 underestimates the MTT. Note that this conclusion holds when the simulated TTD has

a relatively larger long-tail behavior than the exponential distribution. Such observations have also been reported for other real-world aquifers [Basu et al., 2012, Eberts et al., 2012, Kaandorp et al., 2018]. This finding can be seen as an extension of Basu et al. [2012], in which the authors found a moderate discrepancy between the analytical solution using Eq. 3.6 and the numerical solution in a small catchment.

It is obvious that the analytical solution under the RS assumption cannot explicitly include the impact of the distributed hydraulic properties of stratigraphic aquifers and the spatially nonuniform recharge. The above limitations of analytical models may introduce a significant predictive error for the TTD predictions, as shown in Figure 3.7. Moreover, the effective volume of storage related to the transport process S_{eff} is calculated utilizing the numerical solutions of distributed models. As a first-order approximation of effective storage volume, it suggests that only a small fraction of total groundwater volume is involved in the active hydrologic cycle.

The SAS function provides a good interpretability for simulation results using the fully distributed model in terms of characterizing the preference for releasing water of different ages. It can be found that the SAS functions are weakly dependent on the K_s fields in the stratigraphic aquifer system, but the overall preference for young water does not change. This weak dependency can be explained by the fact that different realizations of K_s fields modify the spatial distribution of particle flow paths. The overall tendency for young groundwater in the saturated aquifer has been reported by many past studies [Danesh-Yazdi et al., 2018, Kaandorp et al., 2018, Yang et al., 2018]. Our study links the explicit simulations of travel times and the analytical SAS functions and offers original insights into the uncertainty propagated from recharge and the K_s fields to the SAS functions.

3.6.3 Dependency of TTDs and SAS functions on the spatial pattern of forcings

The sensitivity of the TTDs and SAS functions to the spatial patterns of recharge forcings can be explained mainly by the different flow paths of particle tracers, resulting primarily from the spatially heterogeneous fields of recharge across the study catchment. For the regional groundwater system, the spatial variation of recharge determines the distribution of starting points of the flow pathlines of tracer particles. For example, more

particles will be injected from recharge zones that are typically located in high-elevation regions, resulting in a higher weight of flowlines starting from high-elevation regions. The pronounced spatial variability of recharge also controls the systematic (water age) preference for particles existing from the system (to river discharge) that originated from different regions and therefore exerts a strong control on the shape of the SAS function.

In the study catchment, an oversimplified spatially uniform recharge results in a smaller mean travel time and a stronger preference for discharging young water compared to those taking the spatial variability of recharge. Such observations are conditioned to site-specific features of the study catchment, which is noticed only when the following apply: (a) a site is located in a headwater catchment under a humid climate condition; (b) the recharge rate in areas close to the drainage network is generally lower than that in areas far away from the drainage network; and (c) the system is under (near) natural conditions, meaning that artificial drainage and pumping do not dominate the groundwater budget.

The assumption of spatially uniform input forcing has been widely applied in regional-scale subsurface hydrologic models [Zghibi et al., 2015, Yang et al., 2018]. Our study indicates that a reasonable characterization of spatial pattern of recharge is crucial for reliable TTD prediction. Unfortunately, it is quite challenging to confidently quantify the groundwater recharge at the regional scale under today's technique due to the lack of reliable measurements [Healy, 2010, Cheng et al., 2017, Zink et al., 2017]. Appropriate techniques should be chosen to estimate groundwater recharge according to the study goals and the spatial and temporal scales.

3.6.4 Implications for the applied groundwater modeling

Uncertainty limits the applicability of groundwater models. Most of the applied groundwater models are deterministic models that use direct values of inputs and parameters instead of probabilistic distributions of them. Specifically, both the model inputs and the inversion process are deterministic, leading to a deterministic best-fit parameter set achieved during model calibration. Our study reveals limitations of the above modeling procedure and suggests that the probabilistic distribution of inputs and parameters should be considered for the applied modeling. The main limitation is that the single exclusive assignment of recharge is inadequate for the simulation of transport processes because the error can be propagated from inputs to the conditioned parameters (e.g., hydraulic

conductivities) through the calibration process (Figure 3.4). This accumulated error will further lead to a seriously biased prediction of travel times. Additionally, the modeling workflow used in this study is computationally more efficient than the Bayesian approach and is suitable for complex real-world applications.

The degree of predictive uncertainty is highly dependent on the parameterization scheme. Some highly parameterized models are potentially ill posed due to the paucity of data and therefore cannot be constrained by the available calibration dataset. In this case, the predictive uncertainty of TTDs is potentially high [Weissmann et al., 2002, Danesh-Yazdi et al., 2018]. Stratigraphic aquifer models with zoned parameters are still widely used for the applied groundwater modeling because the field representation of local-scale heterogeneity is difficult. Given that the aquifer model is stratigraphic and the number of parameters is less than the number of observations, most of the adjustable parameters can be effectively bounded. In this case, the uncertainty of input data (e.g., recharge) appears to have a primary influence on the TTD predictions. Note that here we do not account for the error caused by model structural deficiency.

3.7 Conclusions

In this study, we explore the relationship between the uncertainty of recharge, calibration-constrained hydraulic conductivity realizations, and predictions of groundwater TTDs. Using both a physically based numerical model and a lumped analytical model, a comprehensive case study is performed in an agricultural catchment (the Nägelstedt catchment). The RWPT method is used to track the water samples through the modeling domain and compute their travel times. Moreover, the analytical model is fit against the numerical solutions to provide a reference for the effective storage and sampling behavior of the system. Based on this study, the following conclusions are drawn:

1. In the Nägelstedt catchment model, the simulated MTTs are strongly dependent on the recharge rate and weakly dependent on the postcalibrated K_s field. We highlight the importance of recharge quantification and the worth of reliable data in reducing the predictive uncertainty of TTDs.

2. The framework of the SAS function provides a good interpretability of simulated TTDs in terms of characterizing the systematic preference for sampling young/old

water as outflow. On the basis of this framework, we find that the ensemble simulations have a consistent preference for young water, despite the different recharge and hydraulic conductivity realizations. Our study provides a novel modeling framework to explore the effect of input uncertainty and parameter equifinality on TTDs and SAS functions through a combination of calibration-constrained Monte Carlo parameter generation, a numerical model, and a SAS function framework.

3. Both the shape and the breadth of catchment groundwater TTDs and SAS functions are sensitive to the spatial distribution of recharge. Therefore, a reasonable characterization of the spatial pattern of recharge is crucial for the reliable TTD prediction in the catchment-scale groundwater models.

Chapter 4

Assessing the response of groundwater quantity and travel time distribution 1.5, 2 and 3 degrees global warming in a mesoscale central German basin

Acknowledgements

This study was partially performed under a contract for the Copernicus Climate Change Service (edge.climate.copernicus.eu). ECMWF implements this service and the Copernicus Atmosphere Monitoring Service on behalf of the European Commission. This work is also supported by the Deutsche Forschungsgemeinschaft via Sonderforschungsbereich (CRC 1076 AquaDiva) and the German Ministry for Education and Research within the scope of the HOKLIM project (www.ufz.de/hoklim; grant number 01LS1611A). We acknowledge Sabine Sattler from Thuringian State Office for the Environment and Geology (TLUG) for providing geological data. We also acknowledge people from various organizations and projects for the datasets that are used in this study, which include ISI-MIP, JRC, NASA, GRDC, BGR, and ISRIC. We acknowledge the Chinese Scholarship Council (CSC) for supporting Miao Jing's work.

published as:

Jing, M., Kumar, R., Heße, F., Thober, S., Rakovec, O., Samaniego, L., and Attinger, S.: Assessing the response of groundwater quantity and travel time distribution to 1.5, 2 and 3 degrees global warming in a mesoscale central German basin, Hydrol. Earth Syst. Sci. Discuss., https://doi.org/10.5194/hess-2019-9, in review, 2019.

4.1 Abstract

Groundwater is the biggest single source of high-quality freshwater worldwide, which is also continuously threatened by the changing climate. This paper is designed to investigate the response of the regional groundwater system to climate change under three global warming levels (1.5, 2, and 3 °C) in a central German basin (Nägelstedt). This investigation is conducted by deploying an integrated modeling workflow that consists of a mesoscale Hydrologic Model (mHM) and a fully-distributed groundwater model OpenGeoSys (OGS). mHM is forced by five general circulation models under three representative concentration pathways. The diffuse recharges estimated by mHM are used as outer forcings of the OGS groundwater model to compute changes in groundwater levels and travel time distributions. Simulation results indicate that under future climate scenarios, groundwater recharges and levels are expected to increase slightly. Meanwhile, the mean travel time is expected to decrease compared to the historical average. However, the ensemble simulations do not all agree on the sign of relative change. The ensemble simulations do not show a systematic relationship between the projected change and the warming level, but they indicate an increased variability in projected changes with the enhanced warming level from 1.5 to 3 °C. The predictive uncertainties related to climate projections are more pronounced than that related to hydraulic conductivity fields. Our results imply that higher warming levels may introduce more uncertain and extreme events for the studied regional groundwater system. Correspondingly, it is highly recommended to restrain the trend of global warming.

4.2 Introduction

The availability, sustainability, and quality of water resources are threatened by many sources, among which the changing climate plays a critical part [Stocker, 2014]. A significant sign of climate change is global warming, which has been evidenced by the analysis of long-term air temperature records. Not only the earth's surface temperature shows a constant warming trend, but the sea surface temperature has also increased [Stocker, 2014]. There has been adequate proof that the massive greenhouse gas emissions since the eighteenth century accelerate the global warming process [Stocker, 2014]. Consequently, it is urgently needed to estimate the change of meteorological variables

(e.g., precipitation and temperature) in the future global warming scenarios. General circulation models (GCMs) combined with different emission scenarios or representative concentration pathways (RCPs) have been widely employed for climate impact study [Collins et al., 2013, Thober et al., 2018, Marx et al., 2018].

Climate change may significantly alter the pattern of terrestrial hydrological processes, influence the spatial and temporal behavior of shallow water storages, and manipulate the degree and frequency of extreme events such as floods and droughts [van Roosmalen et al., 2009, Sridhar et al., 2017, Thober et al., 2018, Marx et al., 2018]. Hydrological processes and states (e.g., evapotranspiration, soil moisture, and potential recharge) are tightly coupled with the current climate and meteorological variables (e.g., precipitation, humidity, atmosphere temperature). The impact of climate change on the terrestrial water cycle is, unfortunately, uncertain. Climate model projections show a good consistency in future global averaged trends but may disagree on the magnitude of regional-scale variables, particularly when precipitation projection is involved in [Meehl et al., 2007]. Many past studies devote to estimate the control and uncertainty of climate change on hydrological states and fluxes [Hunt et al., 2013, Samaniego et al., 2018, Renée Brooks et al., 2010, Hattermann et al., 2017, Goderniaux et al., 2009]. Among them, some studies indicate that the frequency and intensity of extreme events (e.g., soil moisture drought, heatwave) may be exacerbated owing to anthropogenic warming [Samaniego et al., 2018, Kang and Eltahir, 2018, Marx et al., 2018]. The global water scarcity is likely to be exacerbated due to the potential decline in freshwater resources under the 2 °C global warming scenario [Schewe et al., 2014].

As the single biggest source of the world's fresh water supply, groundwater plays a critical role in the sustainability of the terrestrial ecosystem and the environmental consequences of climate variability. Globally, groundwater makes up 35% of the total freshwater withdrawals, constituting approximately 36%, 27% and 42% of water consumption for households, manufacturing, and agriculture, respectively [Döll et al., 2012]. Although the general knowledge of scale-dependent hydraulic properties of the subsurface hydrologic systems is still quite limited, they prove to be increasingly influenced by anthropogenic factors [Küsel et al., 2016]. The worldwide groundwater system can be affected by climate variability directly by a change in recharge or indirectly by a change in groundwater abstraction [Taylor et al., 2012]. Furthermore, these effects may be adjusted through

anthropogenic activities such as land-use change. Many recent studies devoted to evaluating the impact of climate change on groundwater availability [Engdahl and Maxwell, 2015, Goderniaux et al., 2015, Jackson et al., 2011, Taylor et al., 2012, van Roosmalen et al., 2009, Stisen et al., 2011, Woldeamlak et al., 2007, Maxwell and Kollet, 2008, Havril et al., 2017]. These past studies often use coupled climate-land-surface-subsurface models to investigate the potential response of groundwater storages to the outer forcings under different climate scenarios. Compared with the land surface processes, the groundwater reservoir is less vulnerable to extreme events [Maxwell and Kollet, 2008]. The slow response of groundwater to meteorological variability can be explained by the highly dynamic surface water/groundwater interaction, the existence of a variably thick unsaturated zone, and the big volume of groundwater storage. Quantification of uncertainty in future water resource projections and travel times (decades to centuries) of the regional groundwater system is critically important for regional water sustainability.

Due to the diverse patterns of the terrestrial water cycle in regions under different climate conditions, climate change will have diverse impacts on the groundwater recharge change. Sandström [1995], for instance, found that in Tanzania, a 15% decline in precipitation, without any change in air temperature, will result in a 40-50% decline of groundwater recharge, indicating a potential amplified change of recharge compared to that of precipitation. While some studies found an increasing trend of recharge [Brouyère et al., 2004, van Roosmalen et al., 2009], others indicate that climate change is likely to lead to decreased recharge rates [Pulido-Velazquez et al., 2015, Woldeamlak et al., 2007, Havril et al., 2017]. The changes of recharge, regardless of the sign of change, will significantly influence the groundwater levels and may lead to ecological problems such as the vanishing of wetlands [Havril et al., 2017]. Modification of groundwater recharge will control the flow paths and travel times of pollutants, which is critical to the sustainability of the regional groundwater system. Moreover, the modification of groundwater recharge can change the age distribution for water in both the vadose zone and the saturated zone, as well as significantly change the composite age distribution [Engdahl and Maxwell, 2015].

Groundwater travel time distribution (TTD) is a robust description of the storage and transport dynamics within aquifers under various external forcings. It has many implications for hydrogeological and environmental studies. For instance, significant time-lags of the streamflow response to external forcings have been observed by multiple

studies [Howden et al., 2010, Stewart et al., 2012]. Besides, the legacy pollutants in groundwater reservoirs can have a great impact on the total pollutant loads for agricultural catchments [Wang et al., 2016, van Meter et al., 2017]. Groundwater TTD, as a lumped description of the heterogeneous aquifers, sheds light on the assessment of groundwater responses to non-point source contamination subjected to a changing climate and land use [Böhlke, 2002, Engdahl and Maxwell, 2015].

Although there are plenty of studies that have focused on assessing the impact of future climate change on groundwater recharge [Tillman et al., 2016, Crosbie et al., 2013, Jyrkama and Sykes, 2007, Pulido-Velazquez et al., 2015], groundwater budget [Pulido-Velazquez et al., 2015, Engdahl and Maxwell, 2015, Havril et al., 2017], and groundwater-surface water exchange [Scibek et al., 2007, Smerdon et al., 2007], there is an absence of a systematic evaluation of both the groundwater quantity and TTDs under different warming levels that incorporates the uncertainties in both climate projection and hydrological parameterization. In this study, we analyze the response of groundwater (quantity and travel time distributions) to the 1.5, 2, and 3 °C global warming levels (above the preindustrial levels) in a central German basin (Nägelstedt) using a coupled hydrological model mHM-OGS. The key questions we aim to answer are: (1) How can the flow and transport conditions of a regional groundwater system in future decades differ from the historical period for various possible warming levels? (2) Can we quantify the degree of different uncertainty sources (e.g., uncertainties in climate projections and groundwater models) and their influences on the final simulation results? To answer these questions, we pay particular attention to the assessment of the long-term effect of climate change on the regional groundwater systems considering the buffering effect of groundwater aquifers.

This paper is organized into several sections, with each of them serving its function. Section 4.3 describes the basic topographical, geometrical, and geological properties of the study area. Section 4.4 introduces the methodology and materials for this study. Section 4.5 shows the setup and validation for the mHM and OGS models. The simulation results are presented in Section 4.6. A comprehensive discussion on the simulation results is displayed in Section 4.7 and the main conclusions are drawn at the end of this section.

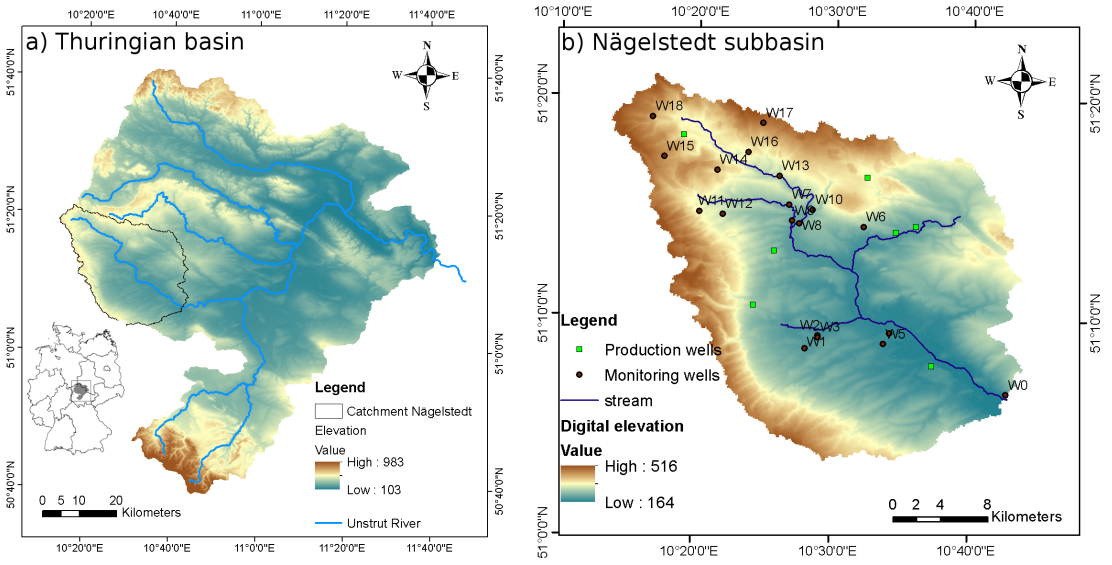

FIGURE 4.1: Study area and locations of pumping and monitoring wells within the Nägelstedt basin. Panel a) shows the relative position of Nägelstedt basin in the Thuringian basin, and Panel b) shows the locations of pumping and monitoring wells in Nägelstedt basin.

4.3 Study Area

As a sub-basin of the Thuringian basin, the Nägelstedt basin is located in central Germany and it has an area of about 850 km^2 (Figure 4.1). It is a headwater catchment of the Unstrut river. The Unstrut river is a typical, meandering lowland river with only moderate flow velocity under natural conditions. The mountains surrounding the Nägelstedt basin drain almost simultaneously into the Unstrut during heavy precipitation events, which in the past led to regular, prolonged flooding of large parts of the floodplains. The topographic elevations of this catchment range from 164 m at the southeastern lowland to 516 m in the Hainich mountainous region. This region is classified as a Cfb climate region based on the Köppen-Geiger classification, where Cfb stands for warm temperate, fully humid, and warm summer climate [Kottek et al., 2006]. It shows a leeward decreasing trend of areal precipitation and rising mean air temperature from the eastern Hainich ridge to the Unstrut Valley [Kohlhepp et al., 2017]. In the larger Thuringian basin, groundwater has been intensively extracted for domestic, industrial and agricultural uses. About 70% of the freshwater requirement for Thuringia is satisfied by groundwater [Wechsung et al., 2008].

The extremely fertile soils in the meadows (wet black soil and loess) make the Thuringian basin one of the best agricultural basins in Germany. Approximately 88% of the total

land use of this region is regarded as arable land [Wechsung et al., 2008]. At the same time, the proportion of woodland and grassland has fallen sharply, leading to an extreme reduction in biodiversity in these areas [Wechsung et al., 2008]. The nitrogen inputs from agriculture fluctuate with time and positions from 5 kg/ha to 31 kg/ha [Wechsung et al., 2008].

The stratigraphy in this area is characterized by a succession of carbonate–siliciclastic alternations. The main aquifer system consists of several sedimentary rocks, including the Middle Keuper (km), the Lower Keuper (ku), the Upper Muschelkalk (mo), the Middle Muschelkalk (mm), and the Lower Muschelkalk (mu) [Seidel, 2003]. The Middle Keuper consists of a marly series with gypsum and dolomite, whereas the Lower Keuper is constituted of grey clays, schieferletten, and dolomitic limestone. The Upper Muschelkalk (Hauptmuschelkalk) is mainly made up of shelly limestone, marl and dolostone. The Middle Muschelkalk consists mainly of evaporites (gypsum, anhydrite, and halite), meanwhile, the Lower Muschelkalk consists of limestone and marls [Seidel, 2003, McCann, 2008, Jochen et al., 2014]. Karstification occurs in the Muschelkalk formation, but has proved to be limited or concentrated in specific zones in this area [Kohlhepp et al., 2017].

The Nägelstedt basin is chosen as the study area for the following reasons: (1) It is a typical agricultural basin where potential non-point source contamination may threaten the sustainability and resilience of groundwater, and (2) the critical zone (CZ) in Nägelstedt basin has been comprehensively investigated using infrastructure platform from the Collaborative Research Center AquaDiva [Küsel et al., 2016, Kohlhepp et al., 2017].

4.4 Methodology and Materials

To investigate the impact of different climate change scenarios, we modified the modeling framework originally developed by Thober et al. [2018] and Marx et al. [2018] from EDgE and HOKLIM projects through coupling it to a three-dimensional subsurface model. Specifically, we use temperature and precipitation derived from five GCMs under three different RCPs to force the mesoscale Hydrologic Model (mHM), aiming to derive the land surface fluxes and states under different future warming scenarios. The projected recharges from mHM calculations are fed to the groundwater model OpenGeoSys (OGS) for the assessment of groundwater quantity and travel time distributions.

4.4.1 Climate scenarios

We use five General Circulation Models (GFDL-ESM2M, HadGEM2-ES, IPSL-CM5A-LR, MIROC-ESMCHEM, and NorESM1-M) gathered from the Coupled Model Intercomparison Projects 5 (CMIP5) to provide the climate variables to the mHM model. Temperature and precipitation are derived from these GCMs under three representative concentration pathways (RCPs; RCP2.6, RCP6.0, and RCP8.5), which are available from ISI-MIP project [Warszawski et al., 2014]. RCPs are representations of emission scenarios, with RCP2.6, RCP6.0, and RCP8.0 representing low, medium, and high emission scenarios, respectively. This multimodel ensemble approach enables the consideration of uncertainty in climate modeling. Climate variables from GCMs are further downscaled to a 0.5 °C spatial resolution employing a trend-preserving bias correction approach [Hempel et al., 2013]. The trend-preserving bias correction approach is capable of representing the long-term mean and extremes of catchment state variables [Hempel et al., 2013]. The 0.5-degree data is further interpolated into 5×5 km^2 grids through the external drift kriging (EDK) approach. The EDK approach can incorporate altitude effects at the sub-grid scale and has been successfully used in many past studies [Wood et al., 2011, Zink et al., 2017, Thober et al., 2018].

We use the period 1971–2000 to represent current climate conditions because 1991–2000 is the latest decade that is available in the GCM data. The GCM data from this period serves as a baseline scenario for the future projection of climate change. A time-sampling approach is applied to estimate the period for different global warming levels of 1.5, 2, and 3 °C [James et al., 2017]. The five GCMs have different degrees of climate sensitivity due to the different climate projections, therefore providing different meteorological forcings to the mHM model. Specifically, different periods of 1.5, 2, and 3 °C global warming are estimated by five GCMs under three RCPs (Table 4.1). We note that some combinations of GCMs and RCPs cannot be identified for the future climate projection before 2099, resulting in a total of 35 GCM/RCP combinations being used in this study (Table 4.1).

4.4.2 The mesoscale Hydrologic Model (mHM)

The disaggregated meteorological data are used as meteorological forcings of the mesoscale Hydrological Model (mHM) for a daily simulation. mHM is a spatially explicit distributed

TABLE 4.1: Time periods of 1.5, 2, and 3 °C global warming in five GCMs under three RCPs.

Warming level	RCPs	GFDL-ESM2M	HadGEM2-ES	IPSL-CM5A-LR	MIROC-ESM-CHEM	NorESM1-M
1.5 °C	2.6	-	2007–2036	2008–2037	2006–2035	2047–2076
	6.0	2040–2069	2011–2040	2009–2038	2012–2041	2031–2060
	8.5	2021–2050	2004–2033	2006–2035	2006–2035	2016–2045
2 °C	2.6	-	2029–2058	2060–2089	2023–2052	-
	6.0	2060–2089	2026–2055	2028–2057	2028–2057	2054–2083
	8.5	2038–2067	2016–2045	2018–2047	2017–2046	2031–2060
3 °C	2.6	-	-	-	-	-
	6.0	-	2056–2085	2066–2095	2055–2084	-
	8.5	2067–2096	2035–2064	2038–2067	2037–2066	2057–2086

hydrologic model that applies grid cells as primary hydrologic units, and accounts for multiple hydrological processes including infiltration, surface runoff, evapotranspiration (ET), soil moisture dynamics, snow accumulation and melting, groundwater recharge, and discharge generation. mHM is forced by hourly or daily meteorological forcings (e.g., precipitation and temperature), and uses accessible physical characteristics including soil textural, vegetation, and geological properties to estimate the spatial variability of parameters using its unique Multiscale Parameter Regionalization (MPR) technique [Samaniego et al., 2010, Kumar et al., 2013a]. The MPR technique is capable of coping with fine-scale features because the effective model parameters are regionalized based on the underlining subgrid-scale information using a consistent upscaling algorithm. The mHM simulations have been successfully established across Europe, and the simulated land surface fluxes have been verified by eddy-covariance stations across Germany [Zink et al., 2017].

4.4.3 OpenGeoSys (OGS)

The porous media simulator OpenGeoSys (OGS) is used to simulate regional groundwater flow and transport processes. OGS has been successfully coupled to mHM through a coupling interface – mHM-OGS [Jing et al., 2018]. The coupling interface interpolates the grid-based recharge produced by mHM into the nodal recharge values spreading over the top surface of OGS-mesh. In doing so, mHM and OGS are dynamically coupled as a surface-subsurface model such that the potential recharge produced by mHM can be fed to OGS and serves as the outer forcing of the groundwater module [Jing et al., 2018]. Specifically in this study, we feed the projected 5×5 km^2 recharge from mHM under future

climate scenarios to the coupling interface (mHM-OGS) to force the groundwater model. OGS is based on the finite element method (FEM) and solves the partial differential equations (PDEs) of fluid flow through linear/non-linear numerical solver. OGS is capable of simulating single processes including saturated zone flow, unsaturated zone flow, and solute transport, as well as coupled processes including saturated/unsaturated flow, multi-phase flow, and reactive transport. Specifically in this study, OGS is used to compute three-dimensional saturated zone flow.

Moreover, a Lagrangian particle tracking method – namely random walk particle tracking (RWPT) – is used to track flow pathways and compute travel time distributions of water parcels [Park et al., 2008a,b, Jing et al., 2019a]. The RWPT method assumes that the advection process is deterministic, while the diffusion/dispersion processes are modeled stochastically [Park et al., 2008a]. The RWPT method has been widely used to account for reactive transport processes and travel times [Park et al., 2008b, Jing et al., 2019a, Engdahl, 2017].

4.5 Model setup

We designed two parallel numerical experiments to investigate the effect of uncertainties in both the climate and groundwater models on the groundwater resources. For the evaluation of climate uncertainty, 35 GCM/RCP pairs are used, whereas only one parameter set is used for the groundwater model. In parallel, to assess the parameter uncertainty in the groundwater model, one sole climate scenario is used, whereas many realizations of parameters constrained by the observations are used for the groundwater model. This climate scenario is produced by calculating the ensemble average of all 35 members of climate scenarios.

4.5.1 mHM model setup

Fed by the five GCMs, the down-scaled meteorological dataset with a spatial resolution of 5×5 km^2 is used as the outer forcing of mHM. The model is set up across Europe using land-use dataset and is forced with spatially distributed meteorologic observations obtained from the E-OBS dataset [Haylock et al., 2008]. Global parameters of mHM are calibrated against discharge observations using the GRDC database. All ensemble

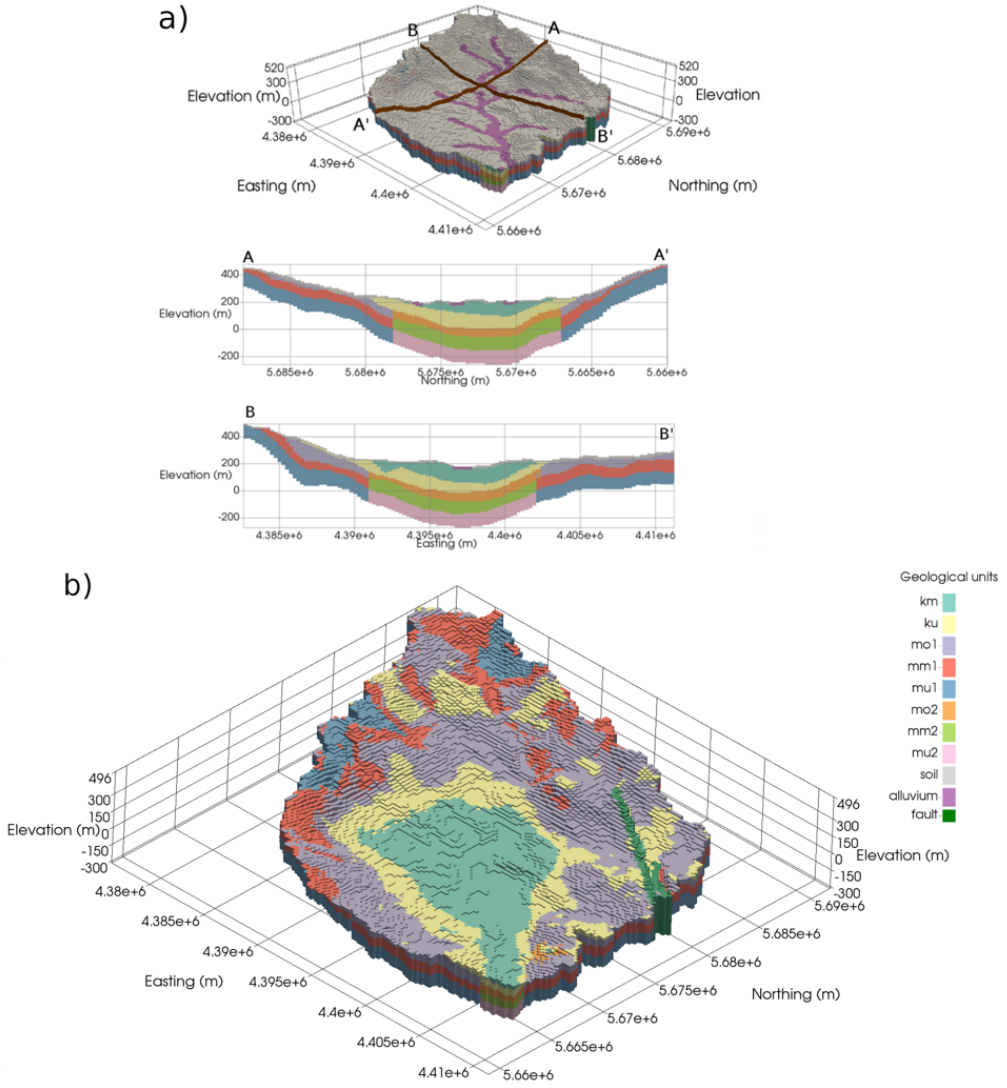

FIGURE 4.2: Geological zonation and three-dimensional mesh for the aquifer system in Nägelstedt basin [Jing et al., 2018]. Panel (a) underlines the spatial pattern of alluvium and soil layers. Panel (b) further displays the zonation of deep geological units. Full names of legends are listed as follows: km – Middle Keuper, ku – Lower Keuper, mo – Upper Muschelkalk, mm – Middle Muschelkalk, mu – Lower Muschelkalk.

simulations are established with the same morphological, land use, and soil type data to keep the relevant parameters consistent throughout this study. Furthermore, the mHM model was validated using observations from many gauging stations across Europe with a period 1966-1995 [Marx et al., 2018]. The calibration-constrained parameter set is derived and used for groundwater recharge projection. The projected groundwater recharge, with a spatial resolution of 5×5 km^2, is further downscaled to a 250×250 m^2 spatial resolution using the bilinear interpolation in the study site for OGS groundwater model.

4.5.2 OGS model setup

A 25-m Digital Elevation Model (DEM) is used to determine the outer bounds of the catchment and the top surface elevation of three-dimensional model domain. A three dimensional stratigraphic mesh is set up based on the above information and bore log data from Thuringian State Office for the Environment and Geology (TLUG) [Fischer et al., 2015]. The mesh consists of 293,041 structured hexagonal elements with a size of 250 m in the x and y direction as well as with a 10 m resolution in the z direction. The parameter zonation approach is used to represent the heterogeneity of hydraulic properties–hydraulic conductivity in this study. The geological zones within the three-dimensional mesh representing Nägelstedt catchment are displayed in Figure 4.2. Ten different sediment units are delineated based on the stratigraphy in this area, including Middle Keuper (km), Lower Keuper (ku), Upper Muschelkalk 1 (mo1), Upper Muschelkalk 2 (mo2), Middle Muschelkalk 1 (mm1), Middle Muschelkalk 2 (mm2), Lower Muschelkalk 1 (mu1), Lower Muschelkalk 2 (mu2), alluvium, and the uppermost soil layer (Figure 4.2). The geological unit "alluvium" represents sandy outwash and gravel near streams, whereas "soil" denotes the uppermost soil layer with a depth of 10 m.

For the uncertainty study of climate scenarios, a post-calibration hydraulic conductivity field sampled from many realizations that are all constrained by head observations is adopted for the OGS groundwater model (Table 4.2). In parallel, to assess the groundwater model uncertainty, 80 realizations of hydraulic conductivity fields randomly sampled from many hydraulic conductivity fields are used to cover a plausible range of values [Jing et al., 2019a]. Meanwhile, a uniform porosity of 0.2 is assigned to each geological layer (Table 4.2).

Given that this study is designed to assess the potential response of the regional groundwater system to global warming scenarios, a steady-state groundwater system could be assumed. This assumption is made because the future warming level is a long-term average, and on such a temporal scale (decadal), the short-time fluctuations of climate forcings are essentially damped in the regional groundwater system [Maxwell and Kollet, 2008].

The bottom and outer boundaries of the model domain are impermeable, and no-flow boundary conditions are assigned onto these geometries. The spatially distributed recharges estimated by mHM under future climate scenarios are mapped onto each grid

TABLE 4.2: Hydraulic parameters used for ensemble simulations with different climate scenarios.

Geological units	Hydraulic conductivity (m/s)	Porosity (-)
km	1.145×10^{-4}	0.2
ku	3.714×10^{-6}	0.2
mo1	3.936×10^{-4}	0.2
mm1	2.184×10^{-4}	0.2
mu1	2.258×10^{-5}	0.2
mo2	3.936×10^{-5}	0.2
mm2	2.184×10^{-5}	0.2
mu2	2.258×10^{-6}	0.2
alluvium	1.445×10^{-3}	0.2
soil	3.026×10^{-4}	0.2

node of the mesh surface by the model interface (mHM-OGS). Long-term averaged pumping rates are assigned as Neumann boundaries to each production well, wherein the pumping rates are obtained from the literature based on long-term historical data [Wechsung et al., 2008]. The total long-term averaged pumping rate over the Nägelstedt catchment is 18870 m^3/day, and it is set constant for all climate scenarios. A fixed head boundary is assigned to the main perennial streams including one mainstream and three tributaries (Figure 4.1). For the Lagrangian particle tracking model, about 100000 spatially distributed particle tracers are injected through the top surface of the mesh. The spatial distribution of particle tracers is consistent with the spatial distribution of simulated diffuse recharges for each climate scenario.

4.5.3 Model calibration

We use the observed discharge and groundwater head over 50 years (1955-2005) to calibrate the mHM and OGS model. The established mHM model for the study area has been calibrated using the observed discharges at the outlet of the catchment in the previous study [Jing et al., 2018]. The OGS groundwater model has also been successfully calibrated using the long-term averaged head observations at many monitoring wells (Figure 4.3). Figure 4.3 reveals that all 80 sets of hydraulic conductivity fields are compatible with the groundwater head observations with a small value of Root Mean Square Error (RMSE) being observed.

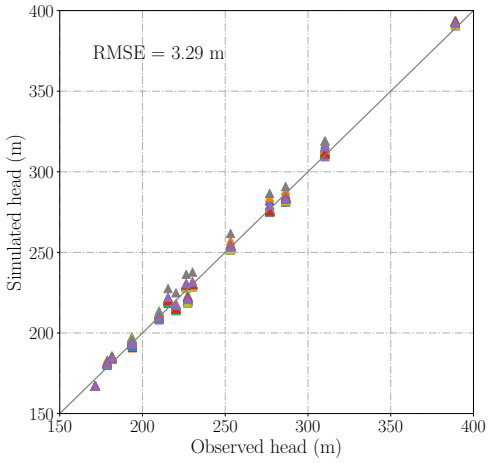

FIGURE 4.3: Groundwater model calibration: comparison of simulated to observed groundwater heads at several monitoring wells using 80 different hydraulic conductivity fields.

4.6 Results

This section displays the ensemble of simulated changes in groundwater recharges, levels and travel time distributions. For the sake of clarity, we use the plus sign to represent simulated values of increases and minus sign to represent decreases.

4.6.1 Climate impact on groundwater recharge

Relative changes of simulated mean annual recharge under 1.5, 2, and 3 °C warming using five GCMs are shown in Figure 4.4. Projected changes of mean annual recharge vary from -4% to +15% for 1.5 °C warming level, meanwhile those range from -3% to +19% for 2 °C warming level. The simulated changes under 3 °C warming scenario range from -8% to +27%. The simulation results from 29 out of 35 total GCM/RCP combinations suggest an increase of groundwater recharge, while only 6 individual simulations projected decreased recharge rates. The projected changes are more dependent on the used GCMs than the RCPs, which can be expected because differences among RCPs are weakened by analyzing different warming levels. Nevertheless, differences in recharge induced by different RCPs can still be seen in Figure 4.4, indicating the necessity of considering multiple GCM/RCP combinations for providing a plausible range of predictive uncertainty. The ensemble averages of relative changes suggest an increase of 8.0%, 8.9%, and 7.2% for the 1.5, 2, and 3 °C warming, respectively. Meanwhile, the standard deviations (SDs) exhibit an increasing tendency with the increasing warming level. With the increase of the global

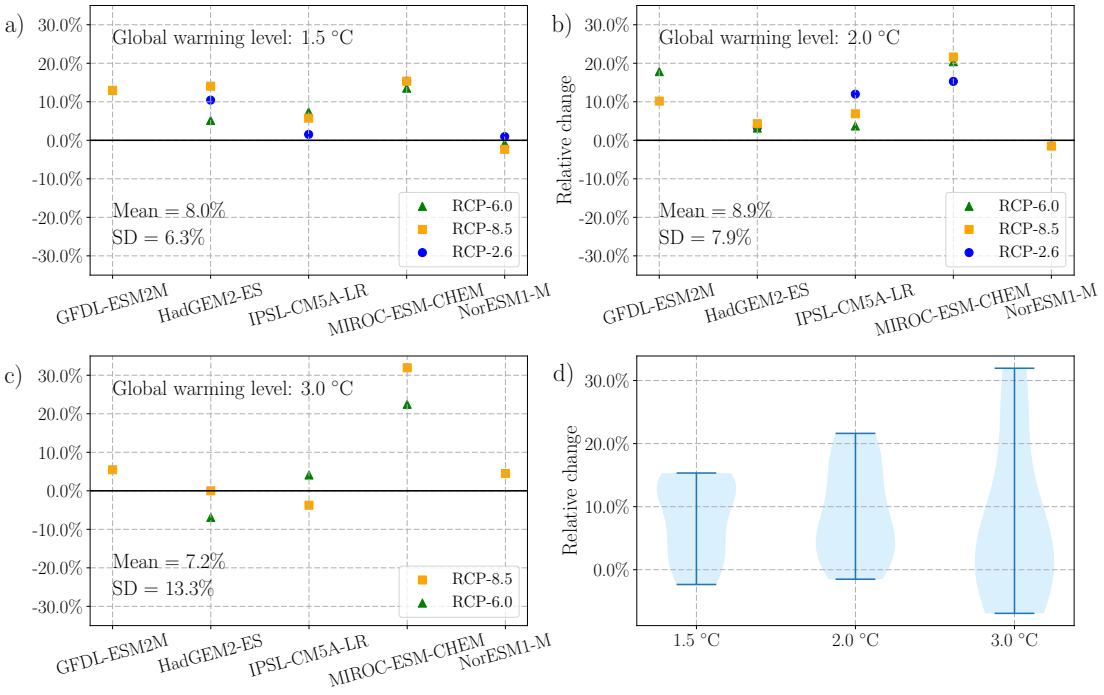

FIGURE 4.4: Projected changes in groundwater recharge rate under three warming scenarios compared to the baseline scenario 1971-2000. Panel a), b), and c) are the scatter plots showing the individual simulation results, and panel d) is the violin plot showing the uncertainty of ensemble simulations.

warming level, the predictive variability in groundwater recharge is also expected to increase (Figure 4.4b).

Generally, calculations indicate that the groundwater recharge rate is expected to be greater than the 1971-2000 average. The increases in groundwater recharge are below 20% in the majority of GCM/RCP realizations, whereas three GCM/RCP realizations suggest a decrease of groundwater recharge in the study area. The simulation under 3 °C warming scenario represents the greatest SD, i.e., the greatest predictive uncertainty. Note that the predictive uncertainty is mainly introduced by the climate projection using various GCM/RCP combinations, given that mHM is the only hydrologic model used in this study and the parameter values are the same for all simulations.

4.6.2 Climate impact on groundwater levels

Changes of simulated spatially distributed groundwater levels under future climate scenarios using the minimum, median, and maximum projected recharge are shown in Figure 4.5. Generally, the areas of topographically-driven flow (e.g., slope) appear to be

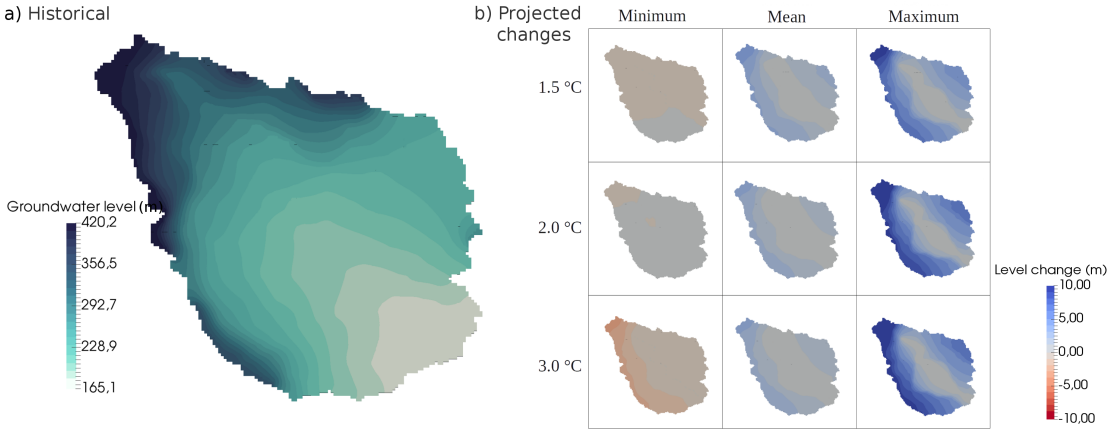

FIGURE 4.5: Contour maps of groundwater levels in Nägelstedt catchment. Panel a) shows the long-term average of groundwater levels in the historical period 1971-2000. Panel b) shows the changes in simulated groundwater levels under 1.5 °C, 2 °C, and 3 °C warming scenarios compared to the baseline scenario 1971-2000 using the maximum, median, and minimum projected recharges.

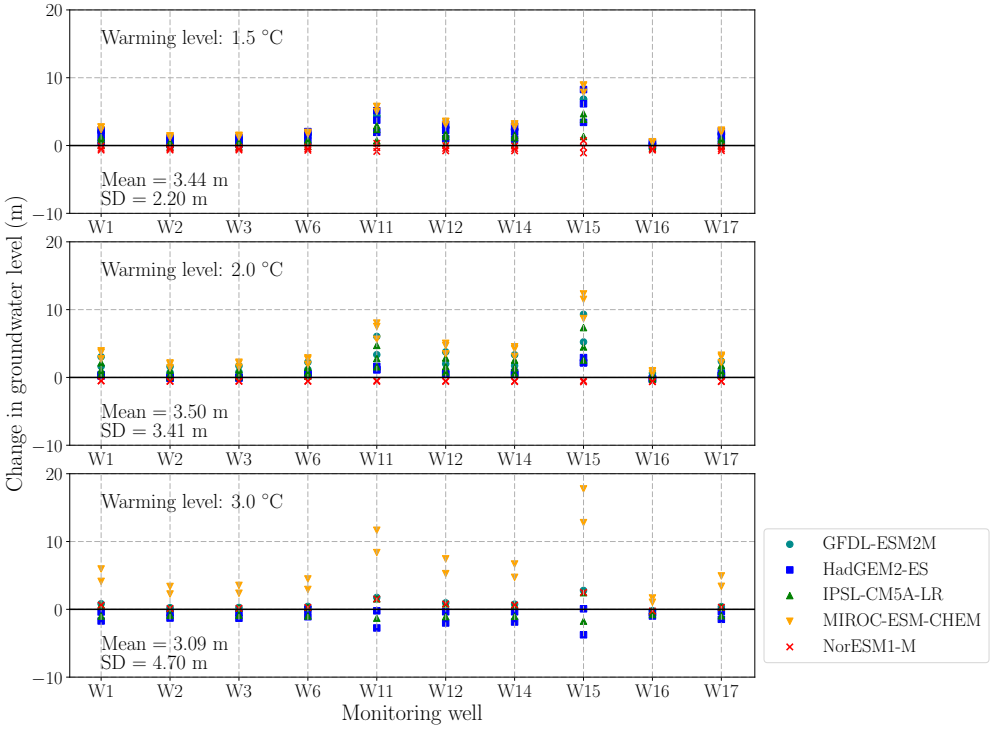

FIGURE 4.6: Changes of simulated groundwater levels in monitoring wells under three warming scenarios compared to the baseline scenario. The positions of monitoring wells are shown in Figure 4.1b.

more sensitive to the changes of recharge compared to the lowland plain. Under 1.5 °C warming scenario, simulated groundwater levels using maximum recharges present an increase ranging from 0 to 10 m compared to those under the baseline scenario, whereas those using minimum recharges exhibit a slight decrease. Under 2 °C warming scenario, groundwater levels are expected to increase compared to the base case using median and maximum projected recharges, whereas marginal differences can be found in the simulated levels using a minimum projected recharge. Under a 3 °C warming scenario, the simulated changes in groundwater levels show the highest variation among the three warming scenarios. Simulations using the maximum recharge suggest a significant increase of groundwater level compared to the 1971-2000 historical average, while simulation using the minimum recharge results in a moderate decrease of groundwater levels (up to a decrease of 5 m at the northeastern mountain).

Figure 4.6 further shows the changes in groundwater levels at several monitoring wells, of which the locations are displayed in Figure 4.1. In general, changes in groundwater levels are induced by the changes in groundwater recharge such that more groundwater recharge results in higher groundwater levels and vice versa. The uncertainty of groundwater level changes increases following the continuous global warming from 1.5 °C to 3 °C, which can be evidenced by an increasing standard deviation of simulated groundwater levels from 2.20 m for 1.5 °C warming to 4.70 m for 3 °C warming (Figure 4.6). The forecasts for groundwater levels present a widespread variation associated with the variability of GCMs. Simulated groundwater levels tend to have the largest increase under three global warming scenarios using meteorological forcings from the MIROC-ESM-CHEM model. In contrast, simulated groundwater levels using meteorological forcings from the NorESM1-M model show minimal changes compared to the baseline scenario. Although differing in magnitude, the changes in groundwater levels for different wells show a consistent trend (either increasing or decreasing) under the same GCM/RCP realization. The simulations show no systematic relationship between the change in groundwater levels and the change in global warming level, but they do indicate an increased variability in groundwater level change following the increased warming level – which can be evidenced by the increased SD values from 1.5 to 3 °C warming level (Figure 4.6).

Overall, calculations of spatially distributed groundwater levels help to understand more of the response of groundwater quantity to the projected climate change, but they provide a little clue on the change in the groundwater transport process. The strong spatial

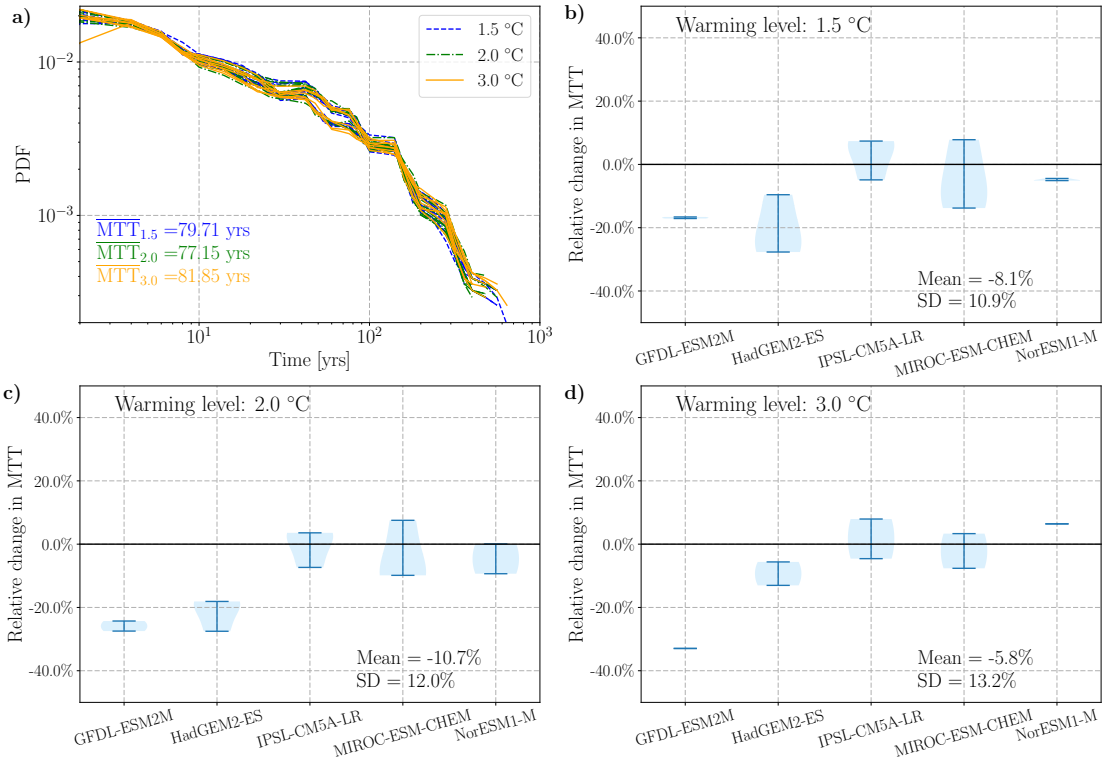

FIGURE 4.7: Simulated TTDs in Nägelstedt catchment under 1.5 °C, 2 °C, and 3 °C warming scenarios. Panel a) shows the probability density function (PDF) of TTDs for the ensemble simulations. Panels b), c), and d) show the relative changes of mean travel times (MTTs) under future climate scenarios compared to the base case.

variability in changes in groundwater levels reveals the high sensitivity for climate change in mountainous areas and relatively low sensitivity in lowland plain areas.

4.6.3 Climate impact on groundwater travel time distributions

Travel time distributions (TTDs) provide a robust description of the flow pathways of water parcels through the subsurface as well as the storage of groundwater within it. Simulated TTDs in Nägelstedt catchment under 1.5, 2, and 3 °C warming scenarios are shown in Figure 4.7. Figure 4.7a) shows the probability density function (PDF) of TTDs for the ensemble simulations. Generally, the simulated PDFs show a fairly consistent shape with a long tail extending to hundreds of years for all GCM/RCP combinations. The long-tail behavior of simulated PDFs of TTDs can be explained by the direct influence of the hydro-stratigraphic aquifer system, whereby some geological units present very low hydraulic conductivity values (e.g., mm2 and mu2) and therefore, remarkably slow down the movements of particles in these layers. The mean travel time (MTT), which by definition is the mass-weighted average of travel times for all water

parcels within the simulated subsurface system, is a typical metric for characterizing the timescales of catchment storage. The calculated ensemble averages of MTTs for 1.5, 2, and 3 °C warming scenarios do not exhibit notable differences (79.71, 77.15, and 81.85 years, respectively).

To analyze the trend of MTTs under future climate scenarios, the relative changes of MTTs under 1.5, 2, and 3 °C warming scenarios are shown in panels b), c), and d) of Figure 4.7. In general, simulations using the data from GFDL-ESM2M and HadGEM2-ES tend to decrease MTTs compared to the base case. Simulations using meteorological data from IPSL-CM5A-LR and MIROC-ESM-CHEM, however, do not agree on the sign of changes in MTTs with a maximum relative change of less than 10%. The ensemble average shows that the MTT is expected to decrease in future periods than the historical average, but a small number of ensemble simulations suggest an increase in MTT. This degree of variability is propagated from the variation in projected recharges using different GCM/RCP combinations. The simulations do not show any systematic relationship between the change in TTDs and the change in warming level, but they do show an increased uncertainty in projected change in TTDs following the increased warming level – which can be demonstrated by the increased SD values from 1.5 to 3 °C warming (Figure 4.7).

Overall, changes in the simulated TTDs provide more details on the response of the system to climate change and how the water cycle is impacted other than considering only the groundwater quantity. The simulated changes in MTTs exhibit a higher variability than the simulated changes in groundwater levels. This is partly because the simulated recharges have different spatial patterns for different GCM/RCP realizations and the TTDs are more sensitive to the spatial pattern of diffuse recharge than the groundwater levels are [Barthel and Banzhaf, 2015, Jing et al., 2019a].

4.6.4 Predictive uncertainty related to the groundwater model

This subsection displays simulation results using 80 different hydraulic conductivity fields that are all conditioned by the head observations and reality. Note that only one climate scenario is used for this group of simulations, which guarantees the simulation results are only controlled by different hydraulic conductivity values. Figure 4.8 displays the spread of changes in simulated groundwater levels and MTTs using 80 different hydraulic

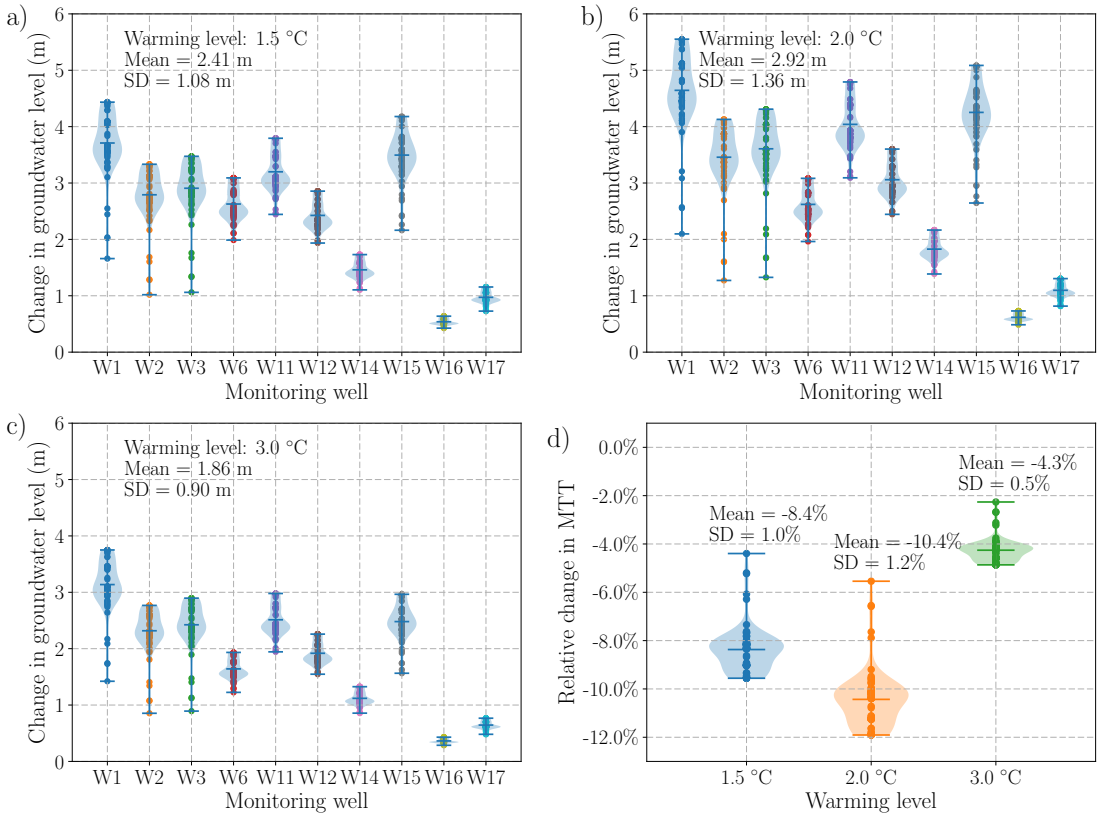

FIGURE 4.8: The predictive uncertainty in simulation results related to different hydraulic conductivity fields. Panel a), b), and c) show the changes in groundwater levels, whereas panel d) shows the projected relative changes in MTTs using 80 different hydraulic conductivity fields.

conductivity fields. The spreads of results vary with the location of monitoring well, provided that the local topographic and hydraulic properties around each monitoring well are different. Wells near the mainstream (e.g., W14 and W16) show smaller variations than those far away from the mainstream (e.g., W1, W3, and W15), indicating the buffering effect of the groundwater aquifer. By comparing the spread of projected changes in groundwater levels in Figure 4.8 to those in Figure 4.6, we find that the spreads induced by different GCM/RCP pairs are remarkably larger than those induced by hydraulic conductivity fields. Moreover, the sign of projected changes in groundwater levels in Figure 4.6 can be either positive or negative, whereas those in Figure 4.8 show a consistent positive sign. The spread of projected relative changes in MTTs ranges from -12.0% to -2.4%, which is also significantly smaller than that related to different climate scenarios (Figure 4.8d). This comparison indicates that predictive uncertainties in groundwater level are primarily contributed by climate projections and secondly by hydraulic parameters.

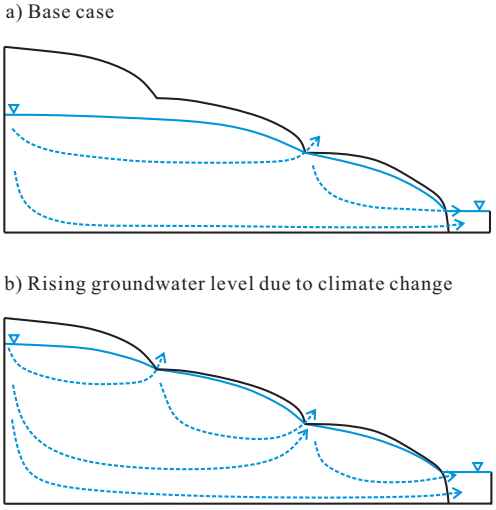

FIGURE 4.9: Conceptual graph showing the influence of rising groundwater level on the regional groundwater flow pattern in due to climate change.

4.7 Discussion and conclusions

We systematically explore the response of a regional groundwater flow system to different global warming scenarios through the sequential coupling of a computationally-efficient land surface model (mHM) and a physically-based groundwater model (OGS). The results of ensemble simulations manifest that groundwater recharge is likely to increase moderately for all three warming levels. However, the ensemble simulations do not all agree on the sign of relative change. This finding is consistent with a previous finding that low flows are expected to increase slightly in this region under future climate scenarios, considering that baseflow is the main component of low flow and recharge feeds the baseflow[Marx et al., 2018]. A similar increasing trend in climate-induced recharge rates has been suggested by many researchers for other regions such as a northern European catchment [Treidel et al., 2012], high plains of USA [Cornaton, 2012], upper Colorado catchment [Tillman et al., 2016] and Snake River basin [Sridhar et al., 2017]. Meanwhile, the seasonal pattern of recharge can be significantly modified by climate change [Chen et al., 2018].

The simulated changes in groundwater levels also manifest similar increases for all three warming scenarios but show a strong spatial variability depending on the local topography and elevation. These changes can be critical to groundwater/surface water interaction because the increase or decrease in groundwater table would modify the dynamics of groundwater discharge into streams [Havril et al., 2017]. In areas with a complex

topography and dense drainage network, rising groundwater levels may activate shallow groundwater flow paths and intensify shallow local flow pathways (Figure 4.9). This way, the mixing behavior of groundwater storage can also change, because the activation of shallow flow paths will lead to a stronger systematic preference for discharging young water [Kaandorp et al., 2018, Jing et al., 2019a]. Those above-mentioned processes can be properly reproduced by the coupled model mHM-OGS, given that the coupled model is physically based and is capable to explicitly represent the spatial heterogeneity. Moreover, changes in groundwater levels will impact the land surface processes such as evapotranspiration, soil moisture dynamics and overland flow [Kollet and Maxwell, 2008, Huntington and Niswonger, 2012].

The remarkable influence of climate change on the catchment-scale groundwater travel time distributions is of critical importance to the sustainability of the hydrological system. Simulated mean travel times suggest a moderate decline for three warming scenarios, which is not surprising since the travel time of water parcels is directly controlled by the recharge rate. With simulated weighted-average MTTs being at a centurial scale, climate-induced variations can significantly affect the long-term sustainability of the regional groundwater system. The decline in groundwater MTTs will remarkably shorten the life span of non-point source pollutants (e.g., nutrient and pesticide) in groundwater aquifers and change the spatial and temporal distributions of pollutant concentrations within the aquifer system. Given that the nutrient budget of the connected surface water body is linked with the groundwater system, the water quality of the surface water body in this region (e.g., the Unstrut river) will respond accordingly in the future, although with a long delay. This finding is in line with many recent studies, wherein they highlight the importance of legacy nutrients in catchments as a reason for long-term catchment response [Haygarth et al., 2014, van Meter et al., 2017].

One essential topic when assessing future climate impact is uncertainty. Within the simulations using the ensemble of GCM/RCP combinations, simulated changes in variables (e.g., recharge, groundwater level, and mean travel time) vary not only in absolute value but also in sign (positive or negative) because of the large variations in different climate projections. The contribution of climate scenarios to the predictive uncertainty is also found to be greater than that of hydraulic parameters in the groundwater model. Within the current modeling framework, predictive uncertainty and error may also be introduced by other sources, such as the internal variability in climate projection using different initial

states, internal parameter uncertainty in the mHM model, and the down-scaling algorithm. Enhancements in climate projection and downscaling algorithms can effectively reduce the variability in the projected impacts of global warming on the regional groundwater system. Nevertheless, the dominant source of uncertainty is highly likely to lie in the climate projections using various GCMs and RCPs [Taylor et al., 2012, Thober et al., 2018, Marx et al., 2018]. Except for the above-mentioned climate projection uncertainty, other uncertainty sources have not been assessed in this study. This fact indicates that the range of predictive uncertainty estimated in this study is only a conservative estimation.

A potential limitation of the current modeling framework lies in the one-way coupling approach that neglects the feedback from groundwater level change to the land surface processes. The change in groundwater table can alter the partitioning of water balances, which further exerts a second-order impact on the groundwater level and travel times [Liang et al., 2003, Leung et al., 2011]. The fully coupled system, based on a mixed form of the Richards equation to solve unsaturated and saturated zone flow simultaneously, is more realistic than the one-way coupled system. However, a fully coupled model consistently suffers from the expensive computational burden, which limits its applicability in large-scale real-world models. It also introduces extra parameters that are essentially unknown at the catchment scale. The current one-way coupling, although less accurate than the two-way coupling, is computationally more efficient – allowing us to understand the first-order control of climatic variability on groundwater characteristics (groundwater level and travel times). Notably, the applied Lagrangian particle tracking in the 3D groundwater model is computationally very expensive. The total computational time performing a single model run is around 14 days using 8 cores on a supercomputer facility. Moreover, we have successfully demonstrated the utility of this model for adequately capturing the observed behavior of groundwater levels across the study basin [Jing et al., 2018]. Accordingly, the one-way coupling method used here is a practical choice, allowing us to perform the large ensemble scenarios with reasonable computational resources (and time).

The second potential limitation of this study is the contradiction between the fine-resolution groundwater model and coarse-resolution mHM simulations. mHM simulations in this study were established within the scope of the HOKLIM project, which focuses on the impact of future climate scenarios on European water resources. All databases used for mHM model setup are on a European scale and typically have coarse spatial

resolutions (e.g., 5×5 km^2). Although the MPR technique embedded in mHM facilitates the characterization of subgrid-scale features, it does not guarantee that all subgrid-scale features can be captured if the resolutions of input data are too coarse. We note that this is a common problem when utilizing coarse-resolution forcings to drive fine-resolution physically-based models. Simulation results in this study can be considered as first-order approximations based on currently available databases. The conclusions drawn in this study can be tentative and therefore, open to revision.

The steady-state nature of simulations is reasonable for the assessment of long-term climate impact on regional groundwater system because 1) it reduce the computational burden, 2) the temporal fluctuations under the future climate cannot be reasonably projected, and 3) high-frequency fluctuations in external forcings have minor influences on long-term travel time distributions [Engdahl, 2017]. However, transient behavior can be very important for many cases where the temporal scale is small and the input forcings are highly dynamic. In recent years, the subject of the transient behavior of TTDs has become more and more prevalent in groundwater hydrology [Woldeamlak et al., 2007, Cornaton, 2012, Engdahl, 2017].

We note that the results in this study are only suitable for the Nägelstedt site in central Europe. In other regions of Europe, groundwater recharge change induced by global warming may have distinct behaviors than those shown in this study. For example, some studies indicate a decrease in groundwater quantity in Mediterranean regions due to the decrease in projected precipitation [Pulido-Velazquez et al., 2015, Moutahir et al., 2016]. Besides, baseflow is also expected to decrease, leading to a potential increase in drought in Mediterranean regions [Marx et al., 2018, Samaniego et al., 2018].

We only consider the direct impact (i.e., impacts exerted through changed precipitations) of climate change on the regional groundwater system. Interactions between the climate and groundwater are exacerbated by land-use change, which is mainly exerted by the intensification of irrigated agriculture. In South Australia and the southwest U.S., the transition from natural catchments to rain-fed cropland significantly changes the groundwater storage through the increase in recharge [Taylor et al., 2012]. The indirect influence of global warming on groundwater systems has not been considered in this study. This influence can be a dominant factor threatening the local groundwater system for many regions worldwide [Taylor et al., 2012]. Future investigations are needed to

incorporate both the direct and indirect impacts of global warming on the sustainability of the regional groundwater system.

To summarize, climate change can significantly alter the quantity and travel time behavior of the regional groundwater system through the modification of recharge, especially for the long term. Ensemble simulations indicate remarkable predictive uncertainties in regional groundwater quantity and travel times, which are introduced primarily by climate projection, and secondly by groundwater model. In the study domain, moderate absolute changes in recharge rates, groundwater levels, and travel times that are nonlinearly related to the amount of global warming are found. However, the variability of these changes increases with the amount of global warming that might also affect the cost of managing the groundwater system. This increased variability indicates an increased possibility of extreme events in the groundwater system following the increase in warming level. Therefore, it is still advisable to restrain global warming to 1.5 °C and avoid global warming of 3 °C.

Chapter 5

Discussion

Based on the results in three previous chapters, this section comprehensively discusses the main findings as well as the significance and limitations of these findings. It is further divided into four subsections, including the discussion on the process representations in hydrological models, that on the estimation of groundwater TTDs, that on the uncertainty evaluation, and that on the climate impact on groundwater resources.

5.1 Process representations in hydrological models

In general, there are two areas in hydrology and hydrogeology where modeling benefits: to understand why a flow system behaves in a certain observed manner and to predict the behavior of a flow system in the future. Besides, models in hypothetical flow scenarios can be used as an indicator of this type of flow system [Anderson et al., 2015].

This dissertation is devoted to develop a coupled surface-subsurface hydrological model (mHM-OGS) and test its applicability in a real-world catchment. Through the coupling, the groundwater representation has been significantly improved for the mHM model concerning the explicit characterization of subsurface heterogeneity and flow path lines. This piece of work sheds light on the improvement of process representation of subsurface components for conceptual hydrological models. In the past few decades, hydrological models have been developed and headed toward complex physically-based representations of processes. The rapid development of computational powers and numerical discretization approaches enables the models going for a large scale (e.g., continental to global scale)

and a fine resolution [Wanders et al., 2019, Greve et al., 2018]. However, it is still a big challenge to effectively combine the increasing computational power and mathematical representations with the incomplete and simplified understanding of the complex real-world hydrological system.

The mHM-OGS coupled model provides a reasonable fit between the simulated and observed time series of groundwater heads for the validation period (1975-2005). Conversely, the mHM-alone simulations without a physically-based groundwater representation cannot reasonably reproduce decadal variations in groundwater heads, and also show less accuracy in estimating baseflow. In the Nägelstedt catchment where the precipitation is around 660 mm yr^{-1}, the coupled model is highly recommended because, in this humid region, the SW-GW exchange is of concern. Other applications where the coupled model is highly recommended include (1) areas where groundwater pumping significantly affects the surface water dynamics and ecological conditions and (2) wetlands where stream network and surface water bodies are closely linked with the groundwater system [Markstrom et al., 2008]. The coupled model can also provide references for water management and the corresponding decision making processes. Meanwhile, the applicability of the coupled model cannot be merely judged by the degree of fit of the model simulations with observed discharge at the outlet of catchment. Instead, coupled models must be carefully assessed based on various sources of observations and data assimilation techniques for the reasonable characterization of changes in near-surface and groundwater flows and reservoirs in the studied region. These observations may include soil moisture, evapotranspiration, snow depth, and concentrations of tracers.

The physically-based hydrologic model offers new opportunities for the integrated SW–GW flow modeling. Integrated catchment modeling is capable to account for the interactions between different hydrologic components, such as the exchanges across the land surface [Maxwell and Miller, 2005, Camporese et al., 2010] and the interactions across the riverbed [Delfs et al., 2012]. Nevertheless, there are a lot of open problems to be addressed for the coupled SW–GW modeling. First, the comprehensive representation of the full complexity of SW–GW interaction is difficult for physically-based hydrologic models. At the hillslope/catchment scale, the surface flow is typically simplified to happen on a two-dimensional Euclidean surface representing the terrain, while the subsurface flow is generally active in a three-dimensional porous media. The coupling of SW–GW flow then must calculate the interaction at the assumed interface represented by the DEM,

which is only a rough representation. Second, the fully-coupled problem is extremely computationally expensive and often suffers from numerical oscillation caused by coarse discretization and strong non-linearity of the equation system. Last but not the least, at the regional scale, fine-scale topographic, geometric, and hydraulic features can hardly be resolved at grid sizes of the large-scale model [Paniconi and Putti, 2015, Jing et al., 2018].

While some highly physically-based hydrological models (e.g., MIKE-SHE, Refsgaard and Storm [1995]) are more complete, they require a lot of parameters and data to support the model setup. It is very time-consuming to establish and calibrate these models [Maxwell et al., 2014]. The mHM-OGS coupled model is relatively easy to set up and computationally efficient. Alternatively speaking, the mHM-OGS model reaches a balance between accuracy and efficiency in hydro(geo)logical process representation. Nevertheless, the gap between the theoretical rigor and the operational difficulties becomes a barrier to the application of all coupled models. Therefore, it is a general trend to study the complex system consisting of various components of the water cycle. Adapting to a wider range of different modeling targets is of critical importance for the development of coupled models of surface water and groundwater [Engdahl and Maxwell, 2015, Bisht et al., 2017]. Besides, the coupling of spatiotemporal scale transformation, the mechanism of soil water movement in the unsaturated zone, the uncertainty of parameters, and the mechanism of dynamic interaction between river and groundwater are highly relevant to this topic and need further investigations.

5.2 Estimating groundwater TTDs at the catchment scale

This dissertation demonstrates the capability of the coupled model (mHM-OGS) in explicitly characterizing large-scale groundwater TTDs through Lagrangian particle tracking. Characterizing travel time behavior is significant to water quality assessment and water resources management for the subsurface hydrological system. Travel time (i.e. transit time, age) denotes the life span of a water parcel or a solute in a control volume, i.e., the time interval from its entrance at the inlet to its exit at the outlet. Travel time distribution (TTD) is a lumped representation of the storage, mixing and transport processes in a hydrologic system [Haitjema, 1995, Leray et al., 2016, Heße et al., 2017, Jing et al., 2019a].

One of the main findings in Chapter 3 is that although being computationally expensive, Lagrangian particle tracking shows better accuracy in linking the shape of TTD to the subsurface heterogeneity. This is a clear advantage of the particle tracking model over the analytical model. Being computationally efficient, the simple analytical model (e.g., exponential model) is able to produce a prediction of MTT to the same order of magnitude with the particle tracking model. To be specific, the particle tracking model is superior to the analytical model if there are sufficient data to build a detailed 3-D hydrogeological model. Conversely, for data-scarce regions where the hydrogeological conditions are partially unclear, the analytical model can serve as a first-order approximation for the MTT, although with less reliability. Note that the exponential solution has a higher accuracy for plain areas rather than mountainous areas because the Dupuit-Forchheimer assumption should be roughly met for using the exponential model. As indicated by the case study in Chapter 3, the difference between the two methods could be around 20%–48 % for a mesoscale catchment.

Chapter 3 also bridges two historically-separate fields with their distinct communities and research methods: surface hydrology and hydrogeology. In the field of surface hydrology, most TTD-related studies focus on the nonstationarity of discharge, aiming to unveil the transient TTDs and their links with residence time distributions. This phenomenon is built on the nature of the fast and dynamic responses of surface fluxes and states to external climate forcings. Spatial heterogeneity has always been implicitly represented by catchment hydrologists using one or a combination of different analytical models, which are built on assumptions of catchment mixing behavior [Benettin et al., 2015, Botter et al., 2011]. Conversely, hydrogeologists focus more on the explicit representation of spatial heterogeneity rather than on that of nonstationarity. Due to the relatively sluggish response of deep groundwater storage to external forcings and the long response time of discharge to groundwater storage, the groundwater flow and transport processes are not as dynamic as the surface processes. Through the coupling of mHM and OGS, it is possible to simultaneously tackle different challenges in characterizing surface and subsurface TTDs [Heße et al., 2017, Jing et al., 2019a]. The coupled model therefore successfully bridges the gap between surface and subsurface hydrology.

The purpose of estimating groundwater TTD is to determine the ages of water samples in the groundwater storage. In this study, water samples are particles in the RWPT method. This age, in turn, represents the age of the groundwater at the corresponding location

in the aquifer, and we can ultimately use that age information for relevant research. The groundwater sample taken at the time of the year is a collection of countless water particles, which are often mixed by water particles of different locations, sources and historical periods [Tóth, 1999]. The age of these groundwater particles may vary greatly from each other and even on different orders of magnitude, while the result of groundwater MTT is only a lumped description of the highly heterogeneous travel times. Therefore, the MTT of groundwater is only statistically significant and should be carefully evaluated in practical applications.

The numerical simulations of TTDs in this dissertation have great implications for groundwater dating techniques as it is a supplement to the traditional isotope-based approaches. Groundwater dating plays a critical part in hydrogeology. Since the evolution of groundwater is controlled by factors such as regional geologic and hydrogeological conditions, geochemical systems, and the activities of human beings, the temporal and spatial patterns of travel times are therefore very complicated. The dating of groundwater is based on various hydrogeological, hydrodynamic and hydrogeochemical information reflected in the complex evolution of groundwater. Therefore, the reliability of the groundwater TTD estimations and their applicability in real-world cases are affected and constrained by this complex process.

A potential limitation of the current approach is the simplification of the impact of human activities on groundwater TTDs. This study does not consider the changing pumping rates along with the changing human activities. On the one hand, groundwater abstraction will change the correspondence between groundwater age and flow field and eventually lead to increasing complexities in modeling groundwater TTDs. In recent years, the depth and intensity of human activities on groundwater have reached an unprecedented level [Taylor et al., 2012]. These activities have broken the natural hydrodynamic state of groundwater for many years and promoted the mixing of groundwater from different sources, locations, and ages, and even led to the change of the entire groundwater flow field [Kang and Eltahir, 2018, Cao et al., 2013]. Although the groundwater TTD behavior can be used to invert these processes, the accuracy and reliability of the inversion results still require careful evaluations, especially when hydrological and topographical conditions are complex.

5.3 Uncertainty evaluation of hydrological models

The process of seeking for values of a parameter set until the residuals between the model outputs and the measurements are minimized is typically called as "calibration" [Doherty, 2015]. Historically, calibration assumes the uniqueness of parameter. A set of best-fit parameter values can be found after the calibration by minimizing the objective function. Numerically, finding one parameter set fit best with observations is much easier and computationally simpler than finding a distribution of parameter values that are all within an acceptable range. For this reason, calibration for a single set of parameters has been excessively used in hydrological modeling for decision-making purpose.

A single best-fit parameter set is not equivalent to the "real" parameter set because of the following reasons: (1) The numerical model is an imperfect reflection of reality. With the different degrees of model structural error, the best-fit parameter set can be slightly or biased from the real one. (2) The measurements may be inaccurate due to measurement error. Assuming that the numerical model is a perfect proxy for reality but the measurements are flawed, the fit values through calibration will also be biased from reality. (3) The existence of null space (Figure 5.1). In cases that the inversion is non-unique (i.e., some of the parameters are insensitive to measurements), many parameter sets can all fit well with measurements, but only one of them is the "real" parameter set. For these reasons, the probability distribution for predictive uncertainty is greater than the posterior predictive probability distribution of that prediction [Doherty and Hunt, 2010, Ajami et al., 2007].

Accordingly, case studies in Chapter 3 and Chapter 4 are devoted to finding the distribution of parameter values that are all compatible with the measurements and reality. Moreover, the input uncertainty is also taken into consideration, allowing a comprehensive evaluation of the uncertainty contribution of different sources for simulation results. This study further manifests the influence of uncertainty in post-calibration parameters on the model predictions. Although as many as 400 realizations are needed to provide a reasonable probability distribution of MTTs (Figure 3.8), they provide far more information and insights into the TTD dynamics than a single set of best-fit parameters. This approach allows for quantifying the calibration-constrained variability of the model outputs and has great implications for decision-making in water resource management.

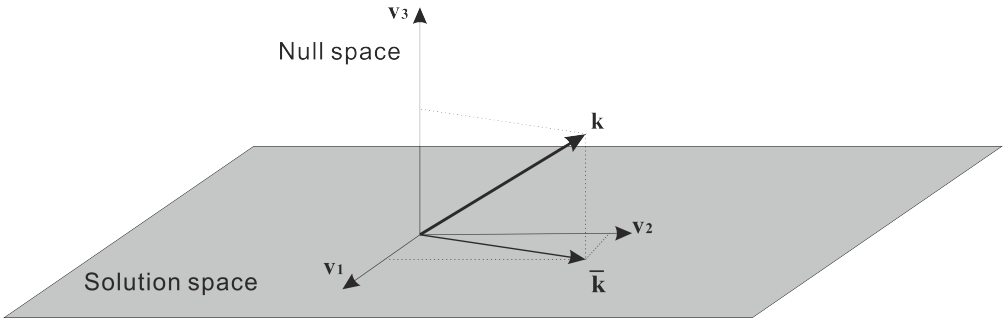

FIGURE 5.1: Illustration of parameter space for model inversion. $\mathbf{k}$ denotes the real parameter set, and $\bar{\mathbf{k}}$ denotes the projection of real parameter set in solution space.

There are also certain limitations in the uncertainty analysis in this study. First, the uncertainty in model structure has not been explicitly evaluated in this study. To establish mathematical expressions (which are easy to solve with existing mathematical methods), the numerical model simplifies some practical hydrogeological conditions. For example, the aquifers in the study are generalized to stratigraphic aquifers. The structural error related to this generalization can be implicitly included in the variability in post-calibration parameters, but it can not be quantified explicitly in the current method [Doherty and Hunt, 2010]. Second, the numerical errors generated by the computation (e.g., the truncation error, numerical fluctuation, and instability of the numerical method in the model solving process) are not included, which can also cause the uncertainty of the numerical solution. Third, other sources of input data have not been evaluated. The accuracy of input data affects the simulation results of hydrological processes to a certain extent. With the development of distributed hydrological models and the increasing impact of human activities on natural hydrological processes, the types of input data are extending to a wider range. Except for the typical precipitation input data, other data have also been used by hydrologists, including temperature, soil type, vegetation type, geological features, as well as human activity data. While using the uncertainty method to quantitatively describe the uncertainty of input data, new data sources such as radar rain, geographic information systems, and computer systems can also help to reduce the errors in traditional data acquisition.

5.4 Evaluation of climate impact on groundwater resources

Global warming potentially influences the water cycle by straightforwardly increasing the ET of near-surface water storages [Schewe et al., 2014, Samaniego et al., 2018]. As a

result, these modifications can influence the rainfall rates, timing, and intensity, and pose a second-order effect on the flow and transport processes in both the near-surface and deep subsurface water reservoirs. While climate change has a straightforward influence on shallow surface water resources employing modifications in meteorological variables and fluxes (e.g., precipitation, temperature, and ET), the impact of it on deep groundwater reservoirs is more complex and needs more investigations.

Correspondingly, Chapter 4 is our first attempt on integrating state-of-the-art models, including an ensemble of climate models, a well-established spatially-distributed hydrologic model, and a fully distributed groundwater model, for the investigation of climate-change influence on regional groundwater quantity and TTDs. The simulation results indicate different degrees of sensitivity of groundwater resources as a response to various climate models. This study highlights the necessity of deploying an ensemble of climate models and RCPs to cover a broad range of uncertainty sources. Additionally, the validation of climate models is also urgently needed to reduce the predictive uncertainty related to climate projections. The three-dimensional groundwater model provides a versatile platform for the evaluation of TTD behavior under various warming levels with its explicit representation of topography, geometry, and geology of the catchment. Climate projections are subject to substantial-high uncertainty, especially when precipitation projection is included [Taylor et al., 2012]. This dissertation also points out that the robustness of simulations is mostly limited by climate uncertainty. Accordingly, the inter-comparison of different climate models is highly relevant to the reliability and confidence in the simulation results and needs to be done in future research. For this reason, the improvement in climate projections will significantly enhance the confidence of current simulations in terms of coping with a changing climate, and thus dramatically improve the applicability of the current modeling approach.

The ensemble simulations in Chapter 4 indicate that groundwater recharge and groundwater levels are likely to increase, and the mean travel time has a high possibility of decline for all tested warming levels. This finding sheds light on the long-term response of catchment-scale groundwater aquifers (in terms of quantity and transport behavior) to climate change in a central European basin. Nevertheless, there are considerable uncertainties in both the magnitude and direction of these changes. As already stated in Chapter 4, there are crucial doubts about the projected effects of climate change on the spatially distributed recharge of groundwater. This phenomenon is directly related to

the uncertainties in climate projections [Taylor et al., 2012, Jing et al., 2019b]. These results are crucial for establishing long-term sustainability targets, as climate projections vary widely and groundwater reservoirs have a long response time for freshwater. Explicit representation of groundwater in climate models, the interactions between land surface flux and groundwater, and anthropogenic disturbances are urgently needed towards a more robust representation of the influence of global warming on the regional groundwater resources.

A potential limitation of the simulations lies in the fact that only one land surface model is used in Chapter 4. This choice has a certain advantage in reducing the computational burden. However, the choice of the land surface model may also affect the simulation results because different land surface models characterize processes differently [Thober et al., 2018, Marx et al., 2018]. Although using an ensemble of land surface models will dramatically increase the computational cost, it is still highly suggested to deploy an ensemble of land surface models for a better estimation of predictive uncertainty.

Affected by climate and human activities, the conditions of land use will inevitably change and affect future water resources. Therefore, it is necessary to study the impact of global change on water resources in combination with future trends of land use. This study only focuses on the direct impact of global warming on water resources and therefore neglects the impact of land-use change on future water resources. Currently, research on future water resources has begun to consider changes in land use [Leung et al., 2011, Samaniego et al., 2018, Treidel et al., 2012]. However, this trend needs to be further strengthened. The integrated investigation of climate and land-use change is highly suggested for future research.

Chapter 6

Conclusions and outlook

6.1 Conclusions

This dissertation offers original insights into several critical aspects of hydrology and hydrogeology, including the coupling of surface and subsurface system, the characterization of catchment TTD, the evaluation of climate impact on groundwater resources, and the uncertainty quantification of hydrological modeling. Based on simulation results and discussions in previous chapters, some solid conclusions are made. The general conclusions are itemized below.

1. The coupling between mHM and OGS is the first attempt to link the predictive capability of two distinct models with different process representations and structures. It provides an explicit representation of groundwater flow and transport processes, which lacks in the original mHM model. The success of model coupling sheds light on the integrated catchment modeling crossing boundaries of surface hydrology and hydrogeology.

   The mHM model is a parsimonious model that is capable to represent the complex and non-linear land surface processes using relatively simple ordinary partial equations (ODEs). The unique well-established parameterization scheme (i.e., the MPR method) enables mHM to cope with fine-scale topographic, geometric, and hydraulic features, thus enhancing its capability of reproducing reasonable land surface flux fields. However, the inherent linear groundwater reservoir within mHM

cannot reproduce complex groundwater flow and transport processes. On the other hand, OpenGeoSys (OGS) is built on the finite element method and is capable to explicitly simulate saturated/unsaturated subsurface processes in heterogeneous porous media. This research is dedicated to bridging the gap between two well-tested models that are developed separately in their respective fields. Through the coupling, the predictive capability of mHM has been augmented to simulate subsurface processes, while the original well-tested features of the two models are fully preserved. The applicability of the coupled model in simulating the regional groundwater system is assessed in a central European basin (Nägelstedt). The simulation results demonstrate that the coupled model is capable to generally reproduce groundwater head dynamics.

2. The coupled model (mHM-OGS) has been successfully used to estimate catchment-scale groundwater TTDs. It can be a valuable tool for large-scale TTD estimation by combining it with the RWPT method. It shows its priority over the analytical models in terms of explicitly characterizing subsurface heterogeneity.

   The coupled model is also capable of explicitly simulating solute transport processes through employing a three-dimensional realistic aquifer model. By combining the numerical model mHM-OGS, the RWPT algorithm, and the analytical framework of SAS function, the TTDs, and SAS functions can be directly calculated without assuming a predefined TTD shape. Although being computationally expensive, this approach can explicitly characterize the heterogeneous topographic, geometric, and hydraulic features and their composite effects on the regional groundwater transport process, therefore it can explicitly represent the heterogeneous groundwater system (e.g., preferential flow pathways). Groundwater TTDs help to understand groundwater movement processes and pollution. In Nägelstedt catchment, the ensemble simulations using the coupled model show that the mean travel times are primarily controlled by the recharge rate and secondarily controlled by the post-calibrated conductivity field. Both catchment-scale TTDs and SAS functions are strongly controlled by the spatial arrangement of recharge. Consequently, the quantification of spatial arrangement in recharge is of crucial importance for estimating groundwater TTDs. As a cutting-edge technique for quantifying the transient behavior of catchment in terms of releasing water and solutes, the framework of SAS functions has been successfully applied for interpreting the results

of tracer tests [Benettin et al., 2015, Rihani et al., 2010]. Unlike those past studies, this study shows that the framework of the SAS function can be also applied for interpreting the results of a fully-distributed numerical model. This combination has good applicability in coping with natural and human-induced changes.

3. Climate change has a strong impact on groundwater resources in Nägelstedt catchment in central Germany. Utilizing a comprehensive numerical investigation using mHM-OGS, this study reveals a high uncertainty of climate impact on groundwater resources. It also provides original insights into future water management under a changing climate.

   Current modeling efforts using mHM-OGS include both surface water and groundwater for the evaluation of climate influence on water resources. Similar approaches using a chain of climate-surface-subsurface models have also been used in some other studies [Engdahl and Maxwell, 2015, Scibek and Allen, 2006]. The projected recharge is subject to high uncertainty, and therefore needs to be carefully assessed for the future adaption to the global change. High uncertainty in climate projections and corresponding changes in precipitation and land use accounts for the predictive uncertainty in projected changes in groundwater resources [Taylor et al., 2012].

4. The uncertainties in climate projection, recharge estimation and model parameters limit the accuracy and reliability of model results. Comprehensive uncertainty evaluation on different sources is highly recommended for both theoretical and practical hydrological modeling efforts.

   In this dissertation, NSMC method-based uncertainty analysis is used to quantify the input data, parameters, and structure of hydrological models. It can guarantee that the simulated groundwater heads and TTDs are within the calculated error limits. Uncertainty in post-calibration parameters indicates that the calibration process does not guarantee a realistic parameter set. Moreover, calibration-constrained Monte Carlo simulations are promising in investigating the post-calibration uncertainty. This dissertation provides important insights on uncertainty evaluation.

6.2 Outlook

This research focuses on three important issues: the coupling of mHM and OGS to better characterize the terrestrial hydrologic cycle, the uncertainty evaluation in predicted travel time distributions using the coupled model, and the assessment of a regional groundwater system under future climate scenarios. Model developments and case studies in this dissertation have great implications for future work.

This dissertation focuses on extending the utility of mHM from surface compartments to simulating groundwater dynamics. Consequently, the dynamic interaction between land surface fluxes and groundwater head changes is not explicitly represented. In contrast to a full coupling, the user can extend the capabilities of mHM with the coupling method described here without compromising the known and proven features. In the next step, however, we will devote ourselves to the implementation of a complete full coupling with the next release of the coupled model. The major restriction of the current coupling approach is that the influence of shallow groundwater depth on soil water dynamics (e.g., precipitation partitioning, soil moisture, and ET) can not be explicitly accounted for. However, the full exchange flux between the surface and groundwater flow can be effectively accounted for with a full coupling scheme. For the implementation of a full coupling scheme, the original groundwater storage in mHM (i.e., the deepest layer in mHM) should be completely replaced by physically-based groundwater storage. In doing so, the original precipitation partitioning and runoff generation will also be modified. After a fully coupled model being established, the fully integrated modeling of catchment flow and transport can become possible.

Besides, the numerical experiments conducted in Chapter 3 are based on the steady-state assumption, therefore they do not consider the time variation in groundwater travel times. This is a reasonable setting for this study given that this study aims to explore the role of inputs and hydraulic properties in TTD predictions. To better understand the relationship between released and stored water, a transient groundwater model and time-varying SAS functions are needed in the future. Moreover, interactions between the climate and subsurface water can be modified by land-use change, which can be attributed to the intensification of irrigated agriculture. This indirect effect of global change to the regional groundwater circulation has not been included in current work and should attract more attention in future research [Jing et al., 2019b].

Uncertainty analysis in this dissertation is built on the NSMC method embedded in PEST inversion codes [Doherty and Hunt, 2010, Doherty, 2015]. The NSMC method offers a robust framework for rapidly generating various parameter fields that meet both the model-to-measurement variance and the real constraints required to study parameter uncertainty after calibration. This method is computationally efficient and relatively easy to implement compared with the Bayesian framework. For these reasons, the NSMC method is used here to efficiently produce the ensemble of parameter sets for computationally-expensive particle tracking calculations.

Nevertheless, Bayesian inversion is superior to the NSMC method because it provides a complete mathematical characterization of what the inversion process can and should accomplish. In the future, the Bayesian inversion is needed to characterize the posterior probabilities distributions of the parameter set. In doing so, the reliability and interpretability of uncertainty analysis could be significantly improved. The prior probability distribution is a key concept of Bayesian theory. However, when implementing prior probability distribution in practical applications, whether it is the distribution of parameters in hydrological frequency analysis or hydrogeological parameters, the estimation of the prior distribution is still very challenging. It is often only possible to use uniform distribution instead of the prior information distribution for Bayesian theory. This limitation needs to be highlighted when applying Bayesian theory in applied hydrological modeling.

Meanwhile, to improve the reliability of groundwater resource assessment results, the following initiatives are highly suggested for future research. First, the expert knowledge of hydrogeological conditions is of vital importance. This helps grasp the medium conditions, water flow conditions and boundary conditions of the aquifer in the simulated area, to establish a correct conceptual model of hydrogeology and corresponding mathematical models. In doing so, the structural error in the model can be minimized. Second, there must be sufficient hydrogeological observation points to make the hydrogeological parameters representative and controllable. Third, if necessary, some field works must be supplemented to accurately calculate the parameters in the source and sink terms of the model, including recharge rate and hydraulic conductivity. Through the quantitative research on the uncertainty contributions in the evaluation of groundwater resources, the main contributions can be selected from the uncertainty sources, which will lay the foundation for the risk analysis of groundwater exploitation decisions.

Following the emergence of new open-source datasets, the method used in this dissertation can be extended to larger-scale applications, i.e., applications in continental or global scales. The current available global datasets include the GRACE satellite dataset [Feng et al., 2013, Fang and Shen, 2017], the UNESCO hydrogeological map [Sutanudjaja et al., 2011, 2014], the Global Runoff Data Centre (http://grdc.bafg.de), among others. These datasets allow hydrologists to set up models on a global scale with satisfying model performances [de Graaf et al., 2015, Wada et al., 2010]. The mHM-OGS coupled model fits well with these global datasets. This is attributed to its capability to read data with different spatial and temporal resolutions while being computationally efficient. Another reason is that mHM can assimilate various sources of data (e.g., remote sensing data) for model validation [Zink et al., 2018]. Global hydrological models can provide important insights and guidelines for groundwater resources management. Meanwhile, the majority of existing global hydrological models do not have an explicit characterization of the groundwater compartment. Only a very limited number of studies attempted to set up global hydrologic models that characterize groundwater systems explicitly [de Graaf et al., 2015, de Graaf et al., 2017]. In the next step, the mHM-OGS coupled model is expected to be applied to a larger scale using multiple global datasets.

Appendix A

Theory of random walk particle tracking

RWPT method is a Lagrangian method for solute transport modeling in saturated/unsaturated zones. The basic idea of RWPT method is to assume that advection process is deterministic and diffusion-dispersion process is stochastic. RWPT solves a diffusion equation at a local Lagrangian coordinates rather than the classical advection-diffusion equation, which can be expressed as:

$$\mathbf{x}(t_i) = \mathbf{x}(t_{i-1}) + \mathbf{v}(\mathbf{x}(t_{i-1}))\Delta t + Z\sqrt{2\mathbf{D}(\mathbf{x}(t_{i-1})\Delta t} \tag{A.1}$$

where $\mathbf{x}$ denotes the coordinates of the particle location, Δt denotes the time step size, and Z denotes a random number with the mean being zero and variance being unity.

The velocity $\mathbf{v}$ in Eq. (A.1) is replaced by $\mathbf{v}_i^*$ to keep consistency with the classical advection-dispersion equation [Kinzelbach, 1986]. The expressions of $\mathbf{v}_i^*$ and the hydrodynamic dispersion tensor $\mathbf{D}_{ij}$ are:

$$\mathbf{v}_i^* = \mathbf{v}_i + \sum_{i=1}^{3} \frac{\partial \mathbf{D}_{ij}}{\partial x_{ij}} \tag{A.2}$$

$$\mathbf{D}_{ij} = \alpha_T |\mathbf{v}| \delta_{ij} + (\alpha_L - \alpha_T) \frac{\mathbf{v}_i \mathbf{v}_j}{|\mathbf{v}|} + \mathbf{D}_{ij}^d \tag{A.3}$$

where δ_{ij} denotes the Kronecker symbol, α_L denotes the longitudinal dispersion length, α_T denotes the transverse dispersion length, $\mathbf{D}_{ij}^{d}$ denotes the tensor of molecular diffusion coefficient and $\mathbf{v}_i$ denotes the mean pore velocity component at the ith direction.

The stochastic governing equation of 3-D RWPT can therefore be expressed as:

$$\begin{aligned}
x_{t+\Delta t} &= x_t + \Big(V_x(x_t, y_t, z_t, t) + \frac{\partial D_{xx}}{\partial x} + \frac{\partial D_{xy}}{\partial y} + \frac{\partial D_{xz}}{\partial z}\Big)\Delta t \\
&\quad + \sqrt{2D_{xx}\Delta t}Z_1 + \sqrt{2D_{xy}\Delta t}Z_2 + \sqrt{2D_{xz}\Delta t}Z_3 \\
y_{t+\Delta t} &= y_t + \Big(V_y(x_t, y_t, z_t, t) + \frac{\partial D_{yx}}{\partial x} + \frac{\partial D_{yy}}{\partial y} + \frac{\partial D_{yz}}{\partial z}\Big)\Delta t \\
&\quad + \sqrt{2D_{yx}\Delta t}Z_1 + \sqrt{2D_{yy}\Delta t}Z_2 + \sqrt{2D_{yz}\Delta t}Z_3 \\
z_{t+\Delta t} &= z_t + \Big(V_z(x_t, y_t, z_t, t) + \frac{\partial D_{zx}}{\partial x} + \frac{\partial D_{zy}}{\partial y} + \frac{\partial D_{zz}}{\partial z}\Big)\Delta t \\
&\quad + \sqrt{2D_{zx}\Delta t}Z_1 + \sqrt{2D_{zy}\Delta t}Z_2 + \sqrt{2D_{zz}\Delta t}Z_3
\end{aligned} \tag{A.4}$$

where x, y, z are the spatial coordinates of particle, Δt is the time step, Z_i is a random number with a mean of zero and a unit variance [Jing et al., 2019a].

Appendix B

Composite parameter sensitivity

The PEST algorithm calculates the sensitivity with respect to each parameter of all observations (with the latter weighted as per user-assigned weights), namely the "composite sensitivity" [Doherty, 2015]. The composite sensitivity of parameter i is defined as $csp_i = \frac{[\mathbf{J}^t\mathbf{Q}\mathbf{J}]_{ii}^{1/2}}{n}$, where $\mathbf{J}$ denotes the Jacobian matrix that includes the sensitivities of all predictions to all model parameters, $\mathbf{Q}$ is the weight matrix, and n is the number of observations with nonzero weights. In this study, all weights assigned to observations are equally set to 1. Table B.1 displays the composite parameter sensitivities in each recharge realization. The mean composite parameter sensitivities of calibrations in all recharge realizations are also included in this table. The hydraulic conductivity of the Middle Muschelkalk (mm) is highly sensitive to groundwater head observations, whereas that of the Lower Muschelkalk (mu) is insensitive to groundwater head observations. The

Table B.1: Composite parameter sensitivities to the groundwater head observations.

Recharge realizations	Parameter sensitivities [-]						
	soil	alluvium	km	ku	mo	mm	mu
R1	6.01	1.89	0.58	1.50	9.47	20.45	0.23
R2	6.15	1.93	0.49	1.52	9.62	20.61	0.35
R3	4.05	1.78	1.38	1.91	7.20	25.84	0.82
R4	5.97	1.91	0.39	1.56	9.41	20.99	0.19
R5	7.31	1.86	0.31	1.34	10.09	19.40	0.015
R6	5.87	1.90	0.39	1.67	9.50	21.03	0.23
R7	7.77	1.93	0.57	1.93	10.53	19.07	0.41
R8	5.03	1.87	0.48	1.81	9.07	22.64	0.11
mean	6.77	1.88	0.57	1.66	9.36	21.25	0.29

sensitivity of mu, however, varies widely between different recharge realizations, from the highest one in R3 (0.82) to the lowest one in R5 (0.015) [Jing et al., 2019a].

Bibliography

T. Aigner. Calcareous Tempestites: Storm-dominated Stratification in Upper Muschelkalk Limestones (Middle Trias, SW-Germany). In *Cyclic and Event Stratification*, pages 180–198, Berlin, Heidelberg, 1982. Springer Berlin Heidelberg.

N. K. Ajami, Q. Duan, and S. Sorooshian. An integrated hydrologic Bayesian multimodel combination framework: Confronting input, parameter, and model structural uncertainty in hydrologic prediction. *Water Resources Research*, 43(1), 2007. doi: 10.1029/2005WR004745.

A. A. Ameli, N. Amvrosiadi, T. Grabs, H. Laudon, I. F. Creed, J. J. McDonnell, and K. Bishop. Hillslope permeability architecture controls on subsurface transit time distribution and flow paths. *Journal of Hydrology*, 543:17–30, 2016. doi: 10.1016/j.jhydrol.2016.04.071.

M. P. Anderson, W. W. Woessner, and R. J. Hunt. *Applied groundwater modeling: Simulation of flow and advective transport*. Academic Press, 2015.

S. Arnold, S. Attinger, K. Frank, and A. Hildebrandt. Uncertainty in parameterisation and model structure affect simulation results in coupled ecohydrological models. *Hydrology and Earth System Sciences*, 13(10):1789–1807, 2009. doi: 10.5194/hess-13-1789-2009.

R. Barthel and S. Banzhaf. Groundwater and Surface Water Interaction at the Regional-scale – A Review with Focus on Regional Integrated Models. *Water Resources Management*, 30(1):1–32, 2015. doi: 10.1007/s11269-015-1163-z.

N. B. Basu, G. Destouni, J. W. Jawitz, S. E. Thompson, N. V. Loukinova, A. Darracq, S. Zanardo, M. Yaeger, M. Sivapalan, A. Rinaldo, et al. Nutrient loads exported from managed catchments reveal emergent biogeochemical stationarity. *Geophysical Research Letters*, 37(23), 2010. doi: 10.1029/2010GL045168.

N. B. Basu, P. Jindal, K. E. Schilling, C. F. Wolter, and E. S. Takle. Evaluation of analytical and numerical approaches for the estimation of groundwater travel time distribution. *Journal of Hydrology*, 475:65 – 73, 2012. doi: 10.1016/j.jhydrol.2012.08.052.

P. Benettin, J. W. Kirchner, A. Rinaldo, and G. Botter. Modeling chloride transport using travel time distributions at Plynlimon, Wales. *Water Resources Research*, 51(5): 3259–3276, 2015. doi: 10.1002/2014WR016600.

P. Benettin, C. Soulsby, C. Birkel, D. Tetzlaff, G. Botter, and A. Rinaldo. Using SAS functions and high-resolution isotope data to unravel travel time distributions in headwater catchments. *Water Resources Research*, 53(3):1864–1878, 2017. doi: 10.1002/2016WR020117.

J. W. Beniston, S. T. DuPont, J. D. Glover, R. Lal, and J. A. Dungait. Soil organic carbon dynamics 75 years after land-use change in perennial grassland and annual wheat agricultural systems. *Biogeochemistry*, 120(1-3):37–49, 2014. doi: 10.1007/s10533-014-9980-3.

D. A. Benson, T. Aquino, D. Bolster, N. Engdahl, C. V. Henri, and D. Fernandez-Garcia. A comparison of Eulerian and Lagrangian transport and non-linear reaction algorithms. *Advances in Water Resources*, 99:15–37, 2017. doi: 10.1016/j.advwatres.2016.11.003.

K. Beven. Interflow. In *Unsaturated Flow in Hydrologic Modeling: Theory and Practice*, pages 191–219. Springer Netherlands, Dordrecht, 1989. doi: 10.1007/978-94-009-2352-2_7.

K. Beven. Prophecy, reality and uncertainty in distributed hydrological modelling. *Advances in Water Resources*, 16(1):41–51, 1993. doi: 10.1016/0309-1708(93)90028-E.

C. Beyer, S. Bauer, and O. Kolditz. Uncertainty assessment of contaminant plume length estimates in heterogeneous aquifers. *Journal of Contaminant Hydrology*, 87(1):73 – 95, 2006. doi: 10.1016/j.jconhyd.2006.04.006.

G. Bisht, M. Huang, T. Zhou, X. Chen, H. Dai, G. E. Hammond, W. J. Riley, J. L. Downs, Y. Liu, and J. M. Zachara. Coupling a three-dimensional subsurface flow and transport model with a land surface model to simulate stream–aquifer–land interactions (CP v1.0). *Geoscientific Model Development*, 10(12):4539–4562, 2017. doi: 10.5194/gmd-10-4539-2017.

J. K. Böhlke. Groundwater recharge and agricultural contamination. *Hydrogeology Journal*, 10(1):153–179, 2002. doi: 10.1007/s10040-001-0183-3.

J. K. Böhlke and J. M. Denver. Combined use of groundwater dating, chemical, and isotopic analyses to resolve the history and fate of nitrate contamination in two agricultural watersheds, atlantic coastal plain, maryland. *Water Resources Research*, 31(9):2319–2339, 1995. doi: 10.1029/95WR01584.

G. Botter, E. Bertuzzo, and A. Rinaldo. Transport in the hydrologic response: Travel time distributions, soil moisture dynamics, and the old water paradox. *Water Resources Research*, 46(3):1–18, 2010. doi: 10.1029/2009WR008371.

G. Botter, E. Bertuzzo, and A. Rinaldo. Catchment residence and travel time distributions: The master equation. *Geophysical Research Letters*, 38(11):1–6, 2011. doi: 10.1029/2011GL047666.

S. Brouyère, G. Carabin, and A. Dassargues. Climate change impacts on groundwater resources: Modelled deficits in a chalky aquifer, Geer basin, Belgium. *Hydrogeology Journal*, 12(2):123–134, 2004. doi: 10.1007/s10040-003-0293-1.

M. Brunke and T. Gonser. The ecological significance of exchange processes between rivers and groundwater. *Freshwater Biology*, 37(1):1–33, 1997. doi: 10.1046/j.1365-2427.1997.00143.x.

M. Camporese, C. Paniconi, M. Putti, and S. Orlandini. Surface-subsurface flow modeling with path-based runoff routing, boundary condition-based coupling, and assimilation of multisource observation data. *Water Resources Research*, 46(2), 2010. doi: 10.1029/2008WR007536.

G. Cao, C. Zheng, B. R. Scanlon, J. Liu, and W. Li. Use of flow modeling to assess sustainability of groundwater resources in the North China Plain. *Water Resources Research*, 49(1):159–175, 2013. doi: 10.1029/2012WR011899.

I. Cartwright and U. Morgenstern. Transit times from rainfall to baseflow in headwater catchments estimated using tritium: the ovens river, australia. *Hydrology and Earth System Sciences*, 19(9):3771–3785, 2015. doi: 10.5194/hess-19-3771-2015.

Z. Chen, A. Hartmann, T. Wagener, and N. Goldscheider. Dynamics of water fluxes and storages in an Alpine karst catchment under current and potential future climate

conditions. *Hydrology and Earth System Sciences*, 22(7):3807–3823, 2018. doi: 10.5194/hess-22-3807-2018.

Y. Cheng, H. Zhan, W. Yang, H. Dang, and W. Li. Is annual recharge coefficient a valid concept in arid and semi-arid regions? *Hydrology and Earth System Sciences*, 21(10): 5031–5042, 2017. doi: 10.5194/hess-21-5031-2017.

O. A. Cirpka and S. Attinger. Effective dispersion in heterogeneous media under random transient flow conditions. *Water Resources Research*, 39(9), 2003. doi: 10.1029/2002WR001931.

M. P. Clark, A. G. Slater, D. E. Rupp, R. A. Woods, J. A. Vrugt, H. V. Gupta, T. Wagener, and L. E. Hay. Framework for Understanding Structural Errors (FUSE): A modular framework to diagnose differences between hydrological models. *Water Resources Research*, 44(12), 2008. doi: 10.1029/2007WR006735.

M. P. Clark, Y. Fan, D. M. Lawrence, J. C. Adam, D. Bolster, D. J. Gochis, R. P. Hooper, M. Kumar, L. R. Leung, D. S. Mackay, R. M. Maxwell, C. Shen, S. C. Swenson, and X. Zeng. Improving the representation of hydrologic processes in Earth System Models. *Water Resources Research*, 51(8):5929–5956, 2015. doi: 10.1002/2015WR017096.

M. Collins, R. Knutti, J. Arblaster, J.-L. Dufresne, T. Fichefet, P. Friedlingstein, X. Gao, W. J. Gutowski, T. Johns, G. Krinner, M. Shongwe, C. Tebaldi, A. J. Weaver, and M. Wehner. Long-term Climate Change: Projections, Commitments and Irreversibility. *Climate Change 2013: The Physical Science Basis. Contribution of Working Group I to the Fifth Assessment Report of the Intergovernmental Panel on Climate Change*, pages 1029–1136, 2013. doi: 10.1017/CBO9781107415324.024.

F. J. Cornaton. Transient water age distributions in environmental flow systems: The time-marching Laplace transform solution technique. *Water Resources Research*, 48(3): 1–17, 2012. doi: 10.1029/2011WR010606.

R. S. Crosbie, B. R. Scanlon, F. S. Mpelasoka, R. C. Reedy, J. B. Gates, and L. Zhang. Potential climate change effects on groundwater recharge in the High Plains Aquifer, USA. *Water Resources Research*, 49(7):3936–3951, 2013. doi: 10.1002/wrcr.20292.

J. A. Cunge. On the subject of a flood propagation computation method (musklngum method). *Journal of Hydraulic Research*, 7(2):205–230, 1969. doi: 10.1080/00221686909500264.

G. Dagan. *Flow and transport in porous formations*. Springer Science & Business Media, 2012.

M. Danesh-Yazdi, J. Klaus, L. E. Condon, and R. M. Maxwell. Bridging the gap between numerical solutions of travel time distributions and analytical storage selection functions. *Hydrological Processes*, 32(8):1063–1076, 2018. doi: 10.1002/hyp.11481.

W. R. Danskin. *Evaluation of the hydrologic system and selected water-management alternatives in the Owens Valley, California*, volume 2370. US Department of the Interior, US Geological Survey, 1999.

I. E. de Graaf, R. L. van Beek, T. Gleeson, N. Moosdorf, O. Schmitz, E. H. Sutanudjaja, and M. F. Bierkens. A global-scale two-layer transient groundwater model: Development and application to groundwater depletion. *Advances in Water Resources*, 102:53–67, 2017. doi: 10.1016/j.advwatres.2017.01.011.

I. E. M. de Graaf, E. H. Sutanudjaja, L. P. H. van Beek, and M. F. P. Bierkens. A high-resolution global-scale groundwater model. *Hydrology and Earth System Sciences*, 19(2):823–837, 2015. doi: 10.5194/hess-19-823-2015.

G. de Marsily, F. Delay, J. Gonçalvès, P. Renard, V. Teles, and S. Violette. Dealing with spatial heterogeneity. *Hydrogeology Journal*, 13(1):161–183, 2005. doi: 10.1007/s10040-004-0432-3.

R. de Rooij, W. araraham, and R. M. Maxwell. A particle-tracking scheme for simulating pathlines in coupled surface-subsurface flows. *Advances in Water Resources*, 52:7–18, 2013a. doi: 10.1016/j.advwatres.2012.07.022.

R. de Rooij, P. Perrochet, and W. Graham. From rainfall to spring discharge: Coupling conduit flow, subsurface matrix flow and surface flow in karst systems using a discrete–continuum model. *Advances in Water Resources*, 61:29–41, 2013b. doi: 10.1016/j.advwatres.2013.08.009.

J. O. Delfs, F. Blumensaat, W. Wang, P. Krebs, and O. Kolditz. Coupling hydrogeological with surface runoff model in a Poltva case study in Western Ukraine. *Environmental Earth Sciences*, 65(5):1439–1457, 2012. doi: 10.1007/s12665-011-1285-4.

J. Doherty. *Calibration and uncertainty analysis for complex environmental models*. Watermark Numerical Computing, 2015.

J. Doherty and R. Hunt. *Approaches to highly parameterized inversion: a guide to using PEST for groundwater-model calibration.* US Department of the Interior, US Geological Survey, 2010.

J. Doherty et al. PEST: a unique computer program for model-independent parameter optimisation. *Water Down Under 94: Groundwater/Surface Hydrology Common Interest Papers; Preprints of Papers*, page 551, 1994.

P. Döll, H. Hoffmann-Dobrev, F. T. Portmann, S. Siebert, A. Eicker, M. Rodell, G. Strassberg, and B. R. Scanlon. Impact of water withdrawals from groundwater and surface water on continental water storage variations. *Journal of Geodynamics*, 59-60:143–156, 2012. doi: 10.1016/j.jog.2011.05.001.

J. É. J. Dupuit. *Études théoriques et pratiques sur le mouvement des eaux dans les canaux découverts et à travers les terrains perméables: avec des considérations relatives au régime des grandes eaux, au débouché à leur donner, et à la marche des alluvions dans les rivières à fond mobile.* Dunod, 1863.

S. M. Eberts, J. K. Böhlke, L. J. Kauffman, and B. C. Jurgens. Comparison of particle-tracking and lumped-parameter age-distribution models for evaluating vulnerability of production wells to contamination. *Hydrogeology Journal*, 20(2):263–282, 2012. doi: 10.1007/s10040-011-0810-6.

N. B. Engdahl. Transient effects on confined groundwater age distributions: Considering the necessity of time-dependent simulations. *Water Resources Research*, 53(8):7332–7348, 2017. doi: 10.1002/2016WR019916.

N. B. Engdahl and R. M. Maxwell. Quantifying changes in age distributions and the hydrologic balance of a high-mountain watershed from climate induced variations in recharge. *Journal of Hydrology*, 522:152 – 162, 2015. doi: 10.1016/j.jhydrol.2014.12.032.

N. B. Engdahl, J. L. McCallum, and A. Massoudieh. Transient age distributions in subsurface hydrologic systems. *Journal of Hydrology*, 543:88–100, 2016. doi: 10.1016/j.jhydrol.2016.04.066.

K. Fang and C. Shen. Full-flow-regime storage-streamflow correlation patterns provide insights into hydrologic functioning over the continental US. *Water Resources Research*, 53(9):8064–8083, 2017. doi: 10.1002/2016WR020283.

W. Feng, M. Zhong, J. M. Lemoine, R. Biancale, H. T. Hsu, and J. Xia. Evaluation of groundwater depletion in North China using the Gravity Recovery and Climate Experiment (GRACE) data and ground-based measurements. *Water Resources Research*, 49(4):2110–2118, 2013. doi: 10.1002/wrcr.20192.

I. M. Ferguson, J. L. Jefferson, R. M. Maxwell, and S. J. Kollet. Effects of root water uptake formulation on simulated water and energy budgets at local and basin scales. *Environmental Earth Sciences*, 75(4):1–15, 2016. doi: 10.1007/s12665-015-5041-z.

C. Fetter. *Applied Hydrogeology*. Waveland Press, Incorporated, 2018.

T. Fischer, D. Naumov, S. Sattler, O. Kolditz, and M. Walther. GO2OGS 1.0: A versatile workflow to integrate complex geological information with fault data into numerical simulation models. *Geoscientific Model Development*, 8(11):3681–3694, 2015. doi: 10.5194/gmd-8-3681-2015.

P. Forchheimer. Uber die ergiebigkeit von brummen, Anlagen und Sickerschlitzen. *Zeitsch Archit. Ing. Ver., Hannover*, 32:539–563, 1986.

J. Garbrecht and G. W. Brunner. A Muskingum-Cunge channel flow routing method for drainage networks. Technical report, Hydrologic Engineering Center Davis CA, 1991.

T. R. Ginn. On the distribution of multicomponent mixtures over generalized exposure time in subsurface flow and reactive transport: Theory and formulations for residence-time-dependent sorption/desorption with memory. *Water Resources Research*, 36(10): 2885–2893, 2000. doi: 10.1029/2000WR900170.

P. Goderniaux, S. Brouyère, H. J. Fowler, S. Blenkinsop, R. Therrien, P. Orban, and A. Dassargues. Large scale surface-subsurface hydrological model to assess climate change impacts on groundwater reserves. *Journal of Hydrology*, 373(1-2):122–138, 2009. doi: 10.1016/j.jhydrol.2009.04.017.

P. Goderniaux, S. Brouyère, S. Wildemeersch, R. Therrien, and A. Dassargues. Uncertainty of climate change impact on groundwater reserves - Application to a chalk aquifer. *Journal of Hydrology*, 528:108–121, 2015. doi: 10.1016/j.jhydrol.2015.06.018.

D. J. Goode. Direct simulation of groundwater age. *Water Resources Research*, 32(2): 289–296, 1996. doi: 10.1029/95WR03401.

A. Gräbe, T. Rödiger, K. Rink, T. Fischer, F. Sun, W. Wang, C. Siebert, and O. Kolditz. Numerical analysis of the groundwater regime in the western Dead Sea escarpment, Israel+ West Bank. *Environmental Earth Sciences*, 69(2):571–585, 2013. doi: 10.1007/s12665-012-1795-8.

T. R. Green, M. Taniguchi, H. Kooi, J. J. Gurdak, D. M. Allen, K. M. Hiscock, H. Treidel, and A. Aureli. Beneath the surface of global change: Impacts of climate change on groundwater. *Journal of Hydrology*, 405(3):532–560, 2011. doi: 10.1016/j.jhydrol.2011.05.002.

P. Greve, T. Kahil, J. Mochizuki, T. Schinko, Y. Satoh, P. Burek, G. Fischer, S. Tramberend, R. Burtscher, S. Langan, et al. Global assessment of water challenges under uncertainty in water scarcity projections. *Nature Sustainability*, 1(9):486, 2018. doi: 10.1038/s41893-018-0134-9.

P. Groenendijk and G. van den Eertwegh. Drainage-water travel times as a key factor for surface water contamination. *Unsaturated zone modeling. Progress, challenges and applications. Wageningen UR Frontis Ser*, 6:145–178, 2004.

L. E. Gulden, E. Rosero, Z. L. Yang, M. Rodell, C. S. Jackson, G. Y. Niu, P. J. F. Yeh, and J. Famiglietti. Improving land-surface model hydrology: Is an explicit aquifer model better than a deeper soil profile? *Geophysical Research Letters*, 34(9):1–5, 2007. doi: 10.1029/2007GL029804.

H. Haitjema. On the residence time distribution in idealized groundwater sheds. *Journal of Hydrology*, 172:127–146, 1995. doi: 10.1016/0022-1694(95)02732-5.

V. C. Hale and J. J. McDonnell. Effect of bedrock permeability on stream base flow mean transit time scaling relations: 1. A multiscale catchment intercomparison. *Water Resources Research*, 52(2):1358–1374, 2016. doi: 10.1002/2014WR016124.

B. A. W. Harbaugh, E. R. Banta, M. C. Hill, and M. G. Mcdonald. MODFLOW-2000 , The U .S . Geological Survey modular graound-water model — User guide to modularization concepts and the ground-water flow process. *U.S. Geological Survey*, page 130, 2000.

G. H. Hargreaves and Z. A. Samani. Reference crop evapotranspiration from temperature. *Applied Engineering in Agriculture*, 1(2):96–99, 1985. doi: 10.13031/2013.26773.

A. H. Haria and P. Shand. Evidence for deep sub-surface flow routing in forested upland Wales : implications for contaminant transport and stream flow generation. *Hydrology and Earth System Sciences*, 8(3):334–344, 2004. doi: 10.5194/hess-8-334-2004.

C. J. Harman. Time-variable transit time distributions and transport: Theory and application to storage-dependent transport of chloride in a watershed. *Water Resources Research*, 51(1):1–30, 2015. doi: 10.1002/2014WR015707.

C. J. Harman, A. S. Ward, and A. Ball. How does reach-scale stream-hyporheic transport vary with discharge? insights from rsas analysis of sequential tracer injections in a headwater mountain stream. *Water Resources Research*, 52(9):7130–7150, 2016. doi: 10.1002/2016WR018832.

A. Hartmann, T. Gleeson, R. Rosolem, F. Pianosi, Y. Wada, and T. Wagener. A large-scale simulation model to assess karstic groundwater recharge over Europe and the Mediterranean. *Geoscientific Model Development*, 8(6):1729–1746, 2015. doi: 10.5194/gmd-8-1729-2015.

F. F. Hattermann, V. Krysanova, S. N. Gosling, R. Dankers, P. Daggupati, C. Donnelly, M. Flörke, S. Huang, Y. Motovilov, S. Buda, T. Yang, C. Müller, G. Leng, Q. Tang, F. T. Portmann, S. Hagemann, D. Gerten, Y. Wada, Y. Masaki, T. Alemayehu, Y. Satoh, and L. Samaniego. Cross-scale intercomparison of climate change impacts simulated by regional and global hydrological models in eleven large river basins. *Climatic Change*, 141(3):561–576, 2017. doi: 10.1007/s10584-016-1829-4.

T. Havril, Á. Tóth, J. W. Molson, A. Galsa, and J. Mádl-Szonyi. Impacts of predicted climate change on groundwater flow systems: Can wetlands disappear due to recharge reduction? *Journal of Hydrology*, 563:1169 – 1180, 2017. doi: 10.1016/j.jhydrol.2017.09.020.

P. M. Haygarth, H. P. Jarvie, S. M. Powers, A. N. Sharpley, J. J. Elser, J. Shen, H. M. Peterson, N.-I. Chan, N. J. K. Howden, T. Burt, F. Worrall, F. Zhang, and X. Liu. Sustainable Phosphorus Management and the Need for a Long-Term Perspective: The Legacy Hypothesis. *Environmental Science & Technology*, 48(15):8417–8419, 2014. doi: 10.1021/es502852s.

M. Haylock, N. Hofstra, A. Klein Tank, E. Klok, P. Jones, and M. New. A European daily high-resolution gridded data set of surface temperature and precipitation for

1950-2006. *Journal of Geophysical Research Atmospheres*, 113(20), 2008. doi: 10.1029/2008JD010201.

W. He, C. Beyer, J. H. Fleckenstein, E. Jang, O. Kolditz, D. Naumov, and T. Kalbacher. A parallelization scheme to simulate reactive transport in the subsurface environment with OGS#IPhreeqc 5.5.7-3.1.2. *Geoscientific Model Development*, 8(10):3333–3348, 2015. doi: 10.5194/gmd-8-3333-2015.

R. W. Healy. *Estimating Groundwater Recharge*. Cambridge University Press, 2010.

S. Hempel, K. Frieler, L. Warszawski, J. Schewe, and F. Piontek. A trend-preserving bias correction – the ISI-MIP approach. *Earth System Dynamics*, 4(2):219–236, 2013. doi: 10.5194/esd-4-219-2013.

F. Heße, M. Zink, R. Kumar, L. Samaniego, and S. Attinger. Spatially distributed characterization of soil-moisture dynamics using travel-time distributions. *Hydrology and Earth System Sciences*, 21(1):549–570, 2017. doi: 10.5194/hess-21-549-2017.

N. J. K. Howden, T. P. Burt, F. Worrall, M. J. Whelan, and M. Bieroza. Nitrate concentrations and fluxes in the River Thames over 140 years (1868–2008): are increases irreversible? *Hydrological Processes*, 24(18):2657–2662, 2010. doi: 10.1002/hyp.7835.

M. Hrachowitz and M. P. Clark. HESS Opinions: The complementary merits of competing modelling philosophies in hydrology. *Hydrology and Earth System Sciences*, 21(8):3953–3973, 2017. doi: 10.5194/hess-21-3953-2017.

M. Hrachowitz, H. Savenije, T. A. Bogaard, D. Tetzlaff, and C. Soulsby. What can flux tracking teach us about water age distribution patterns and their temporal dynamics? *Hydrology and Earth System Sciences*, 17(2):533–564, 2013. doi: 10.5194/hess-17-533-2013.

S. Huang, R. Kumar, M. Flörke, T. Yang, Y. Hundecha, P. Kraft, C. Gao, A. Gelfan, S. Liersch, A. Lobanova, M. Strauch, F. van Ogtrop, J. Reinhardt, U. Haberlandt, and V. Krysanova. Evaluation of an ensemble of regional hydrological models in 12 large-scale river basins worldwide. *Climatic Change*, 141(3):381–397, Apr 2017. doi: 10.1007/s10584-016-1841-8.

R. J. Hunt, J. F. Walker, W. R. Selbig, S. M. Westenbroek, and R. S. Regan. Simulation of Climate - Change effects on streamflow, Lake water budgets, and stream temperature

using GSFLOW and SNTEMP, Trout Lake Watershed, Wisconsin. *USGS Scientific Investigations Report.*, pages 2013–5159, 2013.

J. L. Huntington and R. G. Niswonger. Role of surface-water and groundwater interactions on projected summertime streamflow in snow dominated regions: An integrated modeling approach. *Water Resources Research*, 48(11):1–20, 2012. doi: 10.1029/2012WR012319.

H. T. Hwang, Y. J. Park, E. A. Sudicky, and P. A. Forsyth. A parallel computational framework to solve flow and transport in integrated surface-subsurface hydrologic systems. *Environmental Modelling and Software*, 61:39–58, 2014. doi: 10.1016/j.envsoft.2014.06.024.

V. Y. Ivano, E. R. Vivoni, R. L. Bras, and D. Entekhabi. Catchment hydrologic response with a fully distributed triangulated irregular network model. *Water Resources Research*, 40(11), 2004. doi: 10.1029/2004WR003218.

C. R. Jackson, R. Meister, and C. Prudhomme. Modelling the effects of climate change and its uncertainty on UK Chalk groundwater resources from an ensemble of global climate model projections. *Journal of Hydrology*, 399(1-2):12–28, 2011. doi: 10.1016/j.jhydrol.2010.12.028.

R. James, R. Washington, C.-F. Schleussner, J. Rogelj, and D. Conway. Characterizing half-a-degree difference: a review of methods for identifying regional climate responses to global warming targets. *Wiley Interdisciplinary Reviews: Climate Change*, 8(2):e457, 2017. doi: 10.1002/wcc.457.

K. Jencso, B. McGlynn, M. Gooseff, S. Wondzell, K. Bencala, and L. Marshall. Hydrologic connectivity between landscapes and streams: Transferring reach- and plot-scale understanding to the catchment scale. *Water Resources Research*, 45(4), 2009. doi: 10.1029/2008WR007225.

M. Jing, F. Heße, R. Kumar, W. Wang, T. Fischer, M. Walther, M. Zink, A. Zech, L. Samaniego, O. Kolditz, and S. Attinger. Improved regional-scale groundwater representation by the coupling of the mesoscale Hydrologic Model (mHM v5.7) to the groundwater model OpenGeoSys (OGS). *Geoscientific Model Development*, 11(5):1989–2007, 2018. doi: 10.5194/gmd-11-1989-2018.

M. Jing, F. Heße, R. Kumar, O. Kolditz, T. Kalbacher, and S. Attinger. Influence of input and parameter uncertainty on the prediction of catchment-scale groundwater travel time distributions. *Hydrology and Earth System Sciences*, 23(1):171–190, 2019a. doi: 10.5194/hess-23-171-2019.

M. Jing, R. Kumar, F. Heße, S. Thober, O. Rakovec, L. Samaniego, and S. Attinger. Assessing the response of groundwater quantity and travel time distribution to 1.5, 2 and 3 degrees global warming in a mesoscale central German basin. *Hydrology and Earth System Sciences Discussions*, 2019:1–22, 2019b. doi: 10.5194/hess-2019-9.

L. Jochen, R. D. , and H.-G. Röhling. Lithostratigraphie des Buntsandstein in Deutschland. *Schriftenreihe der Deutschen Gesellschaft für Geowissenschaften*, 69:69–149, 08 2014. doi: 10.1127/sdgg/69/2014/69.

M. I. Jyrkama and J. F. Sykes. The impact of climate change on spatially varying groundwater recharge in the grand river watershed (Ontario). *Journal of Hydrology*, 338(3-4):237–250, 2007. doi: 10.1016/j.jhydrol.2007.02.036.

V. P. Kaandorp, P. G. B. Louw, Y. Velde, and H. P. Broers. Transient Groundwater Travel Time Distributions and Age-Ranked Storage-Discharge Relationships of Three Lowland Catchments. *Water Resources Research*, 54(7):4519–4536, 2018. doi: 10.1029/2017WR022461.

T. Kalbacher, J. O. Delfs, H. Shao, W. Wang, M. Walther, L. Samaniego, C. Schneider, R. Kumar, A. Musolff, F. Centler, F. Sun, A. Hildebrandt, R. Liedl, D. Borchardt, P. Krebs, and O. Kolditz. The IWAS-ToolBox: Software coupling for an integrated water resources management. *Environmental Earth Sciences*, 65(5):1367–1380, 2012. doi: 10.1007/s12665-011-1270-y.

S. Kang and E. A. B. Eltahir. North China Plain threatened by deadly heatwaves due to climate change and irrigation. *Nature Communications*, 9(1):2894, 2018. doi: 10.1038/s41467-018-05252-y.

H. Kim, W. E. Dietrich, B. M. Thurnhoffer, J. K. B. Bishop, and I. Y. Fung. Controls on solute concentration-discharge relationships revealed by simultaneous hydrochemistry observations of hillslope runoff and stream flow: The importance of critical zone structure. *Water Resources Research*, 53(2):1424–1443, 2017. doi: 10.1002/2016WR019722.

M. Kim, L. A. Pangle, C. Cardoso, M. Lora, T. H. M. Volkmann, Y. Wang, C. J. Harman, and P. A. Troch. Transit time distributions and StorAge Selection functions in a sloping soil lysimeter with time-varying flow paths: Direct observation of internal and external transport variability. *Water Resources Research*, 52(9):7105–7129, 2016. doi: 10.1002/2016WR018620.

N. W. Kim, I. M. Chung, Y. S. Won, and J. G. Arnold. Development and application of the integrated SWAT–MODFLOW model. *Journal of Hydrology*, 356(1):1–16, 2008. doi: 10.1016/j.jhydrol.2008.02.024.

W. Kinzelbach. *Groundwater modelling: an introduction with sample programs in BASIC*, volume 25. Elsevier, 1986.

J. W. Kirchner. Aggregation in environmental systems-Part 1: Seasonal tracer cycles quantify young water fractions, but not mean transit times, in spatially heterogeneous catchments. *Hydrology and Earth System Sciences*, 20(1):279–297, 2016. doi: 10.5194/hess-20-279-2016.

B. Kløve, P. Ala-Aho, G. Bertrand, J. J. Gurdak, H. Kupfersberger, J. Kværner, T. Muotka, H. Mykrä, E. Preda, P. Rossi, C. B. Uvo, E. Velasco, and M. Pulido-Velazquez. Climate change impacts on groundwater and dependent ecosystems. *Journal of Hydrology*, 518 (PB):250–266, 2014. doi: 10.1016/j.jhydrol.2013.06.037.

B. Kohlhepp, R. Lehmann, P. Seeber, K. Küsel, S. E. Trumbore, and K. U. Totsche. Aquifer configuration and geostructural links control the groundwater quality in thin-bedded carbonate–siliciclastic alternations of the Hainich CZE, central Germany. *Hydrology and Earth System Sciences*, 21(12):6091–6116, 2017. doi: 10.5194/hess-21-6091-2017.

S. Koirala, P. J.-F. Yeh, Y. Hirabayashi, S. Kanae, and T. Oki. Global-scale land surface hydrologic modeling with the representation of water table dynamics. *Journal of Geophysical Research: Atmospheres*, 119(1):75–89, 2014. doi: 10.1002/2013JD020398.

O. Kolditz, S. Bauer, L. Bilke, N. Böttcher, J. O. Delfs, T. Fischer, U. J. Görke, T. Kalbacher, G. Kosakowski, C. I. McDermott, C. H. Park, F. Radu, K. Rink, H. Shao, H. B. Shao, F. Sun, Y. Y. Sun, A. K. Singh, J. Taron, M. Walther, W. Wang, N. Watanabe, Y. Wu, M. Xie, W. Xu, and B. Zehner. OpenGeoSys: an open-source initiative for numerical simulation of thermo-hydro-mechanical/chemical (THM/C)

processes in porous media. *Environmental Earth Sciences*, 67(2):589–599, 2012. doi: 10.1007/s12665-012-1546-x.

O. Kolditz, H. Shao, W. Wang, and S. Bauer. *Thermo-hydro-mechanical Chemical Processes in Fractured Porous Media: Modelling and Benchmarking*. Springer, 2016.

S. J. Kollet and R. M. Maxwell. Demonstrating fractal scaling of baseflow residence time distributions using a fully-coupled groundwater and land surface model. *Geophysical Research Letters*, 35(7):1–6, 2008. doi: 10.1029/2008GL033215.

V. Koren, S. Reed, M. Smith, Z. Zhang, and D.-J. Seo. Hydrology laboratory research modeling system (HL-RMS) of the US national weather service. *Journal of Hydrology*, 291(3):297–318, 2004. doi: 10.1016/j.jhydrol.2003.12.039.

M. Kottek, J. Grieser, C. Beck, B. Rudolf, and F. Rubel. World map of the Köppen-Geiger climate classification updated. *Meteorologische Zeitschrift*, 15(3):259–263, 2006. doi: 10.1127/0941-2948/2006/0130.

M. Kumar, C. J. Duffy, and K. M. Salvage. A Second-Order Accurate, Finite Volume–Based, Integrated Hydrologic Modeling (FIHM) Framework for Simulation of Surface and Subsurface Flow. *Vadose Zone Journal*, 8(4):873, 2009. doi: 10.2136/vzj2009.0014.

R. Kumar, B. Livneh, and L. Samaniego. Toward computationally efficient large-scale hydrologic predictions with a multiscale regionalization scheme. *Water Resources Research*, 49(9):5700–5714, 2013a. doi: 10.1002/wrcr.20431.

R. Kumar, L. Samaniego, and S. Attinger. Implications of distributed hydrologic model parameterization on water fluxes at multiple scales and locations. *Water Resources Research*, 49(1):360–379, 2013b. doi: 10.1029/2012WR012195.

R. Kumar, J. L. Musuuza, A. F. van Loon, A. J. Teuling, R. Barthel, J. Ten Broek, J. Mai, L. Samaniego, and S. Attinger. Multiscale evaluation of the Standardized Precipitation Index as a groundwater drought indicator. *Hydrology and Earth System Sciences*, 20(3):1117–1131, 2016. doi: 10.5194/hess-20-1117-2016.

W. Kurtz, G. He, S. J. Kollet, R. M. Maxwell, H. Vereecken, and H.-J. Hendricks Franssen. TerrSysMP–PDAF (version 1.0): a modular high-performance data assimilation framework for an integrated land surface–subsurface model. *Geoscientific Model Development*, 9(4):1341–1360, 2016. doi: 10.5194/gmd-9-1341-2016.

K. Küsel, K. U. Totsche, S. E. Trumbore, R. Lehmann, C. Steinhäuser, and M. Herrmann. How Deep Can Surface Signals Be Traced in the Critical Zone? Merging Biodiversity with Biogeochemistry Research in a Central German Muschelkalk Landscape. *Frontiers in Earth Science*, 4(April):1–18, 2016. doi: 10.3389/feart.2016.00032.

S. Leray, N. B. Engdahl, A. Massoudieh, E. Bresciani, and J. McCallum. Residence time distributions for hydrologic systems: Mechanistic foundations and steady-state analytical solutions. *Journal of Hydrology*, 543:67–87, 2016. doi: 10.1016/j.jhydrol.2016.01.068.

L. R. Leung, M. Huang, Y. Qian, and X. Liang. Climate-soil-vegetation control on groundwater table dynamics and its feedbacks in a climate model. *Climate Dynamics*, 36(1):57–81, 2011. doi: 10.1007/s00382-010-0746-x.

X. Liang, D. P. Lettenmaier, E. F. Wood, and S. J. Burges. A simple hydrologically based model of land surface water and energy fluxes for general circulation models. *Journal of Geophysical Research: Atmospheres*, 99(D7):14415–14428, 1994. doi: 10.1029/94JD00483.

X. Liang, Z. Xie, and M. Huang. A new parameterization for surface and groundwater interactions and its impact on water budgets with the variable infiltration capacity (VIC) land surface model. *Journal of Geophysical Research*, 108(D16):8613–8629, 2003. doi: 10.1029/2002JD003090.

N. Linde, P. Renard, T. Mukerji, and J. Caers. Geological Realism in Hydrogeological and Geophysical Inverse Modeling: a Review. *Advances in Water Resources*, 86:86–101, 2015. doi: 10.1016/j.advwatres.2015.09.019.

G. Lindström, B. Johansson, M. Persson, M. Gardelin, and S. Bergström. Development and test of the distributed HBV-96 hydrological model. *Journal of Hydrology*, 201(1-4):272–288, 1997. doi: 10.1016/S0022-1694(97)00041-3.

S. L. Markstrom, R. G. Niswonger, R. S. Regan, D. E. Prudic, and P. M. Barlow. GSFLOW—Coupled Ground-Water and Surface-Water Flow Model Based on the

Integration of the Precipitation-Runoff Modeling System (PRMS) and the Modular Ground-Water Flow Model (MODFLOW-2005). *U.S. Geological Survey*, (Techniques and Methods 6-D1):240, 2008.

A. Marx, R. Kumar, S. Thober, O. Rakovec, N. Wanders, M. Zink, E. F. Wood, M. Pan, J. Sheffield, and L. Samaniego. Climate change alters low flows in Europe under global warming of 1.5, 2, and 3 °C. *Hydrology and Earth System Sciences*, 22(2):1017–1032, 2018. doi: 10.5194/hess-22-1017-2018.

R. M. Maxwell and S. J. Kollet. Interdependence of groundwater dynamics and land-energy feedbacks under climate change. *Nature Geoscience*, 1(10):665–669, 2008. doi: 10.1038/ngeo315.

R. M. Maxwell and N. L. Miller. Development of a coupled land surface and groundwater model. *Journal of Hydrometeorology*, 6(3):233–247, 2005. doi: 10.1175/JHM422.1.

R. M. Maxwell, M. Putti, S. Meyerhoff, J.-O. Delfs, I. M. Ferguson, V. Ivanov, J. Kim, O. Kolditz, S. J. Kollet, M. Kumar, S. Lopez, J. Niu, C. Paniconi, Y.-J. Park, M. S. Phanikumar, C. Shen, E. A. Sudicky, and M. Sulis. Surface-subsurface model intercomparison: A first set of benchmark results to diagnose integrated hydrology and feedbacks. *Water Resources Research*, 50:1531–1549, 2014. doi: 10.1002/2013WR013725.

R. M. Maxwell, L. E. Condon, and S. J. Kollet. A high-resolution simulation of groundwater and surface water over most of the continental US with the integrated hydrologic model ParFlow v3. *Geoscientific Model Development*, 8(3):923–937, mar 2015. doi: 10.5194/gmd-8-923-2015.

J. L. McCallum, N. B. Engdahl, T. R. Ginn, and P. G. Cook. Nonparametric estimation of groundwater residence time distributions: What can environmental tracer data tell us about groundwater residence time? *Water Resources Research*, 50(3):2022–2038, 2014. doi: 10.1002/2013WR014974.

J. L. McCallum, P. G. Cook, S. Dogramaci, and R. Purtschert. Identifying modern and historic recharge events from tracer-derived groundwater age distributions. *Water Resources Research*, 53(2):1039–1056, 2017. doi: 10.1111/j.1752-1688.1969.tb04897.x.

T. McCann. *The Geology of Central Europe Volume 2: Mesozoic and Cenozoic*. Geological Society of London, 2008. doi: 10.1144/CEV2P.

J. J. McDonnell, K. McGuire, P. Aggarwal, K. J. Beven, D. Biondi, G. Destouni, S. Dunn, A. James, J. Kirchner, P. Kraft, S. Lyon, P. Maloszewski, B. Newman, L. Pfister, A. Rinaldo, A. Rodhe, T. Sayama, J. Seibert, K. Solomon, C. Soulsby, M. Stewart, D. Tetzlaff, C. Tobin, P. Troch, M. Weiler, A. Western, A. Wörman, and S. Wrede. How old is streamwater? Open questions in catchment transit time conceptualization, modelling and analysis. *Hydrological Processes*, 24(12):1745–1754, 2010. doi: 10.1002/hyp.7796.

D. McInerney, M. Thyer, D. Kavetski, J. Lerat, and G. Kuczera. Improving probabilistic prediction of daily streamflow by identifying Pareto optimal approaches for modeling heteroscedastic residual errors. *Water Resources Research*, 53(3):2199–2239, 2017. doi: 10.1111/j.1752-1688.1969.tb04897.x.

P. McLachlan, J. Chambers, S. Uhlemann, and A. Binley. Geophysical characterisation of the groundwater–surface water interface. *Advances in Water Resources*, 109(Supplement C):302 – 319, 2017. doi: 10.1016/j.advwatres.2017.09.016.

G. A. Meehl, T. F. Stocker, W. D. Collins, P. Friedlingstein, T. Gaye, J. M. Gregory, A. Kitoh, R. Knutti, J. M. Murphy, A. Noda, et al. *Global climate projections*. Cambridge, UK, Cambridge University Press, 2007.

M. Menning. Deutsche Stratigraphische Kommission (2002) Eine geologische Zeitskala 2002. *Deutsche Stratigraphische Kommission (ed) Stratigraphische Tabelle von Deutschland*, 2002.

G. Merz. Zur Petrographie, Stratigraphie, Paläogeographie und Hydrogeologie des Muschelkalks (Trias) im Thüringer Becken. *Zeitschrift der geologischen Wissenschaften*, 15(4):457–473, 1987.

J. Molnat and C. Gascuel-Odoux. Modelling flow and nitrate transport in groundwater for the prediction of water travel times and of consequences of land use evolution on water quality. *Hydrological Processes*, 16(2):479–492, 2002. doi: 10.1002/hyp.328.

C. Moore and J. Doherty. The cost of uniqueness in groundwater model calibration. *Advances in Water Resources*, 29(4):605–623, 2006. doi: 10.1016/j.advwatres.2005.07.003.

H. Moutahir, P. Bellot, R. Monjo, J. Bellot, M. Garcia, and I. Touhami. Likely effects of climate change on groundwater availability in a Mediterranean region of Southeastern Spain. *Hydrological Processes*, 31(1):161–176, 2016. doi: 10.1002/hyp.10988.

S. P. Neuman. Theory of flow in unconfined aquifers considering delayed response of the water table. *Water Resources Research*, 8(4):1031–1045, 1972. doi: 10.1029/WR008i004p01031.

G.-Y. Niu, Z.-L. Yang, K. E. Mitchell, F. Chen, M. B. Ek, M. Barlage, A. Kumar, K. Manning, D. Niyogi, E. Rosero, and Others. The community Noah land surface model with multiparameterization options (Noah-MP): 1. Model description and evaluation with local-scale measurements. *Journal of Geophysical Research: Atmospheres*, 116(12), 2011. doi: 10.1029/2010JD015139.

A. Ogata. A solution of the differential equation of longitudinal disersion in porous media, us. *USGS Publications Warehouse*, pages paper411–A, 1961. doi: 10.3133/pp411A.

R. K. Pachauri, L. Meyer, G.-K. Plattner, T. Stocker, et al. *IPCC, 2014: Climate Change 2014: Synthesis Report. Contribution of Working Groups I, II and III to the Fifth Assessment Report of the Intergovernmental Panel on Climate Change*. IPCC, 2015.

S. Panday and P. S. Huyakorn. A fully coupled physically-based spatially-distributed model for evaluating surface/subsurface flow. *Advances in Water Resources*, 27(4): 361–382, 2004. doi: 10.1016/j.advwatres.2004.02.016.

C. Paniconi and M. Putti. Physically based modeling in catchment hydrology at 50: Survey and outlook. *Water Resources Research*, 51(9):7090–7129, 2015. doi: 10.1002/2015WR017780.

C. H. Park, C. Beyer, S. Bauer, and O. Kolditz. Using global node-based velocity in random walk particle tracking in variably saturated porous media: Application to contaminant leaching from road constructions. *Environmental Geology*, 55(8):1755–1766, 2008a. doi: 10.1007/s00254-007-1126-7.

C.-H. Park, C. Beyer, S. Bauer, and O. Kolditz. A study of preferential flow in heterogeneous media using random walk particle tracking. *Geosciences Journal*, 12(3):285–297, Sep 2008b. doi: 10.1007/s12303-008-0029-2.

S. Phi, W. Clarke, and L. Li. Laboratory and numerical investigations of hillslope soil saturation development and runoff generation over rainfall events. *Journal of Hydrology*, 493(Supplement C):1–15, 2013. doi: 10.1016/j.jhydrol.2013.04.009.

G. Pinay, S. Peiffer, J. R. de Dreuzy, S. Krause, D. M. Hannah, J. H. Fleckenstein, M. Sebilo, K. Bishop, and L. Hubert-Moy. Upscaling Nitrogen Removal Capacity from Local Hotspots to Low Stream Orders' Drainage Basins. *Ecosystems*, 18(6):1101–1120, 2015. doi: 10.1007/s10021-015-9878-5.

K. Popper. *The logic of scientific discovery*. Routledge, 2005.

M. Pulido-Velazquez, S. Peña-Haro, A. García-Prats, A. F. Mocholi-Almudever, L. Henriquez-Dole, H. Macian-Sorribes, and A. Lopez-Nicolas. Integrated assessment of the impact of climate and land use changes on groundwater quantity and quality in the Mancha Oriental system (Spain). *Hydrology and Earth System Sciences*, 19(4):1677–1693, 2015. doi: 10.5194/hess-19-1677-2015.

Y. Qu and C. J. Duffy. A semidiscrete finite volume formulation for multiprocess watershed simulation. *Water Resources Research*, 43(8), 2007. doi: 10.1029/2006WR005752.

O. Rakovec, R. Kumar, S. Attinger, and L. Samaniego. Improving the realism of hydrologic model functioning through multivariate parameter estimation. *Water Resources Research*, 52(10):7779–7792, 2016a. doi: 10.1002/2016WR019430.

O. Rakovec, R. Kumar, J. Mai, M. Cuntz, S. Thober, M. Zink, S. Attinger, D. Schäfer, M. Schrön, and L. Samaniego. Multiscale and multivariate evaluation of water fluxes and states over european river basins. *Journal of Hydrometeorology*, 17(1):287–307, 2016b. doi: 10.1175/JHM-D-15-0054.1.

J. C. Refsgaard and B. Storm. Mike SHE. *Computer models of watershed hydrology*, 1: 809–846, 1995.

F. Remondi, J. W. Kirchner, P. Burlando, and S. Fatichi. Water Flux Tracking With a Distributed Hydrological Model to Quantify Controls on the Spatiotemporal Variability of Transit Time Distributions. *Water Resources Research*, 54(4):3081–3099, 2018. doi: 10.1002/2017WR021689.

P. Renard and D. Allard. Connectivity metrics for subsurface flow and transport. *Advances in Water Resources*, 51:168–196, 2013. doi: 10.1016/j.advwatres.2011.12.001.

J. Renée Brooks, H. R. Barnard, R. Coulombe, and J. J. McDonnell. Ecohydrologic separation of water between trees and streams in a Mediterranean climate. *Nature Geoscience*, 3(2):100–104, 2010. doi: 10.1038/ngeo722.

R. Rigon, G. Bertoldi, and T. M. Over. GEOtop: A Distributed Hydrological Model with Coupled Water and Energy Budgets. *Journal of Hydrometeorology*, 7(3):371–388, 2006. doi: 10.1175/JHM497.1.

J. F. Rihani, R. M. Maxwell, and F. K. Chow. Coupling groundwater and land surface processes: Idealized simulations to identify effects of terrain and subsurface heterogeneity on land surface energy fluxes. *Water Resources Research*, 46(12):1–14, 2010. doi: 10.1029/2010WR009111.

A. Rinaldo, K. J. Beven, E. Bertuzzo, L. Nicotina, J. Davies, A. Fiori, D. Russo, and G. Botter. Catchment travel time distributions and water flow in soils. *Water Resources Research*, 47(7):1–13, 2011. doi: 10.1029/2011WR010478.

J. Rozemeijer, Y. van Der Velde, R. McLaren, F. van Geer, H. Broers, and M. Bierkens. Integrated modeling of groundwater-surface water interactions in a tile-drained agricultural field: The importance of directly measured flow route contributions. *Water Resources Research*, 46(11), 2010. doi: 10.1029/2010WR009155.

L. Samaniego, R. Kumar, and S. Attinger. Multiscale parameter regionalization of a grid-based hydrologic model at the mesoscale. *Water Resources Research*, 46(5), 2010. doi: 10.1029/2008WR007327.

L. Samaniego, R. Kumar, S. Thober, O. Rakovec, M. Zink, N. Wanders, S. Eisner, H. M. Schmied, E. H. Sutanudjaja, K. Warrach-Sagi, et al. Toward seamless hydrologic predictions across spatial scales. *Hydrology and Earth System Sciences*, 21(9):4323, 2017. doi: 10.5194/hess-21-4323-2017.

L. Samaniego, S. Thober, R. Kumar, N. Wanders, O. Rakovec, M. Pan, M. Zink, J. Sheffield, E. Wood, and A. Marx. Anthropogenic warming exacerbates European soil moisture droughts. *Nature Climate Change*, 8(5):421–426, 2018. doi: 10.1038/s41558-018-0138-5.

K. Sandström. Modeling the Effects of Rainfall Variability on Groundwater Recharge in Semi-Arid Tanzania. *Hydrology Research*, 26(4-5):313, 1995. doi: 10.2166/nh.1995.0018.

H. H. Savenije and M. Hrachowitz. HESS Opinions "catchments as meta-organisms - A new blueprint for hydrological modelling". *Hydrology and Earth System Sciences*, 21 (2):1107–1116, 2017. doi: 10.5194/hess-21-1107-2017.

J. Schewe, J. Heinke, D. Gerten, I. Haddeland, N. W. Arnell, D. B. Clark, R. Dankers, S. Eisner, B. M. Fekete, F. J. Colón-González, S. N. Gosling, H. Kim, X. Liu, Y. Masaki, F. T. Portmann, Y. Satoh, T. Stacke, Q. Tang, Y. Wada, D. Wisser, T. Albrecht, K. Frieler, F. Piontek, L. Warszawski, and P. Kabat. Multimodel assessment of water scarcity under climate change. *Proceedings of the National Academy of Sciences*, 111 (9):3245–3250, 2014. doi: 10.1073/pnas.1222460110.

G. Schoups, N. C. van de Giesen, and H. H. G. Savenije. Model complexity control for hydrologic prediction. *Water Resources Research*, 44(12), 2008. doi: 10.1029/2008WR006836.

J. Scibek and D. Allen. Modeled impacts of predicted climate change on recharge and groundwater levels. *Water Resources Research*, 42(11), 2006. doi: 10.1029/2005WR004742.

J. Scibek, D. M. Allen, A. J. Cannon, and P. H. Whitfield. Groundwater-surface water interaction under scenarios of climate change using a high-resolution transient groundwater model. *Journal of Hydrology*, 333(2-4):165–181, 2007. doi: 10.1016/j.jhydrol.2006.08.005.

G. Seidel. Geologie von Thüringen. *Erdkunde*, 58(1), 2004.

H. G. Seidel, editor. *Geologie von Thüringen*. Schweizerbart Science Publishers, Stuttgart, Germany, 02 2003.

B. Selle, K. Rink, and O. Kolditz. Recharge and discharge controls on groundwater travel times and flow paths to production wells for the Ammer catchment in southwestern Germany. *Environmental Earth Sciences*, 69(2):443–452, 2013. doi: 10.1007/s12665-013-2333-z.

H. Shao, S. V. Dmytrieva, O. Kolditz, D. A. Kulik, W. Pfingsten, and G. Kosakowski. Modeling reactive transport in non-ideal aqueous–solid solution system. *Applied Geochemistry*, 24(7):1287 – 1300, 2009. doi: 10.1016/j.apgeochem.2009.04.001.

H. Shao, T. Nagel, C. Roßkopf, M. Linder, A. Wörner, and O. Kolditz. Non-equilibrium thermo-chemical heat storage in porous media: Part 2 – a 1d computational model for a calcium hydroxide reaction system. *Energy*, 60:271 – 282, 2013. doi: 10.1016/j.energy.2013.07.063.

C. Shen and M. S. Phanikumar. A process-based, distributed hydrologic model based on a large-scale method for surface-subsurface coupling. *Advances in Water Resources*, 33 (12):1524–1541, 2010. doi: 10.1016/j.advwatres.2010.09.002.

B. Smerdon, C. Mendoza, and K. Devito. Simulations of fully coupled lake-groundwater exchange in a subhumid climate with an integrated hydrologic model. *Water Resources Research*, 43(1), 2007. doi: 10.1029/2006WR005137.

M. Sophocleous. Interactions between groundwater and surface water: The state of the science. *Hydrogeology Journal*, 10(1):52–67, 2002. doi: 10.1007/s10040-001-0170-8.

K. Spanoudaki, A. I. Stamou, and A. Nanou-Giannarou. Development and verification of a 3-D integrated surface water–groundwater model. *Journal of Hydrology*, 375(3): 410–427, 2009. doi: 10.1016/j.jhydrol.2009.06.041.

M. Sprenger, C. Stumpp, M. Weiler, W. Aeschbach, S. T. Allen, P. Benettin, M. Dubbert, A. Hartmann, M. Hrachowitz, J. W. Kirchner, J. J. McDonnell, N. Orlowski, D. Penna, S. Pfahl, M. Rinderer, N. Rodriguez, M. Schmidt, and C. Werner. The demographics of water: A review of water ages in the critical zone. *Reviews of Geophysics*, 2019. doi: 10.1029/2018RG000633.

V. Sridhar, M. M. Billah, and J. W. Hildreth. Coupled Surface and Groundwater Hydrological Modeling in a Changing Climate. *Groundwater*, 56(4):618–635, 2017. doi: 10.1111/gwat.12610.

M. K. Stewart, U. Morgenstern, J. J. Mcdonnell, and L. Pfister. The 'hidden streamflow' challenge in catchment hydrology: A call to action for stream water transit time analysis. *Hydrological Processes*, 26(13):2061–2066, 2012. doi: 10.1002/hyp.9262.

M. K. Stewart, U. Morgenstern, M. A. Gusyev, and P. Maloszewski. Aggregation effects on tritium-based mean transit times and young water fractions in spatially heterogeneous catchments and groundwater systems, and implications for past and future applications of tritium. *Hydrology and Earth System Sciences*, 21(9):4615–4627, 2016. doi: 10.5194/hess-2016-532.

S. Stisen, T. O. Sonnenborg, A. L. Højberg, L. Troldborg, and J. C. Refsgaard. Evaluation of Climate Input Biases and Water Balance Issues Using a Coupled Surface–Subsurface Model. *Vadose Zone Journal*, 10(1):37–53, 2011. doi: 10.2136/vzj2010.0001.

T. Stocker. *Climate change 2013: the physical science basis: Working Group I contribution to the Fifth assessment report of the Intergovernmental Panel on Climate Change*. Cambridge University Press, 2014.

F. Sun, H. Shao, T. Kalbacher, W. Wang, Z. Yang, Z. Huang, and O. Kolditz. Groundwater drawdown at Nankou site of Beijing Plain: model development and calibration. *Environmental Earth Sciences*, 64(5):1323–1333, 2011. doi: 10.1007/s12665-011-0957-4.

E. H. Sutanudjaja, L. P. H. van Beek, S. M. de Jong, F. C. van Geer, and M. F. P. Bierkens. Large-scale groundwater modeling using global datasets: A test case for the Rhine-Meuse basin. *Hydrology and Earth System Sciences*, 15(9):2913–2935, 2011. doi: 10.5194/hess-15-2913-2011.

E. H. Sutanudjaja, L. P. H. van Beek, S. M. de Jong, F. C. van Geer, and M. F. P. Bierkens. Calibrating a large-extent high-resolution coupled groundwater-land surface model using soil moisture and discharge data. *Water Resources Research*, 50(1):687–705, 2014. doi: 10.1002/2013WR013807.

R. G. Taylor, B. Scanlon, P. Döll, M. Rodell, R. van Beek, Y. Wada, L. Longuevergne, M. Leblanc, J. S. Famiglietti, M. Edmunds, L. Konikow, T. R. Green, J. Chen, M. Taniguchi, M. F. P. Bierkens, A. MacDonald, Y. Fan, R. M. Maxwell, Y. Yechieli, J. J. Gurdak, D. M. Allen, M. Shamsudduha, K. Hiscock, P. J.-F. Yeh, I. Holman, H. Treidel, R. van Beek, Y. Wada, M. Leblanc, Laurent Longuevergne, J. S. Famiglietti, M. Edmunds, L. Konikow, T. R. Green, J. Chen, M. Taniguchi, M. F. P. Bierkens, A. MacDonald, Y. Fan, R. M. Maxwell, Y. Yechieli, J. J. Gurdak, D. M. Allen, M. Shamsudduha, K. Hiscock, P. J.-F. Yeh, I. Holman, and H. Treidel. Ground water and climate change. *Nature Climate Change*, 3(April):322—329, 2012. doi: 10.1038/NCLIMATE1744.

V. Te Chow. *Applied hydrology*. Tata McGraw-Hill Education, 1988.

D. Tetzlaff, C. Birkel, J. Dick, J. Geris, and C. Soulsby. Storage dynamics in hydropedological units control hillslope connectivity, runoff generation, and the evolution of

catchment transit time distributions. *Water Resources Research*, 50(2):969–985, 2014. doi: 10.1002/2013WR014147.

R. Therrien, R. G. McLaren, E. A. Sudicky, and S. M. Panday. HydroGeoSphere: A three-dimensional numerical model describing fully-integrated subsurface and surface flow and solute transport. *Groundwater Simulations Group, University of Waterloo, Waterloo, ON*, 2010.

S. Thober, R. Kumar, J. Sheffield, J. Mai, D. Schäfer, and L. Samaniego. Seasonal soil moisture drought prediction over europe using the north american multi-model ensemble (nmme). *Journal of Hydrometeorology*, 16(6):2329–2344, 2015. doi: 10.1175/JHM-D-15-0053.1.

S. Thober, R. Kumar, N. Wanders, A. Marx, M. Pan, O. Rakovec, L. Samaniego, J. Sheffield, E. Wood, and M. Zink. Multi-model ensemble projections of European river floods and high flows at 1.5, 2, and 3 degrees global warming. *Environmental Research Letters*, 13(1), 2018. doi: 10.1088/1748-9326/aa9e35.

F. D. Tillman, S. Gangopadhyay, and T. Pruitt. Changes in groundwater recharge under projected climate in the upper Colorado River basin. *Geophysical Research Letters*, 43 (13):6968–6974, 2016. doi: 10.1002/2016GL069714.

A. F. Tompson and L. W. Gelhar. Numerical simulation of solute transport in three-dimensional, randomly heterogeneous porous media. *Water Resources Research*, 26(10): 2541–2562, 1990. doi: 10.1029/WR026i010p02541.

A. F. Tompson, S. F. Carle, N. D. Rosenberg, and R. M. Maxwell. Analysis of groundwater migration from artificial recharge in a large urban aquifer: A simulation perspective. *Water Resources Research*, 35(10):2981–2998, 1999. doi: 10.1029/1999WR900175.

M. Tonkin and J. Doherty. Calibration-constrained Monte Carlo analysis of highly parameterized models using subspace techniques. *Water Resources Research*, 45(1): 1–17, 2009. doi: 10.1029/2007WR006678.

J. Toth. A Theoretical Analysis of Groundwater Flow in Small Drainage Basins. *Journal of Geophysical Research*, 68(16):4795–4812, 1963. doi: 10.1029/JZ068i016p04795.

J. Tóth. Groundwater as a geologic agent: An overview of the causes, processes, and manifestations. *Hydrogeology Journal*, 7(January):1–14, 1999. doi: 10.1007/s100400050176.

H. Treidel, J. L. Martin-bordes, and J. J. Gurdak. *Climate Change Effects on Groundwater Resources: A Global Synthesis of Findings and Recommendations*. CRC Press, 2012.

L. van Beek and M. F. Bierkens. The global hydrological model PCR-GLOBWB: conceptualization, parameterization and verification. *Utrecht University, Utrecht, The Netherlands*, 2009.

Y. van Der Velde, P. J. J. F. Torfs, S. E. A. T. M. van Der Zee, and R. Uijlenhoet. Quantifying catchment-scale mixing and its effect on time-varying travel time distributions. *Water Resources Research*, 48(6):1–13, 2012. doi: 10.1029/2011WR011310.

Y. van der Velde, I. Heidbüchel, S. W. Lyon, L. Nyberg, A. Rodhe, K. Bishop, and P. A. Troch. Consequences of mixing assumptions for time-variable travel time distributions. *Hydrological Processes*, 29(16):3460–3474, 2015. doi: 10.1002/hyp.10372.

M. T. van Genuchten. Analytical solutions for chemical transport with simultaneous adsorption, zero-order production and first-order decay. *Journal of Hydrology*, 49(3-4): 213–233, 1981. doi: 10.1016/0022-1694(81)90214-6.

K. van Meter, N. Basu, J. Veenstra, and C. L. Burras. The nitrogen legacy: emerging evidence of nitrogen accumulation in anthropogenic landscapes. *Environmental Research Letters*, 11(3):035014, 2016. doi: 10.1088/1748-9326/11/3/035014.

K. J. van Meter, N. B. Basu, and P. van Cappellen. Two centuries of nitrogen dynamics: Legacy sources and sinks in the Mississippi and Susquehanna River Basins. *Global Biogeochemical Cycles*, 31(1):2–23, 2017. doi: 10.1002/2016GB005498.

L. van Roosmalen, T. O. Sonnenborg, and K. H. Jensen. Impact of climate and land use change on the hydrology of a large-scale agricultural catchment. *Water Resources Research*, 45(7):1–18, 2009. doi: 10.1029/2007WR006760.

J. E. VanderKwaak and K. Loague. Hydrologic-response simulations for the R-5 catchment with a comprehensive physics-based model. *Water Resources Research*, 37(4):999–1013, 2001. doi: 10.1029/2000WR900272.

Y. Wada, L. P. van Beek, C. M. van Kempen, J. W. Reckman, S. Vasak, and M. F. Bierkens. Global depletion of groundwater resources. *Geophysical Research Letters*, 37 (20), 2010. doi: 10.1029/2010GL044571.

B. J. Wagner and S. M. Gorelick. Optimal groundwater quality management under parameter uncertainty. *Water Resources Research*, 23(7):1162–1174, 1987. doi: 10.1029/WR023i007p01162.

M. Walther, J.-O. Delfs, J. Grundmann, O. Kolditz, and R. Liedl. Saltwater intrusion modeling: Verification and application to an agricultural coastal arid region in oman. *Journal of Computational and Applied Mathematics*, 236(18):4798 – 4809, 2012. doi: http://dx.doi.org/10.1016/j.cam.2012.02.008.

M. Walther, U. Solpuker, N. Böttcher, O. Kolditz, R. Liedl, and F. W. Schwartz. Description and verification of a novel flow and transport model for silicate-gel emplacement. *Journal of contaminant hydrology*, 157:1–10, 2014. doi: 10.1016/j.jconhyd.2013.10.007.

M. Walther, T. Graf, O. Kolditz, R. Liedl, and V. Post. How significant is the slope of the sea-side boundary for modelling seawater intrusion in coastal aquifers? *Journal of Hydrology*, 551(Supplement C):648 – 659, 2017. doi: 10.1016/j.jhydrol.2017.02.031.

N. Wanders, M. T. H. van Vliet, Y. Wada, M. F. P. Bierkens, and L. P. H. R. van Beek. High-Resolution Global Water Temperature Modeling. *Water Resources Research*, 55 (4):2760–2778, 2019. doi: 10.1029/2018WR023250.

H. Wang, C. J. Richardson, M. Ho, and N. Flanagan. Drained coastal peatlands: A potential nitrogen source to marine ecosystems under prolonged drought and heavy storm events—a microcosm experiment. *Science of The Total Environment*, 566-567: 621 – 626, 2016. doi: 10.1016/j.scitotenv.2016.04.211.

W. Wang, G. Kosakowski, and O. Kolditz. A parallel finite element scheme for thermo-hydro-mechanical (THM) coupled problems in porous media. *Computers & Geosciences*, 35(8):1631–1641, 2009. doi: 10.1016/j.cageo.2008.07.007.

W. Wang, O. Kolditz, and T. Nagel. Parallel finite element modelling of multi-physical processes in thermochemical energy storage devices. *Applied Energy*, 185:1954–1964, 2017. doi: 10.1016/j.apenergy.2016.03.053.

L. Warszawski, K. Frieler, V. Huber, F. Piontek, O. Serdeczny, and J. Schewe. The Inter-Sectoral Impact Model Intercomparison Project (ISI–MIP): Project framework. *Proceedings of the National Academy of Sciences*, 111(9):3228–3232, 2014. doi: 10.1073/pnas.1312330110.

F. Wechsung. *Auswirkungen des globalen Wandels auf Wasser, Umwelt und Gesellschaft im Elbegebiet*, volume 6. Weißensee Verlag, 2005.

F. Wechsung, S. Kaden, H. Behrendt, and B. Klöcking, editors. *Integrated Analysis of the Impacts of Global Change on Environment and Society in the Elbe Basin*. Schweizerbart Science Publishers, Stuttgart, Germany, 01 2008.

S. Weill, E. Mouche, and J. Patin. A generalized Richards equation for surface / subsurface flow modelling. *Journal of Hydrology*, 366(1-4):9–20, 2009. doi: 10.1016/j.jhydrol.2008.12.007.

G. S. Weissmann, Y. Zhang, E. M. LaBolle, and G. E. Fogg. Dispersion of groundwater age in an alluvial aquifer system. *Water Resources Research*, 38(10):16–1–16–13, 2002. doi: 10.1029/2001WR000907.

E. Widén-Nilsson, S. Halldin, and C.-y. Xu. Global water-balance modelling with WASMOD-M: Parameter estimation and regionalisation. *Journal of Hydrology*, 340(1): 105–118, 2007. doi: 10.1016/j.jhydrol.2007.04.002.

W. W. Woessner. Stream and Fluvial Plain Ground Water Interactions: Rescaling Hydrogeologic Thought. *Groundwater*, 38(3):423–429, 2000. doi: 10.1111/j.1745-6584.2000.tb00228.x.

S. T. Woldeamlak, O. Batelaan, and F. de Smedt. Effects of climate change on the groundwater system in the Grote-Nete catchment, Belgium. *Hydrogeology Journal*, 15 (5):891–901, 2007. doi: 10.1007/s10040-006-0145-x.

E. F. Wood, D. Lettenmaier, X. Liang, B. Nijssen, and S. W. Wetzel. Hydrological modeling of continental-scale basins. *Annual Review of Earth and Planetary Sciences*, 25(1):279–300, 1997. doi: 10.1146/annurev.earth.25.1.279.

E. F. Wood, J. K. Roundy, T. J. Troy, L. P. H. van Beek, M. F. P. Bierkens, E. Blyth, A. de Roo, P. Döll, M. Ek, J. Famiglietti, D. Gochis, N. van de Giesen, P. Houser, P. R. Jaffé, S. Kollet, B. Lehner, D. P. Lettenmaier, C. Peters-Lidard, M. Sivapalan, J. Sheffield, A. Wade, and P. Whitehead. Hyperresolution global land surface modeling: Meeting a grand challenge for monitoring Earth's terrestrial water. *Water Resources Research*, 47(5), 2011. doi: 10.1029/2010WR010090.

T. Xu and A. J. Valocchi. A Bayesian approach to improved calibration and prediction of groundwater models with structural error. *Water Resources Research*, 51(11):9290–9311, 2015. doi: 10.1002/2015WR017912.

J. Yang, I. Heidbüchel, A. Musolff, F. Reinstorf, and J. H. Fleckenstein. Exploring the Dynamics of Transit Times and Subsurface Mixing in a Small Agricultural Catchment. *Water Resources Research*, 54(3):2317–2335, 2018. doi: 10.1002/2017WR021896.

A. Zech, B. Zehner, O. Kolditz, and S. Attinger. Impact of Heterogeneous Permeability Distribution on the Groundwater Flow Systems of a Small Sedimentary Basin. *Journal of Hydrology*, 532:90–101, 2015. doi: 10.1016/j.jhydrol.2015.11.030.

A. Zghibi, L. Zouhri, I. Chenini, A. Merzougui, and J. Tarhouni. Modelling of the groundwater flow and of tracer movement in the porous and fissured media: chalk aquifer (Northern part of Paris Basin, France). *Hydrological Processes*, 30(12):1916–1928, 2015. doi: 10.1002/hyp.10746.

M. Zink, R. Kumar, M. Cuntz, and L. Samaniego. A high-resolution dataset of water fluxes and states for Germany accounting for parametric uncertainty. *Hydrology and Earth System Sciences*, 21(3):1769–1790, 2017. doi: 10.5194/hess-21-1769-2017.

M. Zink, J. Mai, M. Cuntz, and L. Samaniego. Conditioning a Hydrologic Model Using Patterns of Remotely Sensed Land Surface Temperature. *Water Resources Research*, 54(4):2976–2998, 2018. doi: 10.1002/2017WR021346.

B. Zinn and C. F. Harvey. When good statistical models of aquifer heterogeneity go bad : A comparison of flow , dispersion , and mass transfer in connected and multivariate Gaussian hydraulic conductivity fields. *Water Resources Research*, 39(3):1–19, 2003. doi: 10.1029/2001WR001146.

Acknowledgements

This work would not have been possible without the financial support of the Chinese Scholarship Council (CSC) and the AquaDiva project. Firstly, I would like to express my sincere gratitude to my supervisor Prof. Dr. Sabine Attinger for the continuous support of my doctoral study, for her patience, motivation, and immense knowledge. Her guidance helped me in all the time of research and writing of this thesis. I would like to thank Prof. Dr. Olaf Kolditz for his expertise in environmental informatics and valuable guidance in my research. I would particularly like to thank Prof. Dr. Alexander Brenning for his insightful and constructive comments and suggestions to this cumulative thesis. I would like to thank Prof. Dr. Kai Uwe Totsche and Prof. Dr. Ulrich Wegler for their professional evaluations of my doctoral research. I would particularly like to thank Dr. Falk Heße and Dr. Rohini Kumar, both of whom spent great efforts in helping me design the research and revise the papers. Without their precious support, it would not be possible to conduct this research. I would like to thank Prof. Dr. Anke Hildebrandt for her suggestions on my doctoral thesis. I am grateful to Dr. Wenqing Wang, a master in C++ and mathematics, for his help and encouragement. I am so grateful to Dr. Alraune Zech, Dr. Luis Samaniego, Dr. Lennart Schüler, Dr. Oldrich Rakovec, Dr. Stephan Thober, Dr. Andreas Marx, Dr. Matthias Zink, Dr. Corinna Rebmann, Sebastian Gimper, Timo Houben, Sebastian Müller, Micheal Peichl, Robert Schweppe, Pallav Kumar Shrestha, Johannes Brenner, Maren Kaluza, and all other colleagues from the CHS department at UFZ for the stimulating discussions, for the time we were working together, and for all the fun we have had in the last four years. Particularly, I would like to thank Dr. Lennart Schüler and Timo Houben for their help in the German version of abstract ("Zusammenfassung") of this thesis. I also thank Barbara Timmel at the Foreigner Office, the secretaries – Sindy, Nora, and Catharina, the HIGRADE team, and the EVE cluster team, for their continuous and substantial supports to my stay at Leipzig and study at UFZ. I thank my colleagues from ENVINF department for their great help in my doctoral research.

I am grateful to my Chinese colleagues at UFZ and my Chinese friends at Leipzig. We had a nice time together sharing a similar experience, emotions, and most importantly– the delicious Chinese food. Those moments are some of my most treasured memories.

Last but not the least, I would like to acknowledge the people who mean a lot to me –my mother Yanling Cui, my father Qingquan Jing, and my grandfather – for showing faith in me and giving me the liberty to choose what I desired. Although they hardly understood what I researched, they were willing to support any decision I made. It would be impossible to finish the doctoral research without their encouragement and support.

Publication list

Peer-reviewed Journal

1. **Jing, M.**, Heße, F., Kumar, R., Wang, W., Fischer, T., Walther, M., Zink, M., Zech, A., Samaniego, L., Kolditz, O., and Attinger, S.: Improved regional-scale groundwater representation by the coupling of the mesoscale Hydrologic Model (mHM v5.7) to the groundwater model OpenGeoSys (OGS), Geoscientific Model Development, 11(5): 1989–2007, 2018. doi: 10.5194/gmd-11-1989-2018.

2. **Jing, M.**, Heße, F., Kumar, R., Kolditz, O., Kalbacher, T., and Attinger, S.: Influence of input and parameter uncertainty on the prediction of catchment-scale groundwater travel time distributions, Hydrology and Earth System Sciences, 23(1):171–190, 2019a. doi: 10.5194/hess-23-171-2019.

3. **Jing, M.**, Kumar, R., Heße, F., Thober, S., Rakovec, O., Samaniego, L., and Attinger, S.: Assessing the response of groundwater quantity and travel time distribution to 1.5, 2 and 3 degrees global warming in a mesoscale central German basin, Hydrology and Earth System Sciences Discussion, 2019:1–22, 2019b, in review, doi: 10.5194/hess-2019-9.

Book chapter

1. **Jing, M.**, Heße, F., Wang, W., Fischer, T., Walther, Attinger, S.: HH Processes, in book: Thermo-Hydro-Mechanical-Chemical Processes in Fractured Porous Media: Modelling and Benchmarking, Springer, doi: 10.1007/978-3-319-68225-9_5.

Conference presentation

1. **Jing, M.**, Fischer, T., Zech, A., Walther, M., Heße, F., Kolditz, O., Attinger, S.: Simulation of groundwater circulation considering geological heterogeneity with the truncated pluri-gaussian model: An application in a small sedimentary basin in central Germany. EGU2016, Vienna, Austria; 17-22 April 2016.

2. **Jing, M.**, Zech, A., Schüler, L, Attinger, S.: Characterization of Aquifer Heterogeneity through Pumping Test. Cargese summer school: July 20th - August 1st 2015, - Cargese, France, 2015.

3. **Jing, M.**, Heße, F., Kolditz, O., Attinger, S.: Improved regional scale groundwater representation by the coupling of the mesoscale Hydrologic Model (mHM) to the groundwater model OpenGeoSys (OGS). HIGRADE Conference, Leipzig, Germany; 20 March 2018.

Software

1. **Jing, Miao**, Heße, Falk, Kumar, Rohini, Wang, Wenqing, Fischer, Thomas, Walther, Marc, Attinger, Sabine. (2018, May 16). mHM#OGS v1.0: the coupling interface between the mesoscale Hydrologic Model (mHM) and the groundwater model OpenGeoSys (OGS) (Version 1.0), doi: 10.5281/zenodo.1248005.